This page intentionally left blank


MIDAC


USGS

Volcanic Emissions

Tracking the flow of gases from magma is perhaps the most vexing task of physical volcanology. To play upon a phrase, "gas waits for no man," because the gaseous species are volatile. Also, things get in the way, not the least of which are the volcanic edifice itself and ground water that permeates it.

The 2004–6 Mount St. Helens dacite was a "flat" magma—greatly depleted in excess (exsolved) volatiles compared to the May 18, 1980, dacite. If new magma entered the system as part of the 2004 eruption, it must have been gas poor, on the basis of modeling constrained by cumulative CO_2 emissions, cumulative dacite production, and measurement of dissolved H_2O and other volatile concentrations within the dacite glass.

This view, that the eruption was driven by degassed magma, is supported by chemical trends in hot springs and creek waters that drain the Mount St. Helens crater. Since 1994 these waters have shown decreasing SO_4 and Cl concentrations, most likely reflecting changing release rates of sulfur gases, HCl, and CO_2 from the magma and, to a varying degree, the efficiency of gas scrubbing by the water. Still unanswered is the question of what triggered the eruption of such gas-poor magma—was it influx of a small amount of hotter, gas-rich magma that was otherwise compositionally similar to the 1980s magma, infiltration of rainwater into the upper part of the conduit system, or some other mechanism?

The lessons from the 2004 eruption are clear: Scrubbing or simply having a magma already depleted in gases can mask the more typical signal of shallow magmatic sulfur-species degassing, so early monitoring of CO_2 should accompany early SO_2 monitoring. Indeed, the monitoring of CO_2, SO_2, and H_2S can track the drying out of a volcano and help distinguish the effects of gas scrubbing from the loss of permeability when pathways for gas are sealed by precipitates.

This eruption also provided an opportunity to further test new gas-emission monitoring tools. Results from open-path Fourier-transform infrared spectroscopy support the interpretation that closed-system degassing occurs as shallow as 1–2 km and that open-system degassing characterizes the shallowest part of the magmatic system.

View to south-southwest on September 19, 2005, as spine 6 grew westward away from disintegrating spines 4 and 5 (left of center) and compressed the highly crevassed west arm of Crater Glacier. Rocky terrain in lower right is 1980s dome. USGS photo by J.W. Ewert.

A Volcano Rekindled: The Renewed Eruption of Mount St. Helens, 2004–2006
Edited by David R. Sherrod, William E. Scott, and Peter H. Stauffer
U.S. Geological Survey Professional Paper 1750, 2008

Chapter 25

Pre- and Post-Eruptive Investigations of Gas and Water Samples from Mount St. Helens, Washington, 2002 to 2005

By Deborah Bergfeld[1], William C. Evans[1], Kenneth A. McGee[2], and Kurt R. Spicer[2]

Abstract

Samples of gas and water from thermal springs in Loowit and Step canyons and creeks that drain the crater at Mount St. Helens have been collected since October 2004 to monitor the flux of dissolved magmatic volatiles in the hydrologic system. The changing composition of the waters highlights a trend that began as early as 1994 and includes decreasing SO_4 and Cl concentrations and large increases in HCO_3. Geochemical models indicate that mineral sources and sinks are not the main controls on the changing water chemistry, and carbon and helium isotopes indicate that their sources in the gases and waters have remained unchanged during this time. The present-day molar ratios of C, S, and Cl in the springs approximate ratios measured in plume emissions in August 2005 and provide supporting evidence that changes in water chemistry most likely reflect changes in the release rates of sulfur gases, HCl, and CO_2 from the magma and a varying degree of efficiency of gas scrubbing by the overlying water. Results from coupled chemical analyses and discharge measurements on the creeks yield an estimate of the dissolved flux of magmatic HCl, SO_2, and CO_2 of around 5.2, 4.7, and 22 metric tons per day, respectively.

Introduction

Airborne gas measurements were a valuable tool in tracking magmatic emissions for Mount St. Helens during the 1980–86 eruptive sequence, but flights eventually were suspended as emission rates dropped to low levels. Between September 1988 and September 2004, attempts to measure the flux of magmatic volatiles at Mount St. Helens were restricted to analyses of gases and condensates from vents on the lava dome and thermal waters from springs in Loowit and Step canyons[3] in The Breach. Results from those analyses generally have shown a progressive decrease in magmatic volatile concentrations with time. Airborne gas-flux measurements over the crater at Mount St. Helens were resumed in September 2004 following the onset of seismic activity (Doukas and others, 2005). To date, those measurements have shown that plume CO_2 and SO_2 emission rates are much lower than emission rates during the 1980s eruptions (Gerlach and others, 2005, and this volume, chap. 26). Plume emission rates were one line of evidence that supported an early hypothesis that degassed magma was driving the current eruption.

To track the flux of dissolved magmatic volatiles in the hydrologic system during the current eruption, we established a surface-water sampling program on October 13, 2004. The first samples were collected on the Pumice Plain from two creeks that drain the crater. In mid-April 2005, as conditions nearer the crater stabilized, we expanded the monitoring network to include three locations in The Breach (fig. 1). These five sites were the main focus of our monitoring campaign during the first year after the 2004–5 eruption, but at times we also have collected samples from a warm spring on the west end of the Pumice Plain and from hot springs in Loowit and Step canyons in upper parts of The Breach. Thus far, our sample collection intervals have been irregular, but since October 2005 some continuous temperature and conductivity data have been collected by a probe installed near the top of Step creek.

In this report we present geochemical data from the monitoring sites; data from field campaigns in the crater and

[1] U.S. Geological Survey, 345 Middlefield Road, Menlo Park, CA 94025

[2] U.S. Geological Survey, 1300 SE Cardinal Court, Vancouver, WA 98683

[3] Many geographic features in the Mount St. Helens area are referred to informally by Earth scientists. Capitalization of "canyon," "creek," or "spring" indicates names formally adopted and listed in the Geographic Names Information System, a database maintained by the U.S. Board on Geographic Names. Noncapitalized names are applied informally—eds.

The Breach in 2002 and 2005, which focused on the chemistry of crater gases and hot spring waters; and data from a survey of regional cold springs. We also include data from previous investigations of the geochemistry of the hot springs at Mount St. Helens in order to evaluate long-term changes in gas sources or fluxes and, ultimately, to determine how magmatic processes at an active volcano are reflected in the hydrothermal system. We have adopted the names of the Loowit canyon hot springs that were used by Shevenell and Goff (1993) but have adhered to the policies of the U.S. Board on Geographic Names regarding capitalization of formal and informal names. Additional chemical data not discussed in the paper can be found in appendix 1, which appears only in the digital versions of this work (in the DVD that accompanies the printed volume and online at http://pubs.usgs.gov/pp/1750).

Background

After the May 1980 eruption of Mount St. Helens, gas samples were collected from cracks and fumaroles near the dome in the fall of 1980 (Evans and others, 1981; Gerlach and Casadevall, 1986). Due to dome growth and collapse and extrusions of new lava, the gas-sampling locations varied during the subsequent years. Before our work in 2002, the last

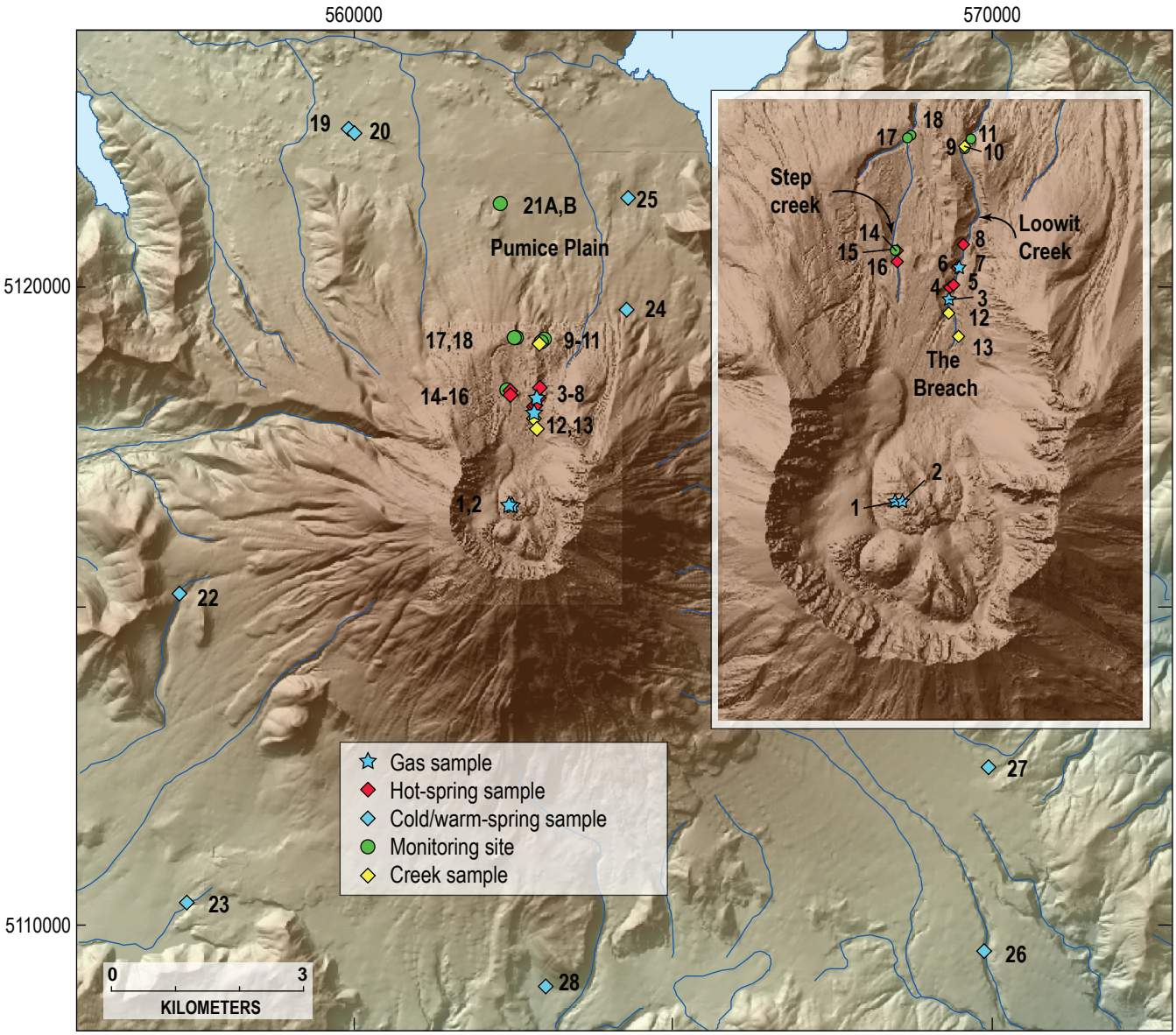

Figure 1. Maps showing sample locations for this study, 2002–2005, Mount St. Helens, Washington. Numbers for sample sites correspond to numbers listed in table 1. Inset shows crater and The Breach sample locations in more detail. Datum for geographic grid and UTM coordinates referenced to WGS84, zone 10.

gas sample from the crater was collected in June 1998 from an 86°C vent on the southwest side of the 1980–86 lava dome on a flow called the September 1984 lobe, herein referred to more briefly as "September lobe." The sampling site was formerly the hottest fumarole on the dome, but in 1998 it had cooled by 260–370°C relative to temperatures recorded in 1994–95 (Symonds and others, 2001).

Downcutting of avalanche deposits in The Breach of Mount St. Helens created Loowit and Step canyons, which drain to the north and represent the main discharge of surface water from the crater (fig. 1). Thermal springs were first observed discharging into Loowit Creek during the summer of 1983, and the first sample of spring water was collected in October 1983 (Thompson, 1990). Lower-temperature, low-discharge springs in Step canyon were discovered at a later date, and the first published analyses of the Step canyon springs are from 1988 (Shevenell and Goff, 1993). It has been estimated that more than 95 percent of the hot spring discharge from both canyons is provided by the springs in Loowit canyon (Shevenell and Goff, 1993). During the 1980s to mid-1990s, the hot springs in Loowit canyon were located in three areas along the length of the canyon. Each area contained clusters of hot springs of varying size and temperature. From south to north, the spring groups are called (1) Loowit source, (2) Loowit boulder basin, and (3) Loowit travertine. The name Loowit travertine is a misnomer that stems from the presence of gypsum-bearing precipitates on the rocks around the vent orifices (Shevenell and Goff, 1993). There are no names for the springs in Step canyon. The waters from both Loowit and Step canyons were sampled throughout the 1980s and 1990s, but because of the larger volume of thermal water, the Loowit canyon springs were sampled with the greatest frequency.

Post-2000 Field Campaigns

Gas and Water Samples from the Crater and The Breach

In August 2002 there were no fumaroles in the crater at Mount St. Helens, but diffuse steam was rising from several locations on the 1980–86 dome. We sampled gas at two locations from the strongest vents we could find on September lobe (fig. 1; table 1). Because of safety concerns we were unable to resample the sites in 2005. In August 2002 and July 2005 we also collected gases from bubbling hot springs in Loowit canyon. To our knowledge these are the first free-gas samples collected from springs in Loowit canyon.

Water samples were collected from the Loowit canyon hot springs in 2002 and 2005, and samples of the Step canyon springs were collected in July and October 2005. At springs with multiple orifices, our strategy was to choose the hottest spring for sample collection, and at times we also sampled water from a nearby spring. In 2002, the hottest vents at the Loowit boulder basin and Loowit travertine sites were along the west bank of Loowit Creek. The outflow from the southernmost spring, which we assume to be the Loowit source spring, was from a single vent on a bench above the canyon floor. The water cascaded down the west canyon wall into Loowit Creek. In July 2005 there was no visible outflow from the Loowit source spring; instead, a new large spring issued from the base of a small fan that abuts the west wall of the canyon. Additional cooler waters discharged from an upper part of the fan and small vents along the west bank of the creek.

The thermal waters in Step canyon occur in clusters and line the banks of the headwaters of Step creek. In 2005 there were no high-discharge vents, and all of the waters issued from areas composed of low-discharge seeps. Intermittent degassing was observed at both of the sites in July, but no gas was visible in October 2005.

Creeks and Regional Springs

The five sites that make up the monitoring network are along creeks that provide the major surface drainage from the crater at Mount St. Helens. The network includes two sites (LCBF and SCBF) on the Pumice Plain (fig. 1; table 1) and three sites (LCAF, EFSCAF, and WFSCAF) closer to the crater above the waterfalls on Loowit and Step creeks. The Pumice Plain sites are the most accessible and serve to monitor the surface drainage from locations just above the confluence of the two creeks. Of the higher-altitude sites, LCAF receives input from all of the hot springs in Loowit canyon and variable seasonal input of glacial meltwater; EFSCAF is on the east fork of Step creek, which is the fork that contains the Step canyon springs; and WFSCAF is a tributary to Step creek that drains the west wall of the crater. This channel (WFSCAF) carries seasonal runoff from the west arm of the Crater Glacier. We have not walked the length of this creek, but there are no obvious thermal waters that discharge to this drainage. In this report we also present water data from the probe locations (fig. 1; table 1) and three other locations on Loowit Creek, which were sampled in 2002 and 2005.

Several studies have used carbon and helium isotopes, together with water chemistry, to demonstrate that cold ground waters in volcanic regions can carry large amounts of dissolved magmatic carbon (Rose and Davisson, 1996; Chiodini and others, 2000; Evans and others, 2002). To investigate outflow of magmatic volatiles from the volcano to regional springs, we sampled eight mostly low-temperature springs in the area surrounding Mount St. Helens in July 2005. Kalama Spring, located southwest of Mount St. Helens, has the largest discharge of any spring in our sample set, followed by carbonate spring, a warm spring on the west end of the Pumice Plain (fig. 1; tables 1 and 2). Because the chemistry of carbonate spring has some similarities with the springs from The Breach, future discussion of this spring will be included with discussions of the hot springs. Of the seven other cold springs in this report, the most well-studied are Kalama, Willow, and Moss Springs, which have been sampled infrequently since

Table 1. Map number and location coordinates for samples collected during 2002–2005, Mount St. Helens, Washington.

[UTM coordinates and altitude are referenced to the WGS84 datum.]

Location	Map No.	Northing	Easting	Altitude (m)
Old dome Mount St. Helens				
September lobe, landing site	1	5116595	562436	2,122
September lobe, upper dome	2	5116600	562487	2,130
Springs in Loowit canyon				
2005 degassing spring	3	5118045	562819	1,664
Loowit source spring	4	5118136	562831	1,635
New spring on fan of Loowit canyon	5	5118157	562856	1,617
Loowit boulder basin spring	6	5118275	562882	1,604
Loowit boulder basin degassing spring	7	5118273	562891	1,604
Loowit travertine spring	8	5118442	562921	1,584
Springs in Step canyon				
Step canyon hottest spring	14	5118396	562453	1,644
Step canyon source spring	16	5118324	562453	1,645
Monitoring network sites				
Probe site, Loowit Creek above falls	9	5119128	562929	1,507
Loowit Creek above falls	11	5119198	562981	1,509
Probe site, east fork Step creek above falls	15	5118401	562446	1,617
West fork Step creek above falls	17	5119212	562519	1,512
East fork Step creek above falls	18	5119224	562546	1,512
Loowit Creek below falls	21A	5121306	562300	1,219
Step creek below falls	21B	5121306	562300	1,219
Other creek locations				
Lower Loowit Creek	10	5119150	562935	1,509
Upper Loowit Creek	12	5117947	562819	1,662
Upper Loowit Creek	13	5117784	562886	1,709
Pumice Plain spring				
Carbonate spring at gage	19	5122487	559926	935
Carbonate spring	20	5122421	560010	945
Regional cold springs				
Springs west of Cold Spring Creek	22	5115219	557268	1,132
Kalama Spring	23	5110368	557390	832
Spring on Loowit trail	24	5119654	564283	1,330
Willow spring	25	5121399	564292	1,125
Spring on Pine Creek	26	5109610	569886	731
Moss spring	27	5112493	569935	882
Spring west of Swift Creek	28	5109062	563021	756

the late 1980s. Four of the springs are unnamed and were identified on 24,000-scale quadrangle maps or were brought to our attention by Mike Clynne of the U.S. Geological Survey (USGS), who has mapped extensively in the area around Mount St. Helens. In the text that follows we refer to the regional springs by their associated map number (fig. 1; table 1). The eight springs we report on here are likely the largest on the margins of the volcano, although assuredly more cold springs are in the Mount St. Helens area.

Field and Laboratory Methods

Water and gas samples were collected for a suite of chemical analyses using standard field and laboratory techniques. At all sites the water temperature and conductivity were measured in the field using portable meters. Spring-water samples collected for bulk chemistry were preserved in the field by filtering them through a 0.45-µm filter into plastic bottles that were first rinsed with filtered water. Samples for cation analyses were preserved with high-purity nitric acid by dropwise addition to a pH < 2. Other nonfiltered (raw) spring-water samples were collected in glass bottles for alkalinity and δD and $\delta^{18}O$ analyses and in preevacuated glass bottles for $\delta^{13}C$ analysis of dissolved inorganic carbon (DIC), which consists of dissolved $CO_2 + HCO_3 + CO_3$. Depending on the sample size, waters collected for $\delta^{13}C$–DIC were acidified with 0.5 to 1.0 mL of high-purity hydrochloric acid to convert DIC to CO_2. Values for $\delta^{13}C$–DIC and ^{14}C–DIC were determined on purified CO_2 extracted from the water samples following methods described in Evans and others (2002).

Samples of creek waters from the monitoring sites typically were collected into prerinsed plastic bottles as raw waters. Filtering, sample preservation, and pH measurements were performed in the laboratory, at Menlo Park, Calif. Because samples from the monitoring sites were sometimes stored before they were received at the lab, we have not determined the bicarbonate concentrations of many of these water samples. A few samples of creek waters were collected for $\delta^{13}C$ analysis of DIC as described above. Creek discharge rate was measured using a pygmy meter. Visual estimates of discharge are identified in table 2.

Anion and cation concentrations in water samples were determined using ion chromatography and inductively coupled argon plasma spectrometry at USGS laboratories in Menlo Park, Calif. Isotope analyses were performed at USGS laboratories in Menlo Park, Calif., and Reston, Va., and at the Center for Accelerator Mass Spectrometry at Lawrence Livermore National Laboratory, Calif. Isotope analyses were performed using techniques outlined in Epstein and Mayeda (1953), Coplen (1973), Vogel and others (1987), and Coplen and others (1991).

Gas samples for bulk composition and $\delta^{13}C$–CO_2 analyses were collected into preevacuated glass bottles through a hollow titanium rod (from gas vents) or a funnel fitted with

Table 2. Spring and creek temperature and discharge measurements 2003–2005, Mount St. Helens, Washington.

[Letters following discharge rate indicate field method: EV, width and depth measured, velocity estimated; E, visual estimate; M, measured. Some locations coded to specify sites: ps, probe site; LCAF, Loowit Creek above falls; LCBF, Loowit Creek below falls; EFSCAF, east fork Step creek above falls; WFSCAF, west fork Step creek above falls; SCBF, Step creek below falls; CARB gs, carbonate spring gage site.]

Location	Date	Temp. (°C)	Discharge (L/s)	Method
Monitoring network sites				
LCAF	08/20/03	27.0	323	M
LCAF	06/17/04	24.4	208	M
LCAF	08/12/04	27.3	320	M
LCAF	04/21/05	27.5	170	E
LCAF	07/26/05	29.1	397	M
LCAF	08/26/05	30.1	408	M
LCAF	10/11/05	30.0	267	M
LCAF ps	10/25/05	25.9	215	M
LCBF	09/28/04	18.1	249	M
LCBF	10/13/04	16.3	306	M
LCBF	10/20/04	10.2	230	E
LCBF	12/02/04	8.4	110	E
LCBF	02/10/05	11.5	110	E
LCBF	04/21/05	16.9	187	M
LCBF	07/26/05	22.5	399	M
LCBF	08/26/05	19.8	279	M
EFSCAF	08/12/04	30.0	80	E
EFSCAF	04/21/05	19.5	60	E
EFSCAF	07/26/05	26.6	45	M
EFSCAF	08/26/05	24.1	40	EV
EFSCAF	10/11/05	17.6	19	M
EFSCAF ps	10/25/05	25.4	27	M
WFSCAF	08/12/04	10.5	120	E
WFSCAF	04/21/05	4.2	<30	E
WFSCAF	07/26/05	10.5	142	M
WFSCAF	08/26/05	16.4	30	EV
WFSCAF	10/11/05	7.5	10	E
SCBF	09/28/04	16.3	95	M
SCBF	10/13/04	14.5	112	M
SCBF	10/20/04	9.1	10	E
SCBF	11/05/04	9.7	10	E
SCBF	12/02/04	4.1	20	E
SCBF	02/10/05	5.6	10	E
SCBF	04/21/05	10.0	3	E
SCBF	07/26/05	21.2	110	M
SCBF	08/26/05	19.2	49	M
Pumice Plain spring				
CARB gs	10/25/05	15.7	354	M
Regional cold springs				
Spring 22	07/29/05	4.4	11	M
Spring 23	07/29/05	4.7	818	M
Spring 24	07/30/05	3.0	16	M
Spring 25	07/30/05	5.4	44	M
Spring 26	07/31/05	7.2	137	M
Spring 27	07/31/05	6.3	82	M
Spring 28	07/31/05	5.2	29	M

Tygon tubing (from bubbling springs). Prior to sampling, the entire collection system was purged of atmospheric gases. Gas samples were analyzed for bulk composition at the USGS in Menlo Park, Calif., using gas chromatography methods reported in Evans and others (1981). Carbon dioxide for stable isotope analysis was separated from the bulk gas sample using standard cryogenic techniques on a vacuum line (Evans and others, 2002). The spring gas samples for $^3He/^4He$ analysis were collected from the funnel and tubing apparatus into copper tubing that was then sealed at both ends with refrigeration clamps. The $^3He/^4He$ determination was run at Lawrence Berkeley National Laboratory in Berkeley, California, following methods outlined by Kennedy and van Soest (2006). Helium isotope ratios are reported as R/R_A values, which represent the $^3He/^4He$ ratio in the gas relative to the $^3He/^4He$ ratio in air. Values for $R/R_A > 1$ indicate that a percentage of the gas is derived from a mantle or magmatic source.

Results and Discussion

Chemistry of the Hot Springs, 1983 to 2005

The chemistry and temperature of the Loowit canyon hot springs changed rapidly after the springs appeared in 1983 (Thompson, 1990; Shevenell and Goff, 1993, 1995). The highest water temperature recorded was 92.6°C from the Loowit travertine spring group in 1986, and by then, concentrations of many of the dissolved constituents in the Loowit springs had peaked (Shevenell and Goff, 1993). The subsequent declining temperatures and variable chemistry were attributed to a rapidly cooling hydrothermal system that had formed just after the 1980 eruption. Several important conclusions were reached by Shevenell and Goff (1993, 1995, 2000) and Goff and McMurtry (2000), including (1) that the Loowit canyon hot springs discharged mixtures of recent meteoric water and about 10 percent magmatic water, (2) that the underground residence time of the mixed water was too short to allow water-rock equilibration or reliable geothermometry, and (3) that Cl, SO_4, and HCO_3 in the springs were mainly derived from magmatic volatiles.

More recent samples show that the chemistry of the hot springs at Mount St. Helens is still changing (F. Goff and the USGS, unpub. data, 1984–94), although water temperatures since 1990 appear to have stabilized (fig. 2). The early trend in anions from SO_4 toward Cl dominance stopped, and water samples from 1994, 2002, and 2005 show declines in both SO_4 and Cl relative to HCO_3 (table 3; fig. 3). The post-1989 data for the Step canyon springs follow a similar trend toward HCO_3-dominated water.

Overall, most elements in the Loowit springs show the effects of dilution by meteoric water over time (fig. 4). The plots in figure 4 may understate the dilution effects because of the increased focus on sampling the hottest springs in 2002 and 2005. Dilution effects also are seen in the δD and $\delta^{18}O$ composition of the waters from 2002 and 2005, which plot on or near the world meteoric water line (table 4; fig. 5). Previous $\delta^{18}O$ values of Loowit hot spring waters through 1994 were shifted by as much as 2 per mil to the right of the meteoric water line.

Simple dilution, however, does not fully explain all of the data. Concentrations of Na and SO_4 have decreased since 1984, whereas Cl and B concentrations remained high throughout the mid- to late 1980s and declined in later years (fig. 4). Concentrations of Mg increased in the 2002 and 2005 samples, and HCO_3 concentrations showed a large increase to concentrations higher than was recorded previously.

A clear response to the renewal of activity in 2004 has not yet been recognized in the hot springs. Just prior to the onset of seismicity in 2004, the discharge and water temperature at a spring in Loowit canyon appeared to be higher than normal (J.S. Pallister, USGS, oral commun., 2004), but no measurements were made. However, any possible temperature increase was short lived, as comparisons between the 2002 and 2005 samples from the hottest springs in Loowit canyon show little change in temperatures (table 3). Similarly, in July 2005 the temperature measured at the hottest spring in Step canyon was substantially higher than temperatures reported from 1994 (fig. 2), but three months later, in October, the temperature at the same location had declined 18°C, although the specific conductance had decreased only slightly. Because the flow from the Step canyon vents is low, this temperature decline is conceivably related to the change in surface air temperature and conductive cooling. The possible causes for rapid swings in temperature at the hot springs need further investigation, but at this point, it is difficult to attribute any temperature changes

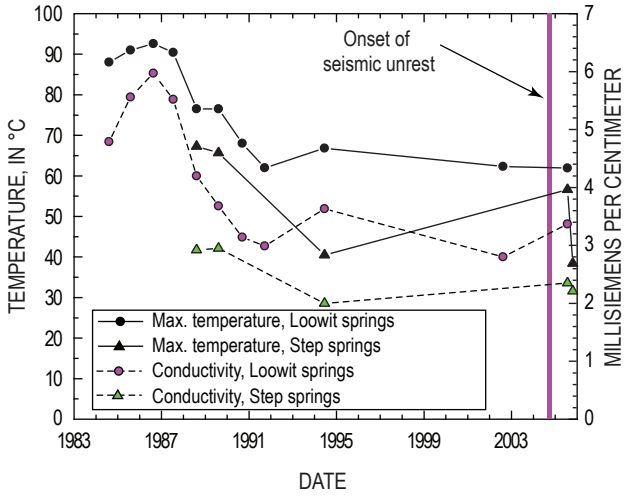

Figure 2. Change in maximum temperature and specific conductance of hot springs in The Breach of Mount St. Helens since 1984. Data from dates before 2002 are from Thompson (1990), Shevenell and Goff (1993), Goff and McMurtry (2000), and unpublished data from the U.S. Geological Survey.

Table 3. Water chemistry data from springs and creeks, 2002-2005, Mount St. Helens, Washington.

[Acidity (pH) and conductivity data in bold are from laboratory measurements, HCO_3 data in bold is determined on the basis of the measured amount of gas from the dissolved inorganic carbon extraction. Unless specified, all units are in parts per million. mS/cm, millisiemens per centimeter; --, no data. Additional chemical analyses are available in the digital appendix that accompanies electronic versions of this work.]

Sample No.	Date	Map No.	Temp. (°C)	pH	Cond (mS/cm)	B	Br	Ca	Cl	F	Fe	HCO_3	K	Li	Mg	Na	SiO_2	SO_4
Springs in Loowit canyon																		
MSH-02-01	08/16/02	4	58.9	6.4	2.6	4.9	0.56	55	310	2.3	3.5	727	44	0.74	24	474	186	330
MSH-02-02	08/17/02	6	61.0	6.3	2.7	5.7	0.61	62	330	2.2	4.0	769	46	0.82	28	497	196	360
MSH-02-03	08/17/02	7	62.3	6.3	2.8	5.9	0.61	68	340	2.2	3.9	844	46	0.83	28	515	197	360
MSH-02-04	08/18/02	8	57.6	6.5	2.8	5.6	0.59	68	350	2.6	2.3	779	45	0.75	31	508	184	360
MSH-05-02	07/26/05	3	59.1	--	2.6	6.0	0.44	67	281	2.5	4.0	--	47	0.94	36	511	196	400
MSH-05-03	07/26/05	3	57.0	**6.5**	3.0	5.9	0.44	66	280	2.6	4.2	761	46	0.90	35	495	191	399
MSH-05-04	07/26/05	5	61.9	**6.7**	3.4	6.7	0.48	69	291	2.4	4.3	807	48	1.01	37	521	205	395
MSH-05-05	07/26/05	5	60.5	--	2.7	6.5	0.48	72	288	2.4	3.3	--	48	1.00	38	512	201	392
Springs in Step canyon																		
MSH-05-07	07/26/05	14	56.6	**6.6**	2.4	5.7	0.32	67	217	1.3	4.7	752	30	0.95	49	375	190	235
MSH-05-06	07/26/05	16	45.1	**6.6**	1.9	4.3	0.24	73	171	1.2	7.7	706	22	0.74	50	271	162	171
MSH-05-22	10/25/05	14	38.4	**6.4**	2.2	5.7	0.36	66	241	1.9	17	--	21	0.84	57	316	166	249
Monitoring network sites																		
LCAF 042105	04/21/05	11	27.5	**8.5**	2.1	3.8	0.32	48	190	2.2	0.34	--	30	0.57	27	334	131	280
LCAF 063005	06/30/05	11	27.9	**8.6**	1.6	--	0.24	--	172	2.6	--	--	--	--	--	--	--	247
MSH-05-11	07/26/05	11	29.1	**8.8**	1.6	3.4	<0.003	54	172	2.2	1.1	487	27	0.52	24	287	123	247
LCAF 082605	08/26/05	11	30.1	**8.3**	1.6	2.9	0.28	32	169	2.3	0.29	--	24	0.46	20	248	105	236
LCAF 101105	10/11/05	11	30.0	**8.6**	1.9	--	0.32	--	197	2.3	--	--	--	--	--	--	--	273
MSH-05-24	10/25/05	9	25.9	**8.7**	1.8	3.5	0.32	55	193	2.5	0.85	**533**	28	0.54	24	304	130	268
LCBF 101304	10/13/04	21A	16.3	**8.5**	1.5	--	0.24	--	147	1.8	--	--	--	--	--	--	--	203
LCBF 102004	10/20/04	21A	10.2	**7.8**	1.6	2.9	0.30	15	151	2.2	<0.08	--	21	0.45	16	260	82	209
LCBF 120204	12/02/04	21A	8.4	**8.5**	1.8	--	0.24	--	167	2.0	--	--	--	--	--	--	--	234
LCBF 021005	02/10/05	21A	11.5	**8.6**	1.8	--	0.24	--	170	2.0	--	--	--	--	--	--	--	260
LCBF 042105	04/21/05	21A	16.9	**8.7**	1.9	3.7	0.32	31	180	2.1	0.48	--	28	0.56	24	312	121	270
LCBF 063005	06/30/05	21A	18.6	**8.7**	1.6	--	0.28	--	174	2.6	--	--	--	--	--	--	--	249
MSH-05-12	07/26/05	21A	22.5	8.9	1.6	3.5	0.26	45	167	2.2	0.47	--	27	0.53	24	291	123	244
LCBF 082605	08/26/05	21A	19.8	8.5	1.6	--	0.28	--	178	2.2	--	--	--	--	--	--	--	249
EFSCAF 042105	04/21/05	18	19.5	8.6	1.5	--	0.32	--	190	1.6	--	--	--	--	--	--	--	160
EFSCAF 063005	06/30/05	18	23.5	8.5	1.6	--	0.24	--	190	1.0	--	--	--	--	--	--	--	154
MSH-05-09	07/26/05	18	26.6	8.8	1.5	4.7	0.24	29	172	1.0	0.13	533	20	0.78	52	245	146	145
EFSCAF 082605	08/26/05	18	24.1	8.2	1.4	3.4	0.20	17	154	0.9	0.32	--	15	0.59	50	179	119	131
EFSCAF 101105	10/11/05	18	17.6	8.3	1.5	--	0.28	--	197	1.4	--	--	--	--	--	--	--	170

Table 3. Water chemistry data from springs and creeks, 2002-2005, Mount St. Helens, Washington.—Continued

[Acidity (pH) and conductivity data in bold are from laboratory measurements, HCO_3 data in bold is determined on the basis of the measured amount of gas from the dissolved inorganic carbon extraction. Unless specified, all units are in parts per million. mS/cm, millisiemens per centimeter; --, no data. Additional chemical analyses are available in the digital appendix that accompanies electronic versions of this work.]

Sample No.	Date	Map No.	Temp. (°C)	pH	Cond (mS/cm)	B	Br	Ca	Cl	F	Fe	HCO_3	K	Li	Mg	Na	SiO_2	SO_4
MSH-05-23	10/25/05	15	25.4	7.2	2.0	5.7	0.36	67	232	1.9	21	**787**	16	0.81	54	237	144	194
WFSCAF 042105	04/21/05	17	4.2	5.7	0.19	0.09	<0.003	12	47	2.2	0.0	--	0.90	0.01	6.0	6.5	19	6.5
WFSCAF 063005	06/30/05	17	6.6	5.7	0.09	--	0.01	--	20	3.2	--	--	--	--	--	--	--	2.5
MSH-05-10	07/26/05	17	10.5	5.8	0.06	0.03	<0.003	3.3	10	2.4	0.01	2.0	0.56	0.004	1.1	2.9	11	2.6
WFSCAF 082605	08/26/05	17	16.4	6.3	**0.05**	0.02	0.01	2.4	6	1.7	0.03	--	0.58	0.004	1.2	3.5	15	6.0
WFSCAF 101105	10/11/05	17	7.5	6.6	0.10	--	0.01	--	17	2.2	--	--	--	--	--	--	--	11
SCBF 101304	10/13/04	21B	14.5	8.5	0.79	--	0.100	--	84	0.9	--	--	--	--	--	--	--	84
SCBF 102004	10/20/04	21B	9.1	7.8	0.20	--	0.03	--	26	1.1	--	--	--	--	--	--	--	68
SCBF 120204	12/02/04	21B	4.1	8.5	1.0	2.6	0.14	31	94	1.3	0.10	--	8.6	0.39	24	135	65	118
SCBF 021005	02/10/05	21B	5.6	8.6	1.4	--	0.20	--	140	1.4	--	--	--	--	--	--	--	156
SCBF 063005	06/30/05	21B	14.5	7.9	0.34	--	0.06	--	48	3.0	--	--	--	--	--	--	--	28
MSH-05-13	07/26/05	21B	21.2	8.4	0.46	1.2	0.07	12	52	2.0	<0.04	--	5.6	0.20	13	69	44	44
SCBF 082605	08/26/05	21B	19.2	8.7	0.89	--	0.12	--	93	1.3	--	--	--	--	--	--	--	89
Other Loowit Creek locations																		
MSH-02-05	08/18/02	10	31.7	7.9	1.9	3.6	0.38	50	220	1.9	0.23	--	29	0.50	20	319	125	240
MSH-02-06	08/18/02	12	2.8	6.0	0.23	<0.02	0.004	23	1.3	1.4	0.62	92	3.4	0.03	6.3	12	39	39
MSH-05-01	07/26/05	13	7.7	**6.4**	0.08	0.04	0.010	7	16	2.3	0.02	4	0.54	0.005	2.0	3.3	17	2.0
Pumice Plain spring																		
CARB 081204	10/13/04	20	17.4	**7.8**	0.9	--	0.12	--	81	1.2	--	--	--	--	--	--	--	144
MSH-05-08	07/26/05	20	25.4	**7.3**	1.2	2.1	0.18	48	107	2.0	0.08	243	11	0.30	12	191	57	224
MSH-05-25	10/25/05	19	15.7	**7.4**	0.8	1.3	0.12	28	71	1.1	0.27	187	6.9	0.19	7.7	114	45	132
Regional cold springs																		
MSH-02-10	08/23/02	23	3.2	7.2	0.05	<0.02	0.003	3.5	1.0	0.1	0.01	25	0.73	0.004	1.2	4.6	22	1.9
MSH-05-15	07/29/05	22	4.4	5.7	0.04	0.004	<0.003	3.4	0.7	0.0	0.01	16	0.66	0.001	0.6	1.9	21	0.4
MSH-05-14	07/29/05	23	4.7	5.8	0.05	0.01	<0.003	3.6	1.1	0.1	0.01	28	0.74	0.006	1.2	4.9	24	1.9
MSH-05-17	07/30/05	24	3.0	8.2	0.08	0.01	<0.003	4.9	3.1	0.2	0.01	11	0.80	0.004	1.2	7.3	18	18
MSH-05-16	07/30/05	25	5.4	6.3	0.13	0.02	<0.003	13	1.4	0.2	<0.04	8	1.5	0.007	3.2	6.9	22	49
MSH-05-19	07/31/05	26	7.2	6.2	0.12	0.10	0.010	4.7	6.5	0.6	<0.04	54	1.8	0.048	2.6	18	43	8.5
MSH-05-18	07/31/05	27	6.3	6.5	0.09	0.08	<0.003	4.3	5.4	0.6	0.01	33	1.0	0.028	2.4	10	33	6.4
MSH-05-20	07/31/05	28	5.2	6.2	0.09	0.03	<0.003	7.0	2.1	0.2	<0.04	52	1.3	0.011	2.9	7.8	32	2.3

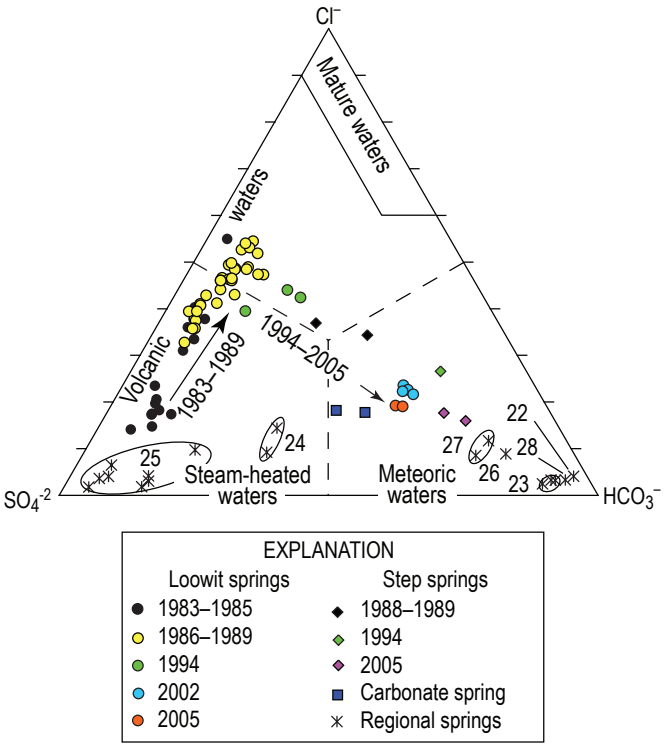

Figure 3. Ternary plot of anion proportion by mass for spring waters at or around Mount St. Helens, Washington (after Giggenbach, 1992). Arrows show change in major anions in Loowit springs since 1983 and Step springs since 1988. Data from dates before 2002 are from Thompson (1990), Shevenell and Goff (1993), Goff and McMurtry (2000), and unpublished data from the U.S. Geological Survey and Fraser Goff (University of New Mexico).

or the minor differences in the chemistry of the Loowit springs between 2002 and 2005 (table 3) to the current eruption.

Chemistry of the Regional Springs

All of the regional springs have temperatures <8°C and conductivities <150 µS/cm but can be divided into three groups based on variations in major anion concentrations (fig. 3; table 3). One group is defined by relatively high SO_4 concentrations, and the other groups are characterized as HCO_3-dominated waters but are subdivided on the basis of Cl concentrations.

The SO_4 waters consist of springs 24 and 25, which are north of Mount St. Helens on the eastern border of the Pumice Plain (fig. 1). Spring 25 has higher SO_4 concentrations than spring 24, and samples collected since 1988 show that anion compositions have been variable (fig. 3). In the late 1980s, SO_4-rich warm springs occurred in the cooling pyroclastic deposits of the Pumice Plain. Shevenell and Goff (1995) noted that these springs were not "steam-heated" waters, which are characteristically SO_4 rich, but instead probably were leaching SO_4 from $CaSO_4$ alteration minerals or from encrustations around the vents of short-lived fumaroles on the pyroclastic flows. Springs 24 and 25 are likely to be cold, dilute examples of this type of water.

The HCO_3-rich waters consist of springs 22, 23, and 28, which are solely HCO_3 waters, and springs 26 and 27, which have slightly elevated Cl in comparison with the other three springs (fig. 3; table 3). Springs 26 and 27 are southeast of Mount St. Helens and are of interest because (1) their anion chemistry lies along the dilution trend defined by the hot springs and (2) their ^{14}C values are greatly reduced relative to modern carbon (table 4), as discussed in more detail below. The elevated Cl in these springs may provide evidence for

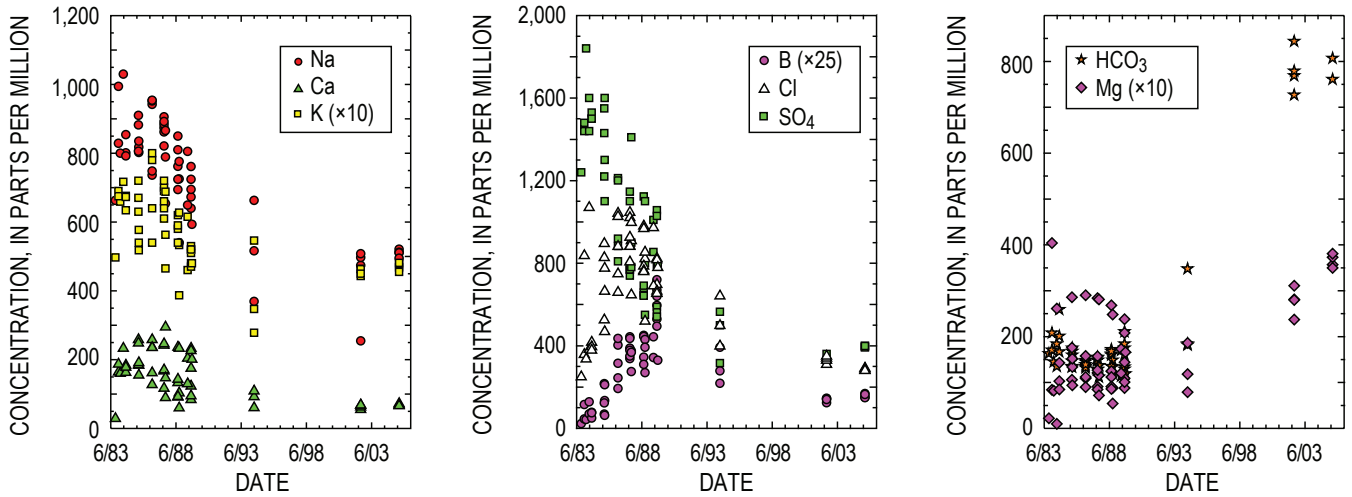

Figure 4. Chemistry of Loowit springs waters from 1983 to 2005, Mount St. Helens, Washington. Data from dates before 2002 are from Thompson (1990), Shevenell and Goff (1993), Goff and McMurtry (2000), and unpublished data (Fraser Goff, University of New Mexico).

some leakage of Loowit-type water through the southeastern wall of the crater.

Gas Transfer from Magma into Water

Gases released from magma can be variably dissolved into overlying cold water or released to a brine phase (Fournier, 1986) that can then mix with cold water. The resulting fluid is acidic, hot, and highly reactive with the surrounding rock. Mineral dissolution converts the acidic gas species H_2S, SO_2, HCl, and CO_2 into the anions SO_4, Cl, and HCO_3. The concentration of these anions in the spring waters can be related back to magmatic degassing only if the effects of variable gas solution and mineral dissolution/precipitation are constrained. Some constraints can be derived from the water chemistry.

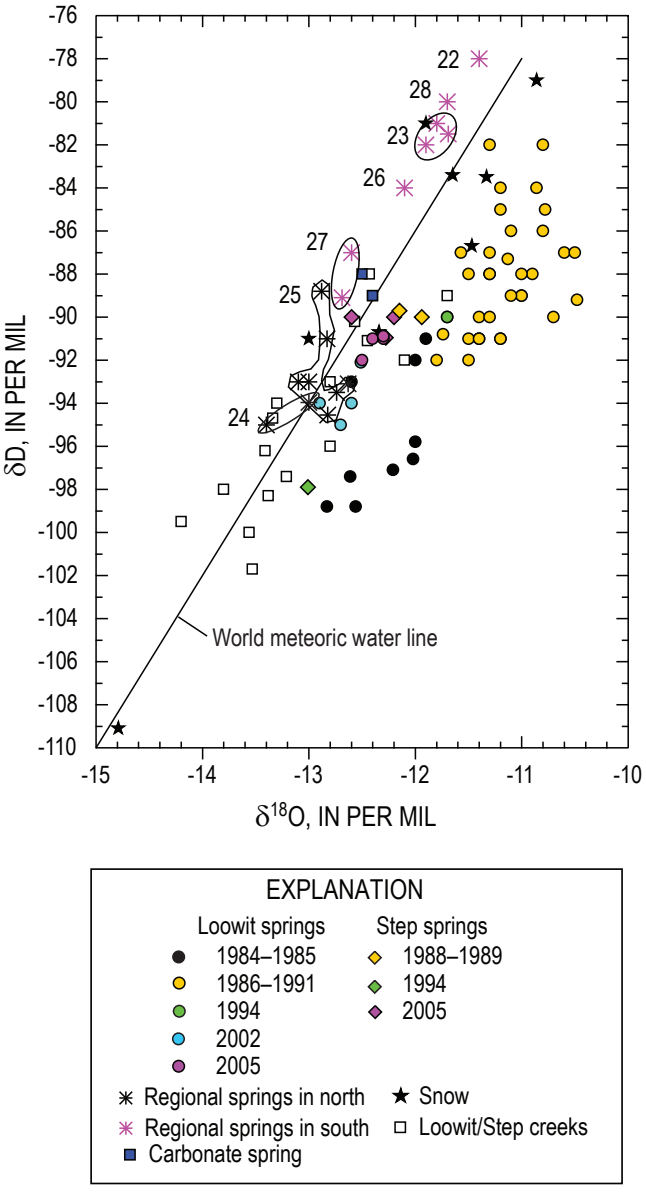

Figure 5. Stable-isotope composition of Loowit springs since 1980s, Mount St. Helens, Washington. Data from dates before 2002 are from Thompson (1990), Shevenell and Goff (1993, 1995), Goff and McMurtry (2000), and unpublished data from the U.S. Geological Survey.

Many metallic ions (such as Ca) are not transported in volatile form (Symonds and others, 1993), requiring that the major source of the cations in the springs be water-rock interaction. This process could ultimately remove SO_4 and HCO_3 from solution via precipitation. Attempts at geothermometry by Shevenell and Goff (1993; 1995) yielded maximum temperatures between 120˚C and 175˚C for the Loowit waters. For an assumed temperature of 150˚C, calculations using SOLMNEQ88 (Kharaka and others, 1988) indicate saturation with anhydrite for waters collected in the 1980s but undersaturation for samples from 2002 and 2005. From the 1980s through 2005, Ca, Na, K, and SO_4 in the spring waters all show similar patterns of decline that are consistent with dilution (fig. 4), so there is no evidence that anhydrite was ever a significant control on SO_4 concentrations. Samples from all collection years are saturated with calcite at all temperatures above the discharge temperature. Calcite formation/dissolution may exert some influence on Ca and HCO_3. However, the large increase in HCO_3 after the 1980s cannot be attributed to calcite dissolution, which would also produce both higher Ca concentrations and higher pH values. Ca and pH have in fact dropped during this time (table 3).

Shevenell and Goff (2000) argued that halite formation in the magmatic fluid component was probably not a significant sink for Cl. Although Br and Cl concentrations in the springs have declined steadily over the years, it is noteworthy that for the past two decades the ratios of these two components have remained at a remarkably constant value around 0.002 (1984–2005, 44 samples, ± 0.001). The Step canyon springs and carbonate spring have lower concentrations of Br and Cl than the Loowit springs but fall along the same trend (fig. 6). The constant Cl/Br ratio shows that halite was never a major control on Cl in fluid sources to the hot springs.

In contrast, fumarole condensates have shown a large range in Cl/Br (fig. 6), possibly indicating that deposition of metal halides in the vent throats (Keith and others, 1981; Edmonds and others, this volume, chap. 27) can be a significant control on fumarolic Cl/Br ratios. The Cl/Br ratio in the springs, which lies within the range of the fumarolic condensates, may better represent the HCl/HBr ratio in gases released from magma. Additional Cl and Br could be leached from the volcanic rocks. Reported Br and Cl ratios in seven samples of andesite and dacite from the crater, The Breach, and Pumice Plain are variable, ranging between 0.002 and 0.01 (table 1 of Shevenell and Goff, 1993). However, the SO_4-rich nature of the transient hot springs in the Pumice Plain (Shevenell and Goff, 1995) indicates that rock leaching is not a major source of halides.

Overall, the data indicate that mineral sources and sinks for SO_4, Cl, and HCO_3 are not the main controls on the anions

Table 4. Isotope values determined for water samples collected during 2002–2005, Mount St. Helens, Washington.

[DIC, dissolved inorganic carbon; --, no data.]

Sample No.	Date	Map No.	Temperature (°C)	δD per mil	$\delta^{18}O$ per mil	$\delta^{13}C$-DIC per mil	^{14}C-DIC percent modern carbon
Springs in Loowit canyon							
MSH-02-01	08/16/02	4	58.9	-94	-12.9	-12.3	--
MSH-02-02	08/17/02	6	61.0	-95	-12.7	--	--
MSH-02-03	08/17/02	7	62.3	-94	-12.6	-12.2	--
MSH-02-04	08/18/02	8	57.6	-92	-12.5	-11.9	--
MSH-05-02	07/26/05	3	59.1	-91	-12.4	--	--
MSH-05-03	07/26/05	3	57.0	-92	-12.5	-12.1	--
MSH-05-04	07/26/05	5	61.9	-91	-12.3	-11.9	--
MSH-05-05	07/26/05	5	60.5	-91	-12.3	--	--
Springs in Step canyon							
MSH-05-06	07/26/05	16	45.1	-90	-12.6	-11.4	--
MSH-05-07	07/26/05	14	56.6	-91	-12.3	-10.9	--
MSH-05-22	10/25/05	14	38.4	-90	-12.2	--	--
Monitoring network sites							
MSH-05-23	10/25/05	15	25.4	-92	-12.1	-7.5	--
MSH-05-24	10/25/05	9	25.9	-89	-12.4	-8.1	--
Other Loowit Creek locations							
MSH-02-06	08/18/02	12	2.8	-98	-13.8	-11.2	--
MSH-05-01	07/26/05	13	7.7	-93	-12.8	--	--
Pumice Plain spring							
MSH-05-08	07/26/05	20	25.4	-89	-12.4	-11.5	5.5
MSH-05-25	10/25/05	19	15.7	-88	-12.5	--	--
Regional cold springs							
MSH-05-15	07/29/05	22	4.4	-78	-11.4	--	--
MSH-02-10	08/23/02	23	3.2	-82	-11.9	-14.2	93.8
MSH-05-14	07/29/05	23	4.7	-81	-11.8	-15.6	--
MSH-05-17	07/30/05	24	3.0	-95	-13.4	--	--
MSH-05-16	07/30/05	25	5.4	-93	-13.0	--	--
MSH-05-19	07/31/05	26	7.2	-84	-12.1	-16.5	50.0
MSH-05-18	07/31/05	27	6.3	-87	-12.6	-16.0	54.8
MSH-05-20	07/31/05	28	5.2	-80	-11.7	-15.9	53.1

in the hot springs. We conclude that the changing anion proportions shown in figure 3 reflect changes in the release rates of sulfur gases, HCl, and CO_2 from the magma and a varying degree of efficiency of gas scrubbing by the overlying water.

The 1983–89 trend in Loowit waters from SO_4 toward Cl (fig. 3) can be explained by the cessation in the supply of magma at the end of the 1980–86 dome-building eruptions. With declining output of sulfur gas from magma, less sulfur was available to be scrubbed into overlying meteoric water. The simultaneous increase in Cl can be attributed to crystallization of extruded and shallowly emplaced magma, with degassing of HCl or partitioning of Cl into an aqueous phase that then mixed with meteoric water. The ensuing trend toward HCO_3 dominance after 1989 (fig. 3) would logically be attributed to continuing declines in the supply of S and Cl as cooling and crystallization of the 1980–86 dome and shallow underlying magma progressed toward completion; CO_2, due to its low solubility even at high pressure, continued to exsolve from magma at greater depths. This scheme does not explain the large increase in HCO_3 concentrations in Loowit springs (fig. 4; table 3). Coupled with the drop in pH, the rise in HCO_3 concentrations between 1989 and 2002 represents an order-of-magnitude jump in DIC, an event of particular interest because it could indicate the ascent of fresh, CO_2-rich magma from depth beneath the chamber, leading up to the renewal of eruptive activity in 2004.

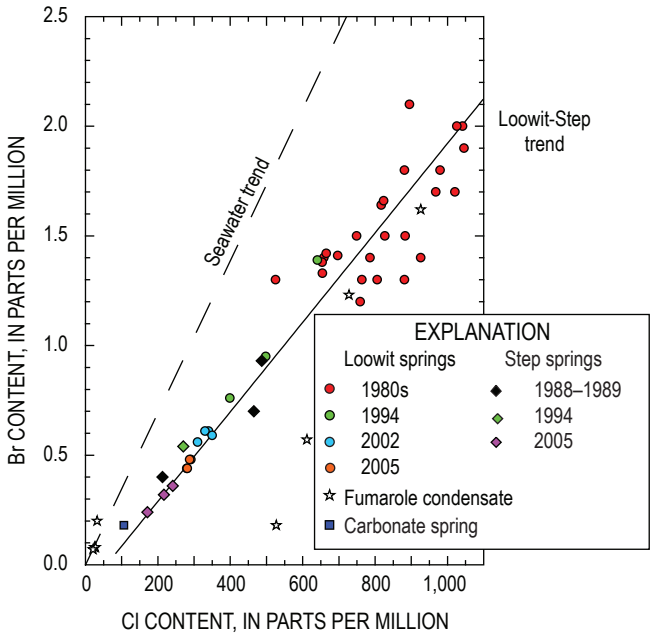

Figure 6. Trends in Br and Cl concentrations for 2002–2005 spring waters, compared with early data from springs and fumarole condensates from the 1980–86 dome at Mount St. Helens, Washington. One 1989 fumarole condensate sample that plots off the scale is not shown. Data from fumarole condensates and waters before 2002 are from Shevenell and Goff (1993, 2000), Goff and McMurtry (2000), and unpublished data (Fraser Goff, University of New Mexico).

However, the HCO_3 increase seems to have begun by 1994 (fig. 4), and carbon isotope data (discussed below) do not indicate CO_2 release from a new source of magma.

By 2002, the molar C:S:Cl ratio in Loowit waters had shifted from ~1:3:8 in the late 1980s to 10:1.4:3.6. This ratio is much closer to the 10:1.1:1.2 ratio measured in plume emissions by various techniques in 2005 (Gerlach and others, 2005; Edmonds and others, this volume, chap. 27). Our preferred explanation for the shift in the ratios is that for many years after dome emplacement in the 1980s, temperatures above boiling in the rocks of the 1980–86 dome prevented shallow waters from completely sealing off escape pathways for gas. Highly soluble HCl and SO_2 were effectively scrubbed by infiltrating water, but the CO_2 was still largely able to escape due to its much lower solubility. Once gas pathways were mostly blocked by liquid water, presumably after 1994, CO_2 scrubbing became efficient, and dissolved C:S:Cl ratios approached those of degassing magma. Note that the timeframe for these changes in chemistry is in fair agreement with the estimate that the 1980–86 dome would cool through its magnetization temperature in 18–36 years after emplacement (Dzurisin and others, 1990).

Carbon and Helium Isotope Evidence on Magmatic End Members

Gas from the Crater and The Breach

In spite of declining fumarole temperatures and the increasing amount of air in gases venting in the crater at Mount St. Helens, the carbon and helium isotopic compositions give evidence of a prolonged magmatic input. Gas collected in November 1980 from a >400°C fumarole near the dome provided the most representative $\delta^{13}C$–CO_2 value for the early magma at Mount St. Helens, −10.5 per mil (Evans and others, 1981; table 5). Over time the carbon isotope composition of CO_2 in fumarole gases shifted to lighter values (fig. 7*A*). The shift cannot be related to the increased air concentrations because the $\delta^{13}C$ value of atmospheric CO_2 is around −7 per mil (Faure, 1986). Since 1994 CO_2 concentrations in gases from the 1980–86 dome have declined, but $\delta^{13}C$–CO_2 values have stabilized (fig. 7). In June 1994, gas from a 560°C fumarole and other lower temperature fumaroles on the dome contained about 32 percent CO_2 and had $\delta^{13}C$ values between −11.7 and −12.0 per mil (Goff and McMurtry, 2000; F. Goff, unpub. data, 1994). In 1998, gas samples collected from an 86°C vent on September lobe contained 5 percent CO_2 with a $\delta^{13}C$ value of −11.9 per mil (Symonds and others, 2003; table 5), and gas samples collected from vents on September lobe in 2002 had less than 3 percent CO_2 with $\delta^{13}C$ values between −12.0 and −11.8 per mil (table 5).

Gas from the bubbling springs in 2002 and 2005 contained mostly CO_2 but also had considerable N_2 and Ar (table 5). The N_2/Ar ratio in the gas falls between the ratios for air and air-saturated meteoric water, but low O_2 values show that

direct air contamination was not a factor. The R/R_A values for $^3He/^4He$ ratios in the gas were 5.5 and 5.8, respectively, similar to a 1989 hot spring water sample that had a value of 5.7 (Goff and McMurtry, 2000). The $\delta^{13}C$ value for the CO_2 in both years was −14.7 per mil, significantly lower than the isotopic composition of CO_2 in the vent gases. Analysis of the 2002 bubbling gas indicates that it is essentially ^{14}C dead, ruling out any significant biogenic CO_2 source (table 5; figs. 7*A*, 7*B*). An important consideration is that equilibrium fractionation processes call for lower $\delta^{13}C$ values in the gas-bubble CO_2, relative to the DIC, consisting of HCO_3 and dissolved CO_2.

Dissolved Inorganic Carbon in Spring Waters

The carbon isotope composition of DIC from the springs in Loowit and Step canyons and carbonate spring has a small range in values that is independent of water temperature (fig. 7*A*). The $\delta^{13}C$–DIC values in all these springs are similar to the $\delta^{13}C$ composition of fumarolic CO_2 from recent years but are lower than the 1980 fumarolic $\delta^{13}C$–CO_2 values. The $\delta^{13}C$–DIC data thus provide additional evidence for a change in the $\delta^{13}C$ of the CO_2 released from the underlying magma. This carbon isotope shift to lower values since 1980 is most easily attributed to fractional loss of ^{13}C-enriched CO_2 during degassing of the magma (Gerlach and Taylor, 1990) and is a strong argument against the involvement of fresh magma. A new pulse of gas-rich magma from great depth would likely cause a return toward heavier $\delta^{13}C$ values in gas vents and DIC, and a new pulse of basalt from mantle depths might bring an increase in $^3He/^4He$ ratios.

The regional springs have much lower HCO_3 concentrations than springs in the crater and The Breach and have lower $\delta^{13}C$–DIC values (tables 3, 4). The ^{14}C content of the DIC in springs 26, 27, and 28 contains about 50 percent modern carbon, and the ^{13}C–^{14}C isotope values fall on a mixing line between typical biogenic carbon and magmatic carbon in the dome vents and hot springs (fig. 7*B*). Springs 26, 27, and 28

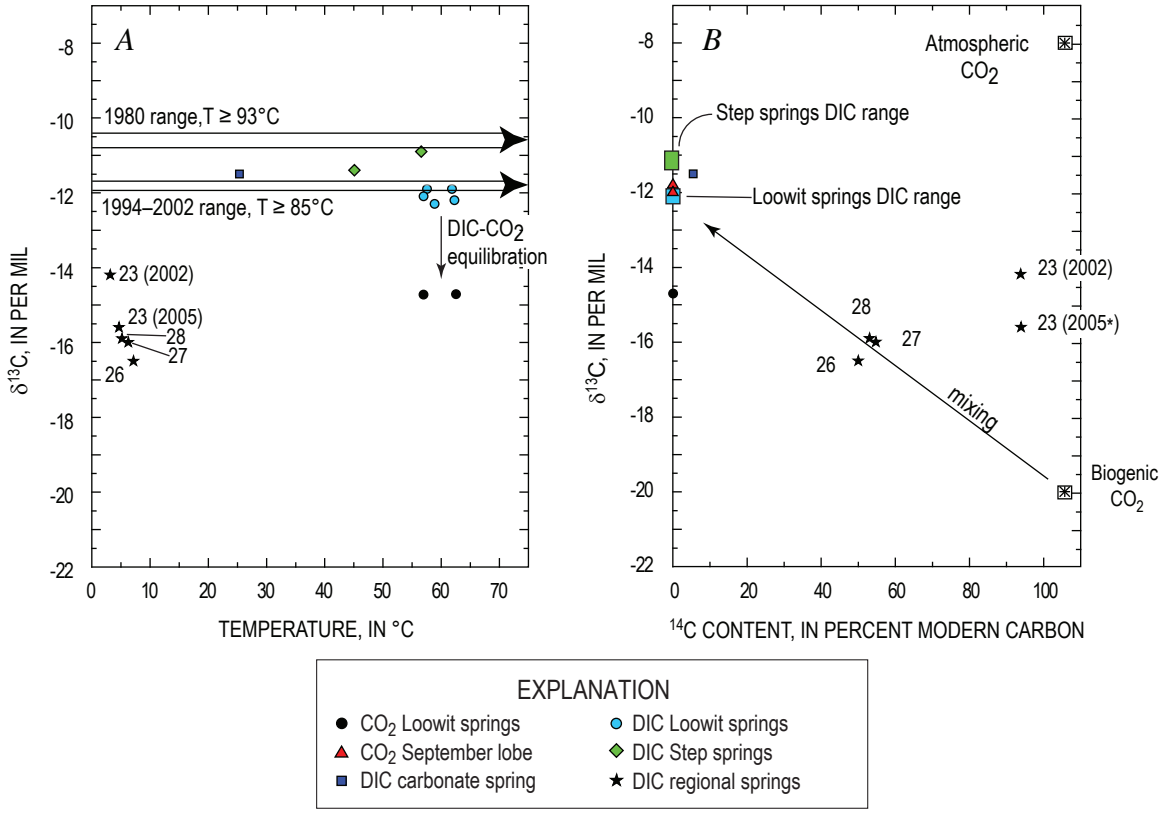

Figure 7. Water temperatures and carbon isotope compositions of dissolved inorganic carbon (DIC) and CO_2 from vents and springs at and around Mount St. Helens, Washington 1980–2005. *A*, $\delta^{13}C$–DIC values for hot and cold springs from this study compared to CO_2 gas collected from the 1980–86 dome. Horizontal arrows represent the range in $\delta^{13}C$–CO_2 values reported for 1980s dome gas samples from Evans (1981), Goff and McMurtry (2000), Symonds and others (2003), and this study. *B*, Comparison of $\delta^{13}C$–DIC and ^{14}C–DIC values for some regional cold springs with values of DIC and CO_2 from hot springs and atmospheric and biogenically derived CO_2. ^{14}C values for DIC in Loowit and Step springs and CO_2 from the September lobe are assumed to be zero. The 2005 analysis of sample 23, shown with asterisk, lacks a ^{14}C–DIC value, so it is arbitrarily assigned the 2002 analytical value, for purposes of plotting the $\delta^{13}C$ results.

Table 5. Chemical and isotopic results from gas analyses, 1980–2005, Mount St. Helens, Washington.

[Concentrations are reported as volume percent; --, no data; R/R_A, the $^3He/^4He$ ratio in the gas relative to the $^3He/^4He$ ratio in air.]

Sample No.	Date	Map No.	Temp. (°C)	He	H_2	Ar	O_2	N_2	CH_4	CO_2	C_2H_6	H_2S	CO	SO_2	N_2 / Ar	$\delta^{13}C$–CO_2 (‰)	$^3He/^4He$ $(R/R)_A$
Dome gas, 1980s dome																	
CQ244IB80 [1]	11/04/80	--	>400	<0.005	8.61	<0.02	0.03	1.6	<0.0002	86.6	<0.01	2.09	0.57	0.84	na	-10.5	--
981214 [2]	06/29/98	--	86	0.0005	0.0014	0.94	19.4	74.5	<0.0002	5.2	<0.0002	<0.0005	<0.001	--	79.1	-11.9	--
MSH-02-08 [3]	08/22/02	2	≥ 86	0.0005	0.0008	0.89	20.6	77.0	<0.0002	1.5	<0.0002	<0.0005	<0.001	--	86.2	-11.8	--
MSH-02-09 [3]	08/22/02	1	≥ 85	0.0006	0.0002	0.90	20.4	76.2	<0.0002	2.4	<0.0002	<0.0005	<0.001	--	84.4	-12.0	--
Hot spring gas, spring in Loowit canyon																	
MSH-02-03 [4]	08/17/02	7	62.3	0.0012	<0.0002	0.26	0.88	18.6	0.06	80.2	<0.0002	<0.0005	<0.001	--	72.4	-14.7	5.5
MSH-05-03	07/26/05	3	57.0	0.0019	0.0003	0.34	<0.0005	23.3	0.05	76.3	<0.0002	0.0026	<0.001	--	69.2	-14.7	5.8

[1] 1980 sample collected from crack near 1980 dome by W.C. Evans, from Evans and others (1981).

[2] 1998 sample collected from September lobe by R. Symonds; ^{13}C–CO_2 from Symonds and others (2003).

[3] Collected from September lobe.

[4] Value for ^{14}C–CO_2 equals 0.07 (percent modern carbon).

may contain some magmatic carbon, and the Cl concentrations in springs 26 and 27 support this idea. The DIC in spring 23 contains 94 percent modern carbon, and two samples from different years had variable $\delta^{13}C$ values that are higher than the other regional springs. The variation in the ^{13}C composition may indicate that some CO_2 degassing occurs from the water prior to its point of emergence. A small magmatic component in the spring is possible, but without additional study (for example, He isotopes), we cannot eliminate the possibility that the dead carbon in all four of these springs is derived from Tertiary-age hydrothermal carbonate in the volcanic rocks that underlie the edifice of Mount St. Helens (Evarts and others, 1987).

Total Discharges of Water, Heat, and Magmatic Volatiles

Creek-Water Discharge

During the course of this investigation, the measured surface discharge from Loowit Creek was about three to six times greater than the discharge from Step creek (table 2). Maximum seasonal discharge at the monitoring sites occurred in the midsummer to fall months. There are no historical data on discharge at Step creek, but measurements at LCAF show that flow rates have increased since 1989 (fig. 8; tables 2 and 6). The increase does not reflect variations in annual precipitation and more likely results from increased input of meltwater as Crater Glacier grew from a persistent snow bank in the shadow of the crater rim to an area of about 1 km^2 by September 2001 (Schilling and others, 2004).

Since October 2004, the emplacement of the new lava dome at Mount St. Helens resulted in extensive deformation of Crater Glacier and a concomitant decrease in the volume of glacial ice, without any large change in the surface flows of the creeks, indicating that some meltwater may exit the crater from leakage through the crater floor (Major and others, 2005; Walder and others, 2007; Walder and others, this volume, chap. 13). A complete hydrologic budget to address this idea has yet to be developed for Mount St. Helens and, until such time, our multiple measurements of stream flow and chemistry for Loowit and Step creeks (table 7) offer the most comprehensive picture of discharge and dissolved fluxes from the crater area.

Two major contributors to conductivity in the creek waters are Cl and SO_4 (fig. 9*A*). During the course of our investigation at both of the Loowit Creek monitoring sites, Cl/SO_4 ratios were essentially constant and mimicked ratios in Loowit springs in 2005 (fig. 9*B*). In contrast, Step creek waters show large variations in Cl to SO_4, which can be attributed directly to changes in the chemistry and discharge of water from WFSCAF. Combining the average flows of Loowit Creek and the east fork of Step creek yields a total thermal water discharge of 335 L/s with an average Cl concentration of 180 mg/L (table 7). The creek waters are composed primarily of meteoric water from melting ice and snow plus water from the

Table 6. Discharge measurements and meter information for Loowit Creek above the falls, 1985–98, Mount St. Helens, Washington.

Date	Discharge (L/s)	Meter type
08/15/85	161	Price AA meter
09/09/85	197	Price AA meter
08/09/88	195	Gurley meter
08/10/89	213	Gurley meter
09/14/89	220	Price AA meter
09/14/89	197	Price AA meter
10/16/89	116	Pygmy meter
01/17/90	109	Pygmy meter
08/24/90	132	Pygmy meter
09/20/90	126	Pygmy meter
10/23/90	109	Pygmy meter
12/07/90	117	Pygmy meter
02/08/91	144	Pygmy meter
05/01/92	161	Pygmy meter
07/28/92	160	Pygmy meter
07/28/92	144	Pygmy meter
05/05/93	118	Pygmy meter
07/07/94	212	Pygmy meter
09/01/98	248	Pygmy meter

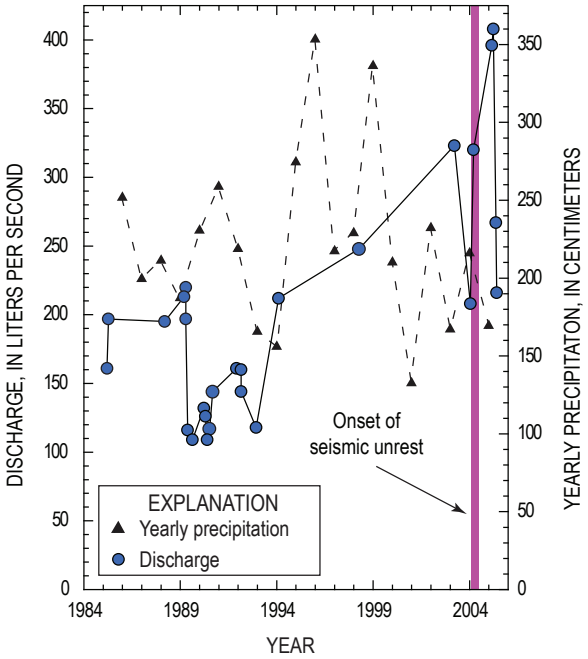

Figure 8. Discharge at site LCAF from 1985 to 2005 and yearly precipitation totals from the SNOTEL station at Spirit Lake, Mount St. Helens, Washington, from 1986 to 2005. Ticks on x axis correspond to month of June. Data from August 1988 and 1989 are from Shevenell (1990).

Table 7. Selected chemistry and discharge measurements for monitoring sites and some springs, 1988–2005, Mount St. Helens, Washington.

[CO_2 t/d, metric tons per day, calculated as CO_2 from measured HCO_3 flux; CO_2 mag., the corrected magmatic flux of CO_2 in metric tons per day based on measured spring pH values (see text); mS/cm, millisiemens per centimeter; ps, probe site; LCAF, Loowit Creek above falls; LCBF, Loowit Creek below falls; EFSCAF, east fork Step creek above falls; WFSCAF, west fork Step creek above falls; SCBF. Step creek below falls; CARB gs, carbonate spring gage site. Data from 1988 and 1989 are from Shevenell (1990). The ^{14}C data in bold were collected at a different time from the time the discharge was measured.]

Sample No.	Location	Date	Temp. (°C)	Conductivity (mS/cm)	Discharge (L/s)	^{14}C (% modern carbon)	HCO_3 (mg/L)	CO_2 (t/d)	CO_2 (mag. t/d)	Cl (mg/L)	SO_4 (mg/L)	Cl (t/d)	SO_4 (t/d)
Monitoring network sites													
MSH-05-11	LCAF	07/26/05	29.1	1.63	396		488	12.1	24	172	247	5.9	8.5
LCAF 082605	LCAF	08/26/05	30.1	1.61	408	--	--	--	--	169	236	5.9	8.3
LCAF 101105	LCAF	10/11/05	30.0	1.94	267	--	--	--	--	197	273	4.5	6.3
MSH-05-24	LCAF ps	10/25/05	25.9	1.83	215	--	533	7.1	14	193	268	3.6	5.0
LCBF 101304	LCBF	10/13/04	16.3	1.49	306	--	--	--	--	147	203	3.9	5.4
LCBF 042105	LCBF	04/21/05	16.9	1.87	187	--	--	--	--	180	270	2.9	4.4
MSH-05-12	LCBF	07/26/05	22.5	1.56	399	--	--	--	--	167	244	5.7	8.4
LCBF 082605	LCBF	08/26/05	19.8	1.63	279	--	--	--	--	178	249	4.3	6.0
Average flux									**19.0**			**4.6**	**6.5**
MSH-05-09	EFSCAF	07/26/05	26.6	1.45	45	--	535	1.5	3	172	145	0.7	0.6
EFSCAF 101105	EFSCAF	10/11/05	17.6	1.52	19	--	--	--	--	197	170	0.3	0.3
MSH-05-23	EFSCAF ps	10/25/05	25.4	1.96	27	--	787	1.3	2.6	232	194	0.5	0.5
Average flux									**2.8**			**0.5**	**0.4**
MSH-05-10	WFSCAF	07/26/05	10.5	0.06	142	--	12	0.1	0.1	10	3	0.1	0.03
SCBF 101304	SCBF	10/13/04	14.5	0.79	112	--	--	--	--	84	84	0.8	0.8
SCBF 082605	SCBF	08/26/05	19.2	0.89	49	--	--	--	--	93	89	0.4	0.4
MSH-05-13	SCBF	07/26/05	21.2	0.46	110	--	--	--	--	52	44	0.5	0.4
Average flux												**0.6**	**0.5**
Pumice Plain spring													
MSH-05-25	CARB gs	10/25/05	15.7	0.80	354	**5.5**	204	4.5	4.3	71	132	2.2	4.0
Regional cold springs													
MSH-05-14	#23	07/29/05	4.7	0.05	818	**93.8**	29	1.5	0.16	--	--	--	--
MSH-05-18 (nr)	#27	07/31/05	6.3	0.08	82	54.8	44	0.2	0.11	--	--	--	--
MSH-05-19	nr #26	07/31/05	7.2	0.12	137	50.0	94	0.8	0.42	--	--	--	--
MSH-05-20	#28	07/31/05	5.2	0.09	29	53.1	73	0.1	0.07	--	--	--	--
Loowit Creek above falls, 1988 and 1989													
SH-45	LCAF	08/09/88	41.0	3.36	195	--	87	1.1	1.1	600	567	10.1	9.6
SH-81	LCAF	08/10/89	41.6	3.02	213	--	88	1.2	1.2	549	507	10.1	9.3
Average flux									**1.1**			**10.1**	**9.4**

hot springs, and we can normalize the creek data to a source spring fluid with 280 mg/L by assuming that the meteoric water has no Cl (table 3). This calculation yields total water outputs of 215 L/s for the Loowit and Step springs. By using the density and enthalpy of water at 56°C, the heat output is ~50 MW. For perspective, a heat output of 50 MW would completely cool the 1980–86 dome in about 125 years.

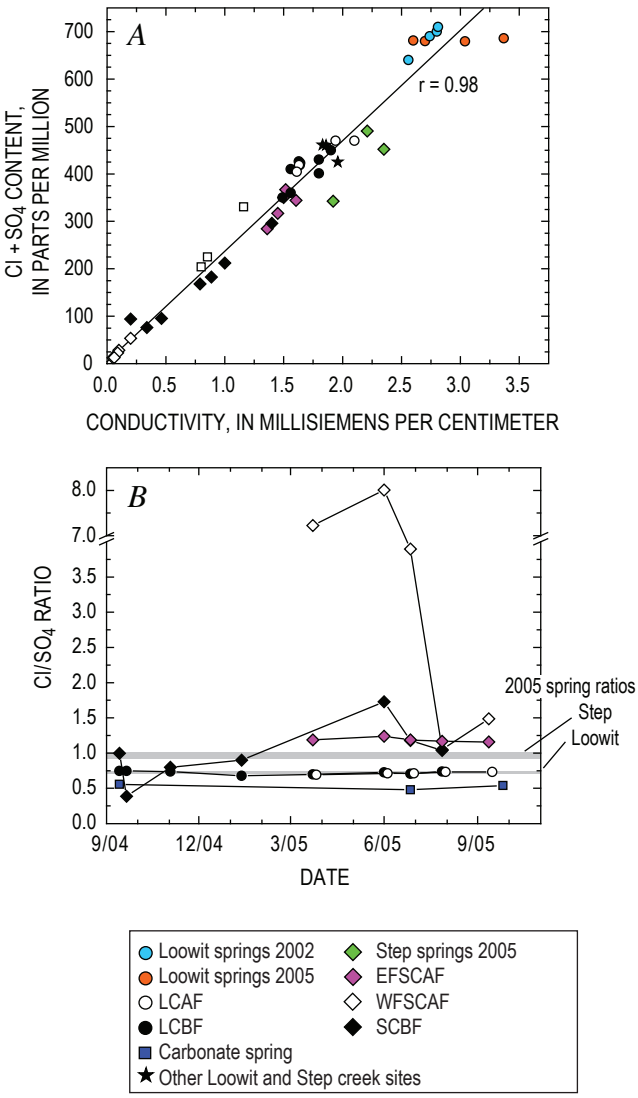

Figure 9. Cl and SO_4 concentrations for Loowit spring waters since 2002 and the creek-monitoring sites since October 2004, Mount St. Helens, Washington. *A*, Cl and SO_4 are major anions controlling conductivity in creek waters. *B*, Temporal plot showing Cl/SO_4 ratios at the monitoring sites. Loowit Creek sites show no change during the first year after the start of the 2004–5 eruption. Sites SCBF and WFSCAF show change in Cl and SO_4 ratios. Gray bars represent range in Cl and SO_4 for Loowit canyon and Step canyon springs in 2005. The LCAF site plot is shifted slightly so data can be shown.

Present-Day Flux of Magmatic Volatiles

Assuming that all of the dissolved carbon in the hot springs is derived from the underlying magma, we can couple the DIC concentration and the discharge to provide an estimate of the magmatic carbon flux. Table 7 shows six datasets for dates when a DIC sample was collected from a monitoring site concurrent with a discharge measurement. The largest flux measured was 12 metric tons per day (t/d), expressed as CO_2, from LCAF in July 2005. On the same day, another 1.5 t/d (as CO_2) discharged from EFSCAF. Measured pH values show that the DIC in Step and Loowit springs consists of approximately equal proportions of dissolved CO_2 and HCO_3, but nearly all of the dissolved CO_2 is outgassed upstream of the monitoring sites. The total output of magmatic carbon from the springs would, therefore, be double the amounts noted above. We did not gage carbonate spring in July 2005, but in October 2005 its magmatic CO_2 flux was 4.3 t/d. That value is adjusted for a small modern, nonmagmatic carbon contribution indicated by the ^{14}C value using mass balance, assuming the modern DIC component contains 105 percent modern carbon (James and others, 1999). Any potential flux of magmatic CO_2 from WFSCAF or the regional springs is less than 1 t/d.

We also estimated Cl and SO_4 fluxes for the creeks using the same methods. Apart from carbonate spring, which may have some nonmagmatic sources of Cl and SO_4, the data in table 7 show that the Loowit Creek sites are the main contributors of Cl and SO_4. Together, the Loowit and Step creeks yield average Cl and SO_4 fluxes of 5.2 t/d (expressed as HCl) and 4.7 t/d (expressed as SO_2) and, adjusting the DIC as discussed above, 22 t/d of CO_2. These data provide a first look at the flux of magmatic components dissolved in the waters at Mount St. Helens. For comparison, HCl and SO_2 fluxes in plume emissions on August 31, 2005, were 14 and 22 t/d, respectively (Edmonds and others, this volume, chap. 27), whereas CO_2 in the crater-plume emissions during the course of the 2004–6 eruption were in hundreds of tons per day (Doukas and others, 2005; Gerlach and others, this volume, chap. 26), and CO_2 emissions from the plume coming off Loowit springs were 27 t/d on June 9, 2005 (Gerlach and others, this volume, chap. 26).

Flux of Magmatic Volatiles 1988–1989

Estimates similar to those made for the 2004–5 data can be made for the flux of magmatic volatiles at LCAF in the late 1980s by using data from Shevenell (1990). Tables 2 and 7 show that the discharge at LCAF in August 1988 and 1989 was roughly 60 percent of the flow measured in the months of July and August 2003–5. In spite of lower discharges of creek water in the late 1980s, dissolved SO_4 and Cl fluxes were 1.4 and 2.2 times higher, respectively, than fluxes in 2004–5 (table 7). The dissolved magmatic CO_2 flux in 1988–89, however, was only 1.1 t/d, in comparison with 19 t/d from this study (table 7). Because the pH of the springs was about 7.2, we made no correction for outgassing of CO_2.

Conclusions

Data from springs and gas discharges in the crater are consistent with plume emission rates (Doukas and others, 2005; Gerlach and others, this volume, chap. 26) that indicate the current eruption is driven by degassed magma. From the early 1980s to 2002, gas vents on the 1980–86 dome grew weaker and more air-dominated, while magmatic Cl and SO_4 inputs to the Loowit springs declined, and the isotopic signal (D and ^{18}O) from magmatic water input disappeared. The large DIC increase in Loowit springs over time could indicate a pulse of new magma, but the $\delta^{13}C$ signatures of the DIC and of CO_2 gas are consistent with degassing of residual magma emplaced in the 1980s. No significant changes in Loowit springs occurred between 2002 and 2005. However, we note that the time for water to flow from the new dome to the spring vents could exceed one year, the time between the onset of unrest and the latest water sampling, so some caution must be applied to interpretations of the Loowit data. Carbon and helium isotope data for gas from the new dome might be more compelling but are unavailable.

Hot or mineralized springs occur on many volcanoes that lack summit plumes or obvious fumaroles and, in these cases, may provide the only opportunity to look for magmatic gases released at depth. The similarity in C:S:Cl ratios of recent Loowit springs samples and the 2005 plume emissions strongly supports the idea that spring geochemistry can accurately reflect magmatic degassing under favorable conditions. In this context, it is important to continue tracking the chemistry of the Mount St. Helens springs during the next few years in a search for responses to the current eruption.

Acknowledgments

We wish to thank several individuals who contributed to our research. Fraser Goff (Earth and Planetary Sciences Dept., Univ. of New Mexico) provided previously unpublished data from his work at Mount St. Helens. Helpful reviews were provided by Fraser Goff and Jon Major (USGS, Cascades Volcano Observatory). Peter Frenzen, the monument scientist at the Mount St. Helens National Volcanic Monument (USDA-Forest Service), provided logistical support and invaluable advice for several of our field campaigns. Student volunteers and interns Bryn Kimball (2002), Taryn López (2005), and Leif Rasmuson (2005) helped with sampling and stream gaging.

References Cited

Chiodini, G., Frondini, F., Cardellini, C., Parello, F., and Peruzzi, L., 2000, Rates of diffuse carbon dioxide Earth degassing estimated from carbon balance of regional aquifers—the case of central Apennine, Italy: Journal of Geophysical Research, v. 105, no. B4, p. 8423–8434.

Coplen, T.B., 1973, A double focusing, double collecting mass spectrometer for light stable isotope ratio analysis: International Journal of Mass Spectrometry and Ion Physics, v. 11, p. 37–40.

Coplen, T.B., Wildman, J.D., and Chen, J., 1991, Improvements in the gaseous hydrogen-water equilibration technique for hydrogen isotope-ratio analysis: Analytical Chemistry, v. 63, p. 910–912.

Doukas, M.P., McGee, K.A., and Gerlach, T.M., 2005, Airborne measurement of CO_2, SO_2, and H_2S emissions rates during the 2004–2005 eruption of Mount St. Helens [abs.]: Eos (American Geophysical Union Transactions), v. 86, no. 52, Fall Meet. Suppl., Abstract V53D-1590.

Dzurisin, D., Denlinger, R.P., and Rosenbaum, J.G., 1990, Cooling rate and thermal structure determined from progressive magnetization of the dacite dome at Mount St. Helens, Washington: Journal of Geophysical Research, v. 95, no. B3, p. 2763–2780.

Edmonds, M., McGee, K.A., and Doukas, M.P., 2008, Chlorine degassing during the lava dome-building eruption of Mount St. Helens, 2004–2005, chap. 27 *of* Sherrod, D.R., Scott, W.E., and Stauffer, P.H., eds., A volcano rekindled; the renewed eruption of Mount St. Helens, 2004–2006: U.S. Geological Survey Professional Paper 1750 (this volume).

Epstein, S., and Mayeda, T., 1953, Variation of ^{18}O content of waters from natural sources: Geochimica et Cosmochimica Acta, v. 4, no. 5, p. 213–224.

Evans, W.C., Banks, N.G., and White, L.D., 1981, Analyses of gas samples from the summit crater, *in* Lipman, P.W., and Mullineaux, D.R., eds., The 1980 eruptions of Mount St. Helens, Washington: U.S. Geological Survey Professional Paper 1250, p. 227–232.

Evans, W.C., Sorey, M.L., Cook, A.C., Kennedy, B.M., Shuster, D.L., Colvard, E.M., White, L.D., and Huebner, M.A., 2002, Tracing and quantifying magmatic carbon discharge in cold groundwaters—Lessons learned from Mammoth Mountain, USA: Journal of Volcanology and Geothermal Research, v. 114, p. 291–312.

Evarts, R.C., Ashley, R.P., and Smith, J.G., 1987, Geology of the Mount St. Helens area; record of discontinuous volcanic and plutonic activity in the Cascade arc of southern Washington: Journal of Geophysical Research, v. 92, no. B10, p. 10155–10169.

Faure, G., 1986, Principles of isotope geology: New York, John Wiley, 589 p.

Fournier, R.O., 1986, Conceptual models of brine evolution in magma-hydrothermal systems, chap. 55 *of* Decker, R.W., Wright, T.L., and Stauffer. P.H., eds., Volcanism in Hawaii: U.S. Geological Survey Professional Paper 1350, v. 2, p. 1487–1506.

Gerlach, T.M., and Casadevall, T.J., 1986, Fumarole emissions

at Mount St. Helens volcano, June 1980 to October 1981; degassing of a magma-hydrothermal system: Journal of Volcanology and Geothermal Research, v. 28, nos. 1–2, p. 141–160, doi:10.1016/0377-0273(86)90009-0.

Gerlach, T.M., and Taylor, B.E., 1990, Carbon isotope constraints on degassing of carbon dioxide from Kilauea Volcano: Geochimica et Cosmochimica Acta, v. 54, no. 7, p. 2051–2058.

Gerlach, T.M., McGee, K.A., and Doukas, M.P., 2005, Emission rates, pre-eruption gas saturation and ascent degassing during the 2004–2005 eruption of Mount St. Helens [abs.]: Eos (American Geophysical Union Transactions), v. 86, no. 52, Fall Meet. Suppl., Abstract V52B-07.

Gerlach, T.M., McGee, K.A., and Doukas, M.P., 2008, Emission rates of CO_2, SO_2, and H_2S, scrubbing, and preeruption excess volatiles at Mount St. Helens, 2004–2005, chap. 26 *of* Sherrod, D.R., Scott, W.E., and Stauffer, P.H., eds., A volcano rekindled; the renewed eruption of Mount St. Helens, 2004–2006: U.S. Geological Survey Professional Paper 1750 (this volume).

Giggenbach, W.F., 1992, Chemical techniques in geothermal exploration, *in* D'Amore, F., ed., Applications of geochemistry in geothermal reservoir development: Rome, UNITAR/UNDP Guidebook, Center on Small Energy Resources, p. 119–144.

Goff, F., and McMurtry, G.M., 2000, Tritium and stable isotopes of magmatic waters: Journal of Volcanology and Geothermal Research, v. 97, p. 347–396.

James, E.R., Manga, M., and Rose, T.P., 1999, CO_2 degassing in the Oregon Cascades: Geology, v. 27, no. 9, p. 823–826.

Keith, T.E.C., Casadevall, T.J., and Johnston, D.A., 1981, Fumarole encrustations; occurrence, mineralogy and chemistry, *in* Lipman, P.W., and Mullineaux, D.R., eds., The 1980 eruptions of Mount St. Helens, Washington: U.S. Geological Survey Professional Paper 1250, p. 239–250.

Kennedy, B.M., and van Soest, M.C., 2006, A helium isotope perspective on the Dixie Valley, Nevada, hydrothermal system: Geothermics, v. 35, p. 26–43.

Kharaka, Y.K., Gunter, W.D., Aggarwal, P.K., Perkins, E.H., and DeBraal, J.D., 1988, SOLMINEQ.88—A computer program for geochemical modeling of water-rock interactions: U.S. Geological Survey Water Resources Investigation Report 88–4227, 420 p.

Major, J.J., Scott, W.E., Driedger, C., and Dzurisin, D., Mount St. Helens erupts again; activity from September 2004 through March 2005: U.S. Geological Survey Fact Sheet 2005–3036, 4 p.

Rose, T.P., and Davisson, M.L., 1996, Radiocarbon in hydrologic systems containing dissolved magmatic carbon dioxide: Science, v. 273, p. 1367–1370.

Schilling, S.P., Carrara, P.E., Thompson, R.A., and Iwatsubo, E.Y., 2004, Posteruption glacier development within the crater of Mount St. Helens, Washington, USA: Quaternary Research, v. 61, no. 3, p. 325–329.

Shevenell, L., 1990, Chemical and isotopic investigation of the new hydrothermal system at Mount St. Helens, Washington, USA: Reno, University of Nevada, Ph.D. dissertation, 282 p.

Shevenell, L., and Goff, F., 1993, Addition of magmatic volatiles into the hot spring waters of Loowit Canyon, Mount St. Helens, Washington, USA: Bulletin of Volcanology, v. 55, no. 7, p. 489–503, doi:10.1007/BF00304592.

Shevenell, L., and Goff, F., 1995, Evolution of hydrothermal waters at Mount St. Helens, Washington, USA: Journal of Volcanology and Geothermal Research, v. 69, p. 73–94.

Shevenell, L., and Goff, F., 2000, Temporal geochemical variations in volatile emissions from Mount St. Helens, USA, 1980–1994: Journal of Volcanology and Geothermal Research, v. 99, p. 123–138.

Symonds, R.B., and Reed, M.H., 1993, Calculation of multicomponent chemical equilibria in gas-solid-liquid systems; calculation methods, thermochemical data, and applications to studies of high-temperature volcanic gases with examples from Mount St. Helens: American Journal of Science, v. 293, no. 8, p. 758–864.

Symonds, R.B., Gerlach, T.M., and Reed, M.H., 2001, Magmatic gas scrubbing—implications for volcano monitoring: Journal of Volcanology and Geothermal Research, v. 108, nos. 1–4, p. 303–341, doi:10.1016/S0377-0273(00)00292-4.

Symonds, R.B., Poreda, R.J., Evans, W.C., Janik, C.J., and Ritchie, B.E., 2003, Mantle and crustal sources of carbon, nitrogen, and noble gases in Cascade-Range and Aleutian-Arc volcanic gases: U.S. Geological Survey Open-File Report 03–436, 26 p.

Thompson, M.J., 1990, Chemical data from thermal and nonthermal springs in Mount St. Helens National Monument, Washington: U.S. Geological Survey Open-File Report 90-0690–A, 16 p.

Vogel, J.S., Southon, J.R., and Nelson, D.E., 1987, Catalyst and binder effects in the use of filamentous graphite for AMS: Nuclear Instruments and Methods in Physics Research, v. B29, p. 50–56.

Walder, J.S., LaHusen, R.G., Vallance, J.W., and Schilling, S.P., 2007, Emplacement of a silicic lava dome through a crater glacier—Mount St Helens, 2004–06: Annals of Glaciology, v. 45, p. 14–20.

Walder, J.S., Schilling, S.P., Vallance, J.W., and LaHusen, R.G., 2008, Effects of lava-dome growth on the Crater Glacier of Mount St. Helens, Washington, chap. 13 *of* Sherrod, D.R., Scott, W.E., and Stauffer, P.H., eds., A volcano rekindled; the renewed eruption of Mount St. Helens, 2004–2006: U.S. Geological Survey Professional Paper 1750 (this volume).

Appendix 1. Trace-Element and Isotopic Data from Springs and Creeks in the Mount St. Helens Area, Washington, 2002–2005

[This appendix appears only in the digital versions of this work—in the DVD-ROM that accompanies the printed volume and as a separate file accompanying this chapter on the Web at: http://pubs.usgs.gov/pp/1750.]

This appendix is a spreadsheet of analytical data.

A Volcano Rekindled: The Renewed Eruption of Mount St. Helens, 2004–2006
Edited by David R. Sherrod, William E. Scott, and Peter H. Stauffer
U.S. Geological Survey Professional Paper 1750, 2008

Chapter 26

Emission Rates of CO_2, SO_2, and H_2S, Scrubbing, and Preeruption Excess Volatiles at Mount St. Helens, 2004–2005

By Terrence M. Gerlach[1], Kenneth A. McGee[1], and Michael P. Doukas[1]

Abstract

Airborne surveillance of gas emissions began at Mount St. Helens on September 27, 2004. Reconnaissance measurements—SO_2 column abundances and CO_2, SO_2, and H_2S concentrations—showed neither a gas plume downwind of the volcano nor gas sources within the crater. Subsequent measurements taken during the period of unrest before the eruption began on October 1 and for several days after October 1 showed only small point sources of gas within the crater. These sources defined a pattern of scrubbed degassing that evolved from near-zero emissions, to scattered CO_2-only sources, to growing sources of CO_2 with minor H_2S and SO_2, and finally to myriad sources of CO_2 with increasingly SO_2-dominant sulfur gases. Scrubbing strongly hydrolyzed SO_2 but also affected CO_2 and H_2S.

From October 7 on, a coherent plume spilled over the crater rim, yielding emission rates for CO_2 and SO_2, but not always for H_2S. Virtually all SO_2 and most CO_2 outgassed from the growing dome of new dacite; some CO_2 came from sources on the 1980–86 lava dome and in the Loowit springs area. The 2004–5 emission rates were notably low and variable. Emission rates for CO_2 peaked early (10/7/2004) at 2,415 metric tons per day (t/d), but the median rate was 655 t/d; only about 20 percent of the rates were greater than 1,000 t/d and about 45 percent were less than 500 t/d. Emission rates of SO_2 never exceeded 240 t/d, and the median rate was only 72 t/d; 70 percent of SO_2 emission rates were <100 t/d and about 40 percent were <50 t/d. Emission rates of H_2S were <10 t/d. Cumulative outputs through November 2005 were about 231,000 t CO_2 and 30,000 t SO_2.

The CO_2 and SO_2 emission rates are distinctly lower than those of the early 1980s, but they are similar to those of the 1980s lava-dome eruptions, possibly back as far as late 1981 or late 1980. However, the CO_2/SO_2 ratio of the 2004–5 emissions (11±1) is higher than that of the 1980s emissions (8) because of scrubbing during the early part of the eruption. The nonscrubbed CO_2/SO_2 of the 2004–5 gases is 9±1, similar to the1980s emissions.

Modeling constrained by cumulative CO_2 emissions, cumulative dacite production, and melt H_2O concentration confirms that the 2004–5 dacite is a "flat" magma—that is, a dacite magma greatly depleted in excess (exsolved) volatiles compared to May 18, 1980, dacite. The inferred excess-volatile content of the current dacite is only 1.2 volume percent (vol. percent), or 0.2 weight percent (wt. percent), compared to the 15 vol. percent (3 wt. percent) of the May 18 dacite at 900°C and 220 megapascals (MPa) (8.6 km depth). At the much lower pressure of 130 MPa prior to ascent from the shallowest part of the reservoir (5.2 km depth), the current dacite's inferred excess-volatile content is 1.2 wt. percent—significantly less than the 3 wt. percent of the May 18 dacite and on the low end of the 1–6-wt. percent range of deeper intermediate to silicic magmas commonly involved in explosive volcanism.

The modeling further indicates that before ascent from 5.2 km depth, the dacite's excess volatile phase was H_2O rich (X_{H_2O} = ~0.96, X_{CO_2} = ~0.04, mole fraction basis) with $H_2S/SO_2 > 40$, and its rhyolitic melt phase contained about 4.4 wt. percent H_2O and 37 parts per million (ppm) CO_2. After closed-system ascent to the depth range of groundmass crystallization (~0.5–1 km), X_{H_2O} is 0.98, H_2S/SO_2 is 4–7, and the melt contains 1.1–1.5 wt. percent H_2O and 1–3 ppm CO_2. Sulfur dioxide becomes dominant over H_2S at depths less than 0.2 km. Because of excess-volatile depletion, open-system degassing involves depths shallower than about 2.5 km, weak CO_2 and SO_2 emissions prone to the effects of scrubbing, and—in contrast to early 1980 degassing—no measurable effect on the equilibrium ($^{210}Pb/^{226}$ Ra) values of the 2004–5 dacite.

The 2004–5 gas emissions are incompatible with "new" gas-rich magma introduced into the reservoir in the months

[1] U.S. Geological Survey, 1300 SE Cardinal Court, Vancouver, WA 98683

just before or since the onset of unrest and eruptive activity. However, the gas emissions are compatible with a flat magma—either leftover dacite from 1986 or dacite injected into the reservoir since 1986 as excess volatile-depleted magma, or as gas-rich magma subsequently mixed with larger amounts of leftover dacite or stripped of its excess volatiles by degassing prior to the current eruption.

Introduction

Airborne surveillance of gas emissions began on September 27, 2004, four days after a shallow earthquake swarm beneath the 1980–86 lava dome signaled Mount St. Helens' reawakening after 18 years (Scott and others, this volume, chap. 1; Moran and others, this volume, chap. 2). In this chapter we report the CO_2, SO_2, and H_2S gas emissions from the eruption's inception to the end of 2005, documenting their measurement, sources, and the magnitude and variability of the emission rates—presented in the context of gas-emission rates at Mount St. Helens in the 1980s and at several Cascade Range volcanoes since the late 1990s. The outstanding feature of the 2004–5 gas emissions is their persistently low emission rates. We attribute these low rates mainly to the extreme depletion of excess (that is, exsolved) volatiles in the current dacite compared to the May 18, 1980, dacite and secondarily to gas scrubbing. VolatileCalc modeling (Newman and Lowenstern, 2002) quantifies and confirms our hypothesis of excess-volatile depletion in the 2004–5 dacite. We exploit the modeling to reveal the amount and composition of excess-volatile fluid in the source dacite at depth, to track its evolution as the dacite ascends, and to quantify several related aspects of the degassing.

Background

Airborne Emission-Rate Measurements at Mount St. Helens in the 1980s

Airborne monitoring from a fixed-wing aircraft of SO_2 emission rates began at Mount St. Helens in May 1980 by making correlation spectrometer (COSPEC) measurements on the plume. More than 1,000 COSPEC flights followed during the next 8 years (McGee, 1992; McGee and Casadevall, 1994), most of which were made 1–2 km downwind of source vents during episodes of dome-building eruptions, endogenous dome growth, or intervening noneruptive periods. Casadevall and others (1981, 1983) describe the measurement technique and discuss the SO_2 emissions through 1982. McGee (1992) describes the structure, dynamics, and SO_2 cross sections of noneruptive plumes at Mount St. Helens that occurred from 1980 to 1988. McGee and Sutton (1994) discuss measurements made during four 1984–86 dome-building eruptions and compare results with various geophysical monitoring data. Early SO_2 emission rates frequently exceeded 1,000 metric tons per day (t/d), but rates declined to negligible levels by September 1988 when airborne COSPEC measurements ended, nearly 2 years after the last dome-building eruption of the 1980s (McGee and Casadevall, 1994). Airborne monitoring also included 119 measurements of CO_2 emission rates that ranged from >20,000 t/d in July 1980 to <1,000 t/d by the end of August 1981, when measurements were halted because concentrations of plume CO_2 had declined to levels indistinguishable from ambient atmospheric CO_2 by the analyzer employed at the time (Harris and others, 1981; McGee and Casadevall, 1994). McGee and Casadevall (1994) tabulate the 1980–1988 airborne emission-rate measurements and supplementary data, all of which can be downloaded from the USGS publications Web site, http://pubs.usgs.gov/of/1994/of94-212/ (last accessed March 14, 2008).

Airborne Emission-Rate Measurements in the Cascades Since the 1980s

We initiated a program of volcanic gas emission-rate measurements at Cascade Range volcanoes in the late 1990s after developing improved airborne monitoring techniques (described below). The program comprised airborne plume measurements at major volcanic centers, from Mount Baker in Washington to Lassen Peak in California, to establish baseline emission rates of CO_2, SO_2, and H_2S for identifying anomalous gas emissions at times of volcano unrest in the Cascade Range (table 1). Several volcanic centers—Glacier Peak, Mount Rainer, Mount Adams, Mount Jefferson, Medicine Lake caldera and Mount Shasta—produce no detectable emissions of the three gases; however, these airborne results do not rule out minor diffusive degassing and scattered spring and fumarole gas discharges derived from underlying magma. Other centers, such as Newberry caldera and South Sister, though lacking coherent plumes, do produce trace quantities of gas from small point sources that can be detected in airborne gas measurements. Besides Mount St. Helens, only three volcanoes in the Cascade Range produce coherent plumes with measurable gas output at the present time—Mount Baker, Mount Hood, and Lassen Peak. All of these volcanoes emit small amounts of gas: emission rates are <300 t/d for CO_2 and <10 t/d for H_2S; SO_2 is below detection.

Airborne Measurements at Mount St. Helens in 1998

In May 1998, background seismicity at Mount St. Helens increased markedly from the low levels recorded for the previous few years. Located directly below the lava dome, these small earthquakes clustered mainly in two distinct depth bands: 2–5 km and 7–9 km. Throughout June and the first half of July 1998, the seismicity continued to increase, with earthquake depths spanning the entire range from 2 to 9 km. The first of several airborne gas-surveillance flights recorded

Table 1. Gas measurements in the Cascade Range and nearby calderas after 1988.

[Platform indicates aircraft: FX, fixed-wing; Heli, helicopter. t/d, metric tons per day; –, no data; 0, measurement taken but gas was not detected; tr, trace.]

Volcano	Date	Platform	CO_2 (t/d)	SO_2 (t/d)	H_2S (t/d)
Mount Baker	07/08/1998	FX	273	0	–
	09/13/2000[1]	FX	187	0	5.5
	03/21/2001	FX	0	0	0
Glacier Peak	07/08/1998	FX	0	0	–
Mount Rainer	07/08/1998	FX	0	0	–
Mount Adams	08/03/1998	FX	0	0	–
	08/10/2005	FX	0	0	0
Mount St. Helens	06/22/1998	FX	1,900	0	–
	07/08/1998[2]	FX	tr	0	–
	07/08/1998[3]	FX	tr	0	–
	08/03/1998	FX	0	0	–
	09/14/1998	FX	0	0	–
Mount Hood	06/22/1998	FX	0	0	–
	08/03/1998	FX	0	0	–
	08/10/2005	FX	0	0	0
	09/15/2005	Heli	144	0	6.4
Mount Jefferson	08/11/1998	FX	0	0	–
Newberry caldera	09/19/2000	FX	tr	0	–
South Sister	04/25/2001	Heli	tr	0	–
	09/21/2001	Heli	0	0	–
Medicine Lake caldera	08/11/1998	FX	0	0	–
Mount Shasta	08/11/1998	FX	0	0	–
Lassen Peak	08/11/1998	FX	110	0	–
	09/19/2000	FX	20	0	2

[1]Data from McGee and others (2001).

[2]Morning flight.

[3]Afternoon flight.

a CO_2 emission rate of 1,900 t/d on June 22 (table 1). By July 8, morning and afternoon gas-measurement flights detected only trace CO_2 degassing, and by the end of July, seismicity returned to levels similar to those prior to May. Additional gas-surveillance flights on August 3 and September 14 failed to detect CO_2 degassing. All 1998 flights failed to detect SO_2; there were no H_2S measurements.

Instrumentation and Configuration of the Airborne Monitoring System

In this study, we used an airborne system developed during the past decade for measuring volcanic CO_2, SO_2, and H_2S emissions and intended primarily for application in the Cascade Range and the Aleutian arc. Sites of interest in these regions are remote, ground access is difficult, climates are wet, and thick snow pack and glaciers are present locally. Large volumes of recharge water foster hydrothermal systems and bodies of ground water and surficial water capable of scrubbing acidic magmatic volatiles (especially SO_2, HCl, HF) and masking magma degassing at depth during the early stages of unrest—hence the emphasis on an airborne system capable of measuring CO_2 and H_2S emissions (Doukas and Gerlach, 1995; Symonds and others, 2001).

The airborne system incorporates a LI-COR Model LI-6252 nondispersive infrared CO_2 analyzer and flow control unit to measure CO_2 concentrations. This instrument, with a fast 1-s response time and a high sensitivity to low concentrations of CO_2, is well suited for measuring small changes in CO_2 concentration. Its use for determining CO_2 in volcanic plumes is described in detail elsewhere (Gerlach and others, 1997; Gerlach and others, 1999). We used an Interscan Model 4170 H_2S analyzer to measure plume H_2S in the 0–1 ppm range. This instrument consists of an electrochemical voltametric sensor coupled to a 1-L/min sample-draw pump with H_2S concentration recorded from calibrated analog output. McGee and others (2001) describe the application of the Interscan analyzer to measuring H_2S in volcanic plumes. Similarly, an Interscan Model 4240 SO_2 analyzer with a 0–2 ppm range provides direct measurements of SO_2 in the plume. Assuming ambient air is largely devoid of H_2S and SO_2, our measurements indicate typical instrument noise values of 3–4 parts per billion (ppb)for these analyzers. Interscan analyzers show some cross sensitivity to other gases, so these gases are removed by appropriate chemical scrubbers installed on input lines. Because Interscan analyzers measure gas partial pressures, all calibrated output is corrected for the pressure and temperature at the altitude of measurement.

The airborne system is configured to employ two types of optical ultraviolet spectrometers for measuring SO_2 column abundances. For some of the early measurements in this study, we employed a Barringer correlation spectrometer (COSPEC V)—long the standard tool for monitoring volcanic SO_2 emission rates (Stoiber and Jepsen, 1973; Crafford, 1975; Malinconico, 1979; Stoiber and others, 1983). A data logger records the analog output of the instrument for later processing using USGS software. For the majority of the SO_2 flux measurements, we used a FLYSPEC built and configured as described in Horton and others (2006). This new, miniaturized, lightweight and low-power, ultraviolet correlation spectrometer incorporates an Ocean Optics USB2000 ultraviolet spectrometer with a fiber-optic collimating lens, a UV band-pass filter, and two SO_2 calibration cells. A subnotebook computer provides FLYSPEC power, control, and data collection through a USB port, and a small GPS receiver supplies location data for cosine corrections of traverses not perpendicular to the direction of plume travel.

The airborne instrument package also includes a type-K thermocouple, shielded from wind and direct sunlight, for measuring ambient air temperature and a chart recorder for in-flight logistical use. A pressure transducer mounted within the LI-COR analyzer provides measurements of ambient atmospheric pressure inside the unpressurized aircraft cabin. An onboard Rockwell GPS receiver continuously records the precise latitude, longitude, and altitude, so that the location of each measurement can be retrieved later for data processing. The data from all instruments except the FLYSPEC are recorded at 1-s frequency in a handheld PSC Falcon Model 310 portable data-collection terminal. Figure 1 illustrates schematically the configuration of all the instruments of the airborne system. Figure 2 displays instrument placement in both helicopter and fixed-wing aircraft and the external helicopter mounting of a FLYSPEC.

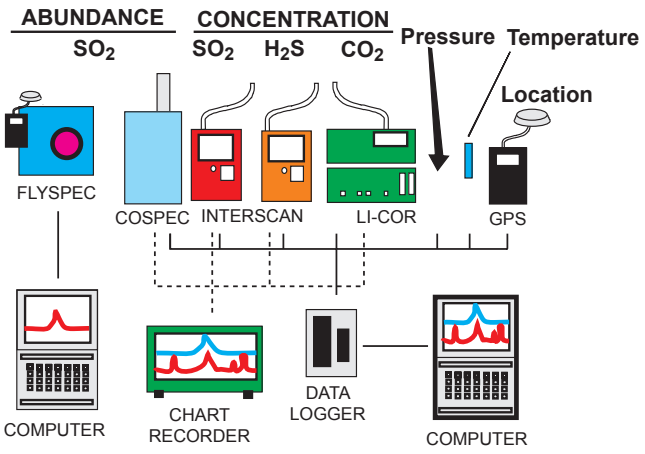

Figure 1. Airborne instrument package showing instruments used for measuring SO_2 column abundances (FLYSPEC and COSPEC); instruments for measuring CO_2, SO_2, and H_2S gas concentration (LI-COR and Interscan); sensors for measuring temperature, pressure, and location; and other components used during a typical airborne mission (computer, data logger, and chart recorder).

Procedures and Methods

The gas measurements began on September 27, 2004. The five flights during the first week were primarily for reconnaissance purposes. At this stage of unrest, the volcano lacked a coherent gas plume but produced small fragmentary and ephemeral parcels of gas that—although detectable by the airborne system—were only useful for rough estimates of gas emission rates. Nevertheless, we were able to discover and follow the development of point sources of emerging gas emissions within the crater by mounting the direct-sampling instruments (LI-COR and Interscans) in a helicopter with an air intake tube attached to the lower left strut and making reconnaissance flights of the 1980–86 lava dome, the crater floor, and the crater walls (fig. 3).

After the first week of October 2004, a coherent plume developed and spilled over the crater rim, and accurate emission-rate determinations became feasible (fig. 4). We mounted and flew the direct-sampling instruments and the COSPEC V in a twin-engine aircraft configured for open-flow sampling of external air (Gerlach and others, 1997, 1999). The use of a twin-engine aircraft prevented contamination by combustion products from engine exhaust. Upward-looking COSPEC measurements taken while flying traverses beneath the plume perpendicular to the direction of plume transport provided SO_2 column abundances across an orthogonal section of the plume (fig. 5*A*). Flying traverses across the plume at different altitudes, each normal to its transport direction, allowed in-plume measurements and profiling of entire orthogonal sections of the plume by the direct-sampling instruments (LI-COR and Interscans) (fig. 5*B*). Figure 6 illustrates a series of airborne traverses across the plume, showing where the Interscan analyzer detected SO_2 in the orthogonal plume cross section. Later processing of these data into emission rates included corrections for curvature in the flight paths and for deviations from orthogonality. Contour maps of gas concentrations in the orthogonal plume cross section were produced using mapping software (Surfer v. 8).

By November 10, 2004, we made a transition to the use of a helicopter as the airborne platform for gas measurements, for these reasons: the availability of a helicopter for field work, the superior maneuverability of a helicopter for making plume measurements at the crater rim and within the crater, and the slower airspeed of the helicopter, which permits more measurements per meter across small plumes. Use of the helicop-

Figure 2. Gas-monitoring equipment installation for airborne surveillance, 2004–2005. *A*, FLYSPEC being attached to the strut of helicopter. The instrument's narrow field of view allows it to be mounted near the body of the aircraft without blocking the light. *B*, Typical mounting arrangement of instrumentation in helicopter. *C*, Instrumentation placed in a fixed-wing aircraft. Note COSPEC panel (right) protruding from behind copilot's seat. USGS photos by K.A. McGee (*A*, *C*) and M.P. Doukas (*B*).

ter also marked the transition to exclusive use of the FLYSPEC ultraviolet spectrometer for SO_2 emission-rate measurements. Although it is possible to utilize the COSPEC in a helicopter, "chopping" of light to the COSPEC telescope by the rotor blades creates interference in the signal output. This requires selection of longer time constants to dampen the interference, which negates the advantageous spatial resolution of the helicopter (Caltabiano and others, 1992; Galle and others, 2002; Elias and others, 2006). The FLYSPEC, however, is relatively immune to interference by the rotor blades, and no special filtering or processing of the data is required. The switch from COSPEC to FLYSPEC did not introduce inconsistencies into the SO_2 emission-rate dataset—side-by-side testing of these instruments shows they produce statistically equivalent results (Elias and others, 2006; Horton and others, 2006).

The relatively small field of view (2.5°) of the FLYSPEC allows it to be mounted on an external structural member close to the body of the helicopter and positioned to point vertically without loss of signal due to light obstruction (fig. 2*A*). We fed the USB signal and power cable through a side window of the helicopter to connect with the subnotebook computer. Prior to the plume measurements, we landed the helicopter at a calibration station high on the flank of Mount St. Helens and collected instrument spectra for the high and low calibration cells along with spectra for dark current and clear sky. Once the FLYSPEC was calibrated, we flew several traverses beneath the plume that were averaged to obtain the SO_2 column abundances of the plume. We reduced the data with the FluxCalc software program written by staff at the Hawai'i Institute of Geophysics and Planetology, University of Hawai'i at Mānoa. The program compares absorption values of as many as nine peak-and-trough combinations in each sample SO_2 spectrum to the two calibration cell spectra and then computes the column abundance of SO_2.

The standard method for determining emission rates from airborne in-plume measurements by the direct-sampling instruments is based on the volcanic gas concentrations measured in the cross section through the plume normal to wind direction, the average plume pressure and temperature in that section, and the wind speed (Harris and others, 1981; Gerlach and others, 1997). Gerlach and others (1999) adapted the method by using orbital traverses around a volcano and correcting the data from curved plume cross sections approximately normal to wind direction. McGee and others (2001) further adapted the method by using H_2S peaks as a guide for resolving the boundary between atmospheric-only CO_2 and atmospheric plus volcanic plume CO_2. In this study, we often used the location of SO_2 peaks recorded by the Inter-scan analyzer as markers to distinguish plume CO_2 from the atmospheric background CO_2 because H_2S was not always detected in the plume. Direct measurement of CO_2 and SO_2

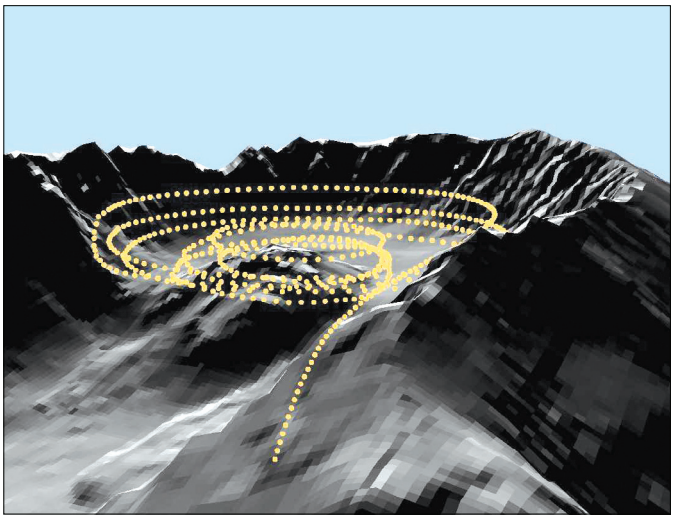

Figure 3. Shaded-relief elevation model of Mount St. Helens' crater indicating the flight path of a gas-measurement flight in October 2004. Early gas flights in fall 2004 before the emergence of a discrete plume, such as the flight illustrated here, were geared toward detecting point sources of CO_2, SO_2, and H_2S. View is to the southeast.

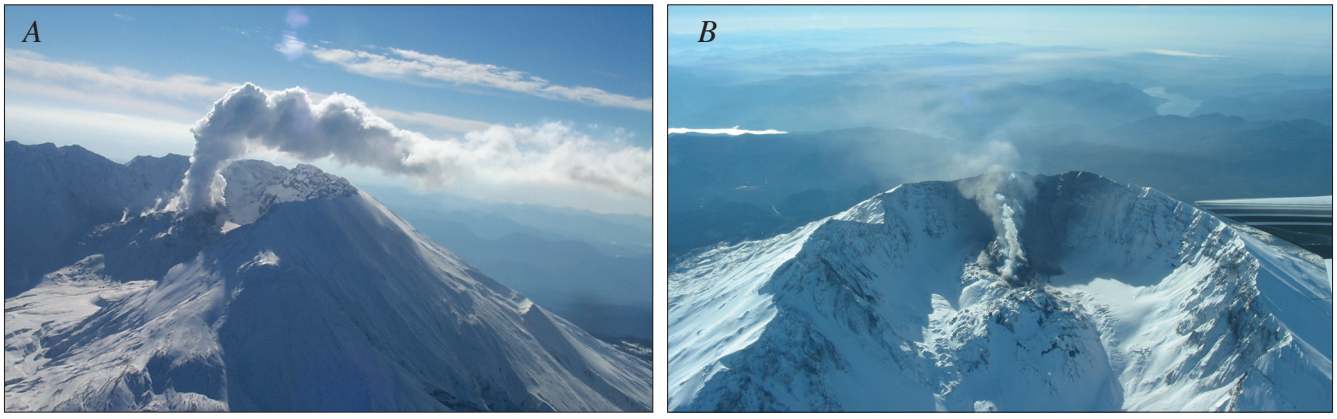

Figure 4. Typical gas plumes from Mount St. Helens early in the 2004–2005 eruption. *A*, Plume observed on October 27, 2004. View is to southeast. *B*, Plume on November 4, 2004. View is to south. Crater diameter is about 2.1 km.
USGS photos by M.P. Doukas (*A*) and K.A. McGee (*B*).

also allowed calculation of CO_2/SO_2 ratios at many locations in the plume.

Knowing the velocity of plume travel is essential in computing accurate gas-emission rates from either gas concentrations in a plume cross section or column-abundance measurements made beneath the plume. It is assumed that the speed of the plume as it moves downwind is the same as the ambient wind speed. We used the Doukas (2002) method of wind-speed measurement, in which a GPS receiver records the rate and direction of drift of the aircraft while flying neutral wind circles at the altitude of the plume. This information allows determination of wind speed and wind direction at the altitude of the plume with a windspeed uncertainty of <10 percent.

The equation of Gerlach and others (1997),

$$E_{CO_2} = 0.457329(ASP_{CO_2})/T, \quad (1)$$

calculates the CO_2 emission rate, E_{CO_2}, in t/d where A is the area of the plume cross section after corrections for curvature of orbital traverses (in m^2), S is the average plume speed (in m/s), P_{CO_2} is the average partial pressure of CO_2 in the plume (in pascals (Pa), calculated from the product of average barometric pressure in the plume and the average mole fraction concentration of CO_2 in the plume), and T is the average air temperature in the plume (in K). The constant (units: s t K Pa^{-1} m^{-3} d^{-1}) includes the kilogram molecular weight of CO_2 (0.04401 kg/mol), the universal gas constant (8.314510 Pa m^3 mol^{-1} K^{-1}), and the conversion factors 86,400 s/d and 10^3 kg/t. When calculating E_{H_2S}, P_{CO_2} is replaced by P_{H_2S}, and the con-

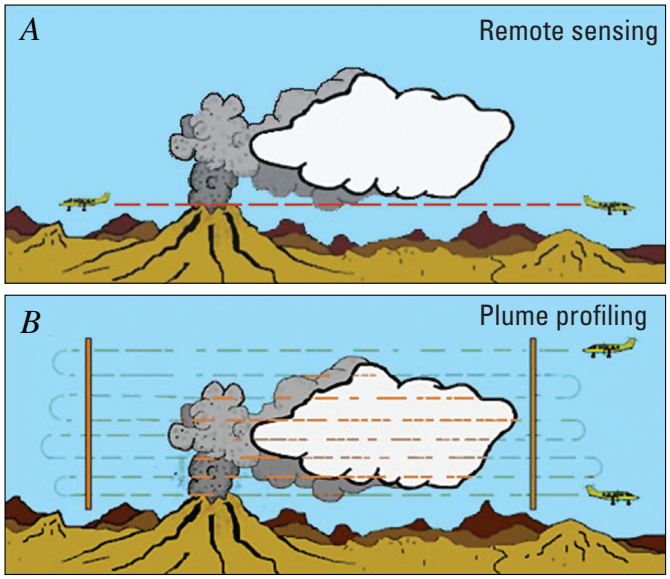

Figure 5. Schematic flight patterns for plume monitoring. *A*, Flight pattern for remote measurement of SO_2 column abundances in the plume. Flight traverses with the upward-looking FLYSPEC or COSPEC spectrometer are made beneath the plume perpendicular to its direction of travel. *B*, Instruments that measure concentration and require direct sampling of the plume, such as LI-COR and Interscan, are flown directly through the plume, perpendicular to its travel direction, in a series of top-to-bottom profiles forming a vertical plume cross section.

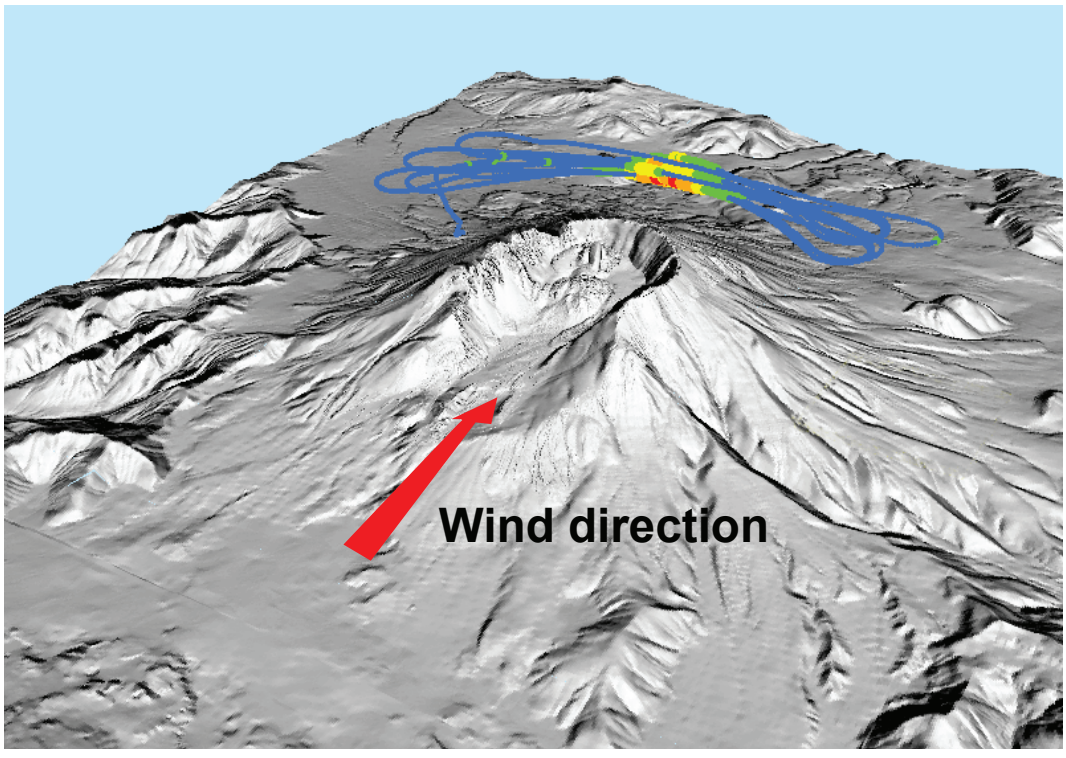

Figure 6. Illustration of a downwind airborne measurement of the plume from Mount St. Helens on July 13, 2005, plotted on shaded-relief elevation model. View is to the southeast. Blue line represents GPS tracks of several traverses through the plume, with hotter colors (yellow, orange, and red) representing locations where SO_2 was measured. Red arrow indicates wind direction; wind is from the north.

stant is 0.354141 (McGee and others, 2001); when calculating E_{SO_2}, P_{SO_2} and the constant 0.665665 are used.

Flight frequency varied because of a mix of factors, which included perceived flight safety, apparent necessity of the data for hazard assessments, rate of change of eruptive activity, and current and forecasted weather. Starting on September 27, 2004, we made 11 flights in the first 3 weeks, 1 to 2 flights per week during the next 5 weeks, and 1 or 2 flights per month thereafter throughout 2005, except during December 2005 when weather conditions did not permit access to the plume. Flight dates and aircraft platforms deployed (helicopter or fixed-wing) are recorded in table 2.

Description of Data and Statistical Tests

Gas emission-rate data, which form the backbone data of this report, tend to have skewed rather than symmetrical distributions. The skewed distributions are a reflection of two fundamental properties of gas emission-rate data: they can take on only positive values, and their standard deviations are typically large—commonly about as large or larger than their means. When distributions are skewed, means and standard deviations may no longer adequately describe population distributions, and interpreting these statistics in terms of a normal distribution can produce a misleading picture. It is preferable instead to report the median for skewed distributions (Glantz, 2005); we also report upper and lower percentile information as appropriate to give an indication of the dispersion of values in the sampled population.

If populations are skewed from normal distributions, parametric statistical tests may become unreliable, and nonparametric or distribution-free statistical tests should be used (Glantz, 2005). Therefore, we used statistical software (SigmaStat v. 3.1) to calculate the nonparametric Mann-Whitney rank-sum test (MWRST), instead of the parametric Student's *t* test, to test for significant differences in two groups of data. The MWRST can be used to evaluate significant difference in the medians of two groups, significant difference in the underlying population distributions of two groups, and significant difference between two groups caused by random sampling variations. We report the probability level (*P*) of MWRST results. Following the tradition of most physical-science research, the critical significance level for *P* is 5 percent ($P = 0.05$) in this report; that is, $P \leq 0.05$ indicates a significant difference. Several of the statistical calculations also included Kolmogorov-Smirnov normality testing (SigmaStat v. 3.1).

Results and Observations

Emission Rates, Cumulative Emissions, and CO_2/SO_2 Ratios

The measured CO_2, SO_2, and H_2S emission rates of the 2004–5 eruption spanned the period from September 27, 2004, to November 22, 2005 (fig. 7, table 2). Emission rates frequently were below detection limits before October 7, 2004 (fig. 7, table 2). Time series of the 24 CO_2 and 28 SO_2 emission rates measured from October 7, 2004, until the last 2005 measurement on November 22 were notably low and variable. Emission rates ranged from 2,415 t/d to 146 t/d for CO_2 and from 240 t/d to 14 t/d for SO_2; both CO_2 and SO_2 had low medians: 655 t/d for CO_2 and 72 t/d for SO_2. Less than 5 percent of the CO_2 emission rates were >2,000 t/d, about 80 percent were <1,000 t/d, more than 40 percent were <500 t/d, and about 25 percent were <250 t/d. Of the SO_2 emission rates, only 7 percent were >200 t/d, almost 70 percent were <100 t/d, and 40 percent were <50 t/d. At times, emission rates fell to <150 t/d for CO_2 and to <30 t/d for SO_2. Emission rates of H_2S were always low (<10 t/d). Multiple traverses under the plume gave comparable SO_2 emission rates, so the observed variation was not simply from puffing during times of measurement.[2]

Cumulative CO_2 and SO_2 emissions—calculated from the areas under emission-rate time-series plots—indicate total outputs of 231,150 t CO_2 and 29,700 t SO_2 from October 7, 2004, through November 22, 2005 (fig. 8; table 2). Weighted emission rates—calculated from cumulative emissions on measurement dates (fig. 8; table 2) divided by the number of days since October 7, 2004—are like multiday averages and thus smoother than measured emission rates. Although less variable, weighted emission rates also have low medians—830 t/d for CO_2 and 99 t/d for SO_2. However, these median rates are somewhat higher than the medians of measured values. Nevertheless, statistical tests confirm that no significant dif-

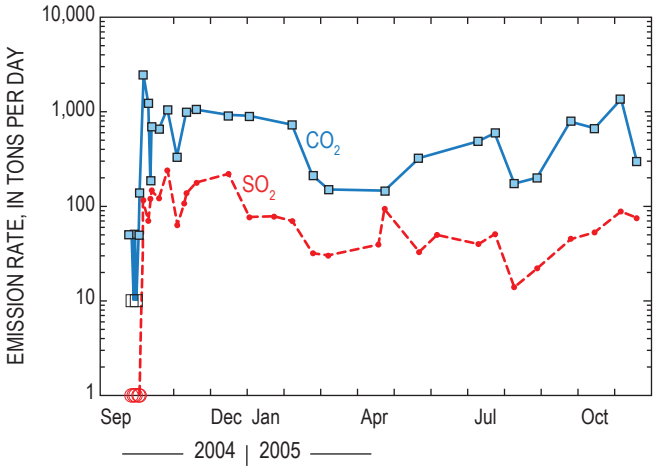

Figure 7. Time-series plots of CO_2 and SO_2 emission rates from September 27, 2004, to November 22, 2005 (table 2). The open symbols for some earlier measurements between September 27 and October 1, 2004, indicate estimated detection limit values of 10 t/d (CO_2) and 1 t/d (SO_2).

[2] Note added in proof: Low emission rates of 150–300 t/d CO_2, 5–35 t/d SO_2, and < 0.1 t/d H_2S persisted during 12 gas-monitoring flights from 2006 until the eruption paused in late January 2008.

Table 2. Emission rates and cumulative emissions for CO_2, SO_2, and H_2S during 2004–2005, Mount St. Helens, Washington.

[Emission rates are measured rates used in calculations of this study; significant figures were exaggerated to reduce roundoff errors. Cumulative emissions were determined as described in the text. Platform indicates aircraft: FX, fixed-wing; Heli, helicopter. t/d, metric tons per day; nd, not determined.]

Date	Platform	CO_2 (t/d)	SO_2 (t/d)	H_2S (t/d)	CO_2 (t)	SO_2 (t)
09/27/2004	Heli	50	1 [1]	0.1 [1]	nd	nd
09/29/2004	Heli	10 [1]	1 [1]	0.1 [1]	nd	nd
09/30/2004	Heli	50	1 [1]	0.1 [1]	nd	nd
10/01/2004	Heli	10 [1]	1 [1]	0.1 [1]	nd	nd
10/03/2004	Heli	50	1 [1]	0.1 [1]	nd	nd
10/04/2004	Heli	140	1 [1]	0.4	nd	nd
10/07/2004	FX	2,415	115	8	2,415	115
10/11/2004	FX	1,222	70	4	7,274	370
10/13/2004	FX	186	120	6	8,682	560
10/14/2004	FX	710	148	0.1 [1]	9,130	694
10/20/2004	FX	652	121	8	13,216	1,501
10/27/2004	Heli	1,060	240	8	19,208	2,764
11/04/2004	FX	332	63	0.1 [1]	24,776	3,976
11/10/2004	Heli	nd	107	6	nd	4,486
11/12/2004	Heli	981	138	nd	30,028	4,732
11/20/2004	Heli	1,053	177	6	38,164	5,993
12/17/2004	Heli	914	221	5	64,718	11,370
01/03/2005	Heli	887	76	0.1 [1]	80,027	13,893
01/24/2005	Heli	nd	78	11	nd	15,509
02/08/2005	Heli	718	70	0.3	108,917	16,619
02/25/2005	Heli	211	32	0.6	116,814	17,485
03/10/2005	Heli	149	30	0.3	119,154	17,888
04/21/2005	Heli	nd	40	0	nd	19,347
04/26/2005	Heli	146	94	0	126,086	19,681
05/25/2005	Heli	325	33	0	132,916	21,522
06/09/2005	Heli	nd	50	nd	nd	22,145
07/13/2005	Heli	485	40	nd	152,760	23,675
07/27/2005	Heli	594.3	51	0.1 [1]	160,316	24,312
08/12/2005	Heli	174	14	0.1 [1]	166,462	24,832
08/31/2005	Heli	198	22	0.1 [1]	169,996	25,174
09/28/2005	Heli	789	45	0.1 [1]	183,814	26,112
10/18/2005	Heli	658	53	0.3	198,284	27,092
11/09/2005	Heli	1,353	88	0.1 [1]	220,405	28,643
11/22/2005	Heli	300	75	0.1 [1]	231,150	29,702

[1]Estimated detection limits for CO_2, SO_2, and H_2S emission rates.

ference exists between the medians of measured and weighted CO_2 and SO_2 emission rates and the populations they sample (P >0.05).

The 24 contemporaneous CO_2 and SO_2 emission rates measured from October 7, 2004, to November 22, 2005, have a median molar CO_2/SO_2 ratio of ~12; about half of the CO_2/SO_2 ratios are between 7 and 18. The corresponding weighted emission rates have a median CO_2/SO_2 of ~10 and about half the CO_2/SO_2 ratios are between 9 and 11. Statistical tests confirm there is no significant difference between CO_2/SO_2 ratios calculated from measured and weighted emission rates (P >0.05). Total emissions for the entire period—231,150 t CO_2 and 29,700 t SO_2—indicate a CO_2/SO_2 of ~11. Thus, we employ a grand median CO_2/SO_2 ratio of 11±1 in this report.

Early Degassing

From the start of airborne gas measurements on September 27, 2004, throughout the period of unrest before the eruption began on October 1 and for almost a week thereafter, a volcanic plume was either absent or present as small fragmentary and ephemeral parcels of gas, yielding only rough gas-emission rates (table 2). Flights during this period served mainly as reconnaissance surveys for gas-emitting sources on the 1980–86 dome, the crater floor, and the crater walls (fig. 3) and led to the discovery and observation of point sources of gas emission that, over time, established a record of emergent degassing. The record began with SO_2 and H_2S concentrations at detection limits at all locations and CO_2 concentrations at ambient atmospheric levels at most locations (fig. 9), although sporadic CO_2 sources occurred with minor peaks <1.5 ppm above ambient levels. Similar results persisted through September 30. After the first steam-and-ash explosion at the start of the eruption on October 1, new CO_2 concentration peaks above ambient levels appeared—one new source on the northwest face of the 1980s dome produced an above-background peak of 36 ppm—but SO_2 and H_2S still remained largely at noise levels. There was some evidence, however, of the presence of H_2S—one minor peak was observed, and some observers in the air and on the ground downwind of the volcano reported the odor of H_2S.

The number of fumarole sources increased significantly by October 2, as did the number of above-ambient CO_2 concentration peaks—one reaching up to 16 ppm—while SO_2 and H_2S continued to be mostly absent, although field crews again reported H_2S odors (fig. 10). A further increase in the number of fumaroles and a broadening of CO_2 anomalies along with coincident low H_2S peaks (<0.02 ppm) appeared in the record on October 3. By October 4, CO_2 anomalies were as broad as a kilometer or more across, and SO_2 and H_2S formed coinci-

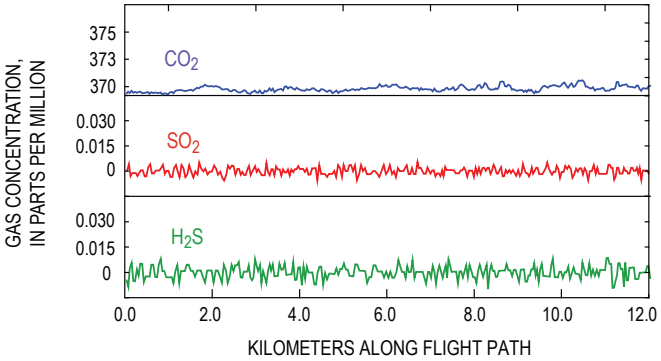

Figure 9. Concentrations of CO_2, SO_2, and H_2S measured along a helicopter flight path in Mount St. Helens crater on September 27, 2004. Concentrations of CO_2 are similar to ambient atmospheric levels; concentrations of SO_2 and H_2S are at sensor detection limits.

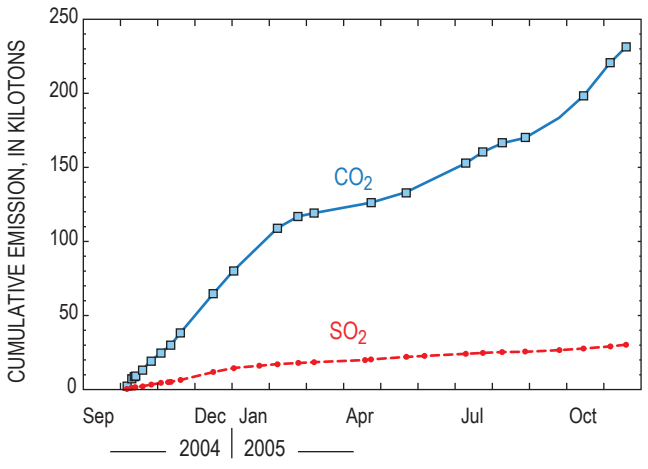

Figure 8. Time-series plots of cumulative CO_2 and SO_2 emissions from October 7, 2004, to November 22, 2005, when emission rates for both gases were above detection limits (fig. 7; table 2).

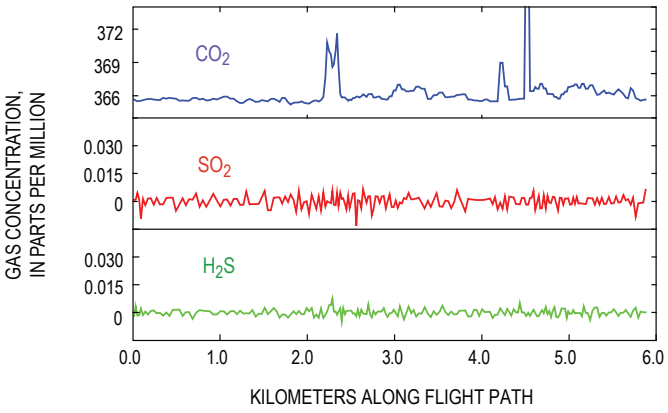

Figure 10. Concentrations of CO_2, SO_2, and H_2S measured along a helicopter flight path in Mount St. Helens crater on October 2, 2004. Concentrations of CO_2 show sporadic spikes above ambient atmospheric levels; concentrations of SO_2 and H_2S remain at sensor detection limits. The clipped CO_2 peak rises to 382 ppm.

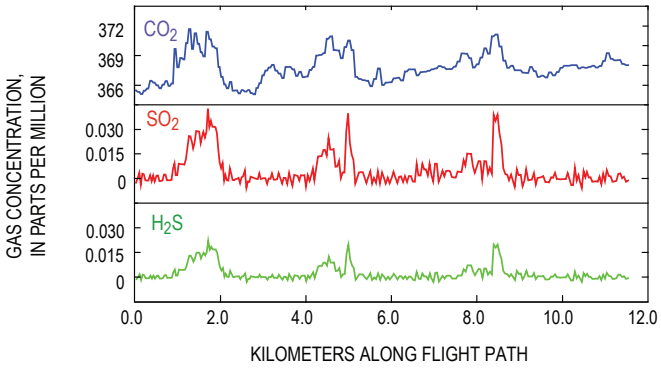

Figure 11. Concentrations of CO_2, SO_2, and H_2S measured along a helicopter flight path in Mount St. Helens crater on October 4, 2004. Concentrations of CO_2 show broad anomalies above ambient atmospheric levels; concentrations of SO_2 and H_2S show sharply coincident anomalies spiking above sensor detection limits. Note that SO_2 and H_2S anomalies have concentration levels of roughly similar magnitude.

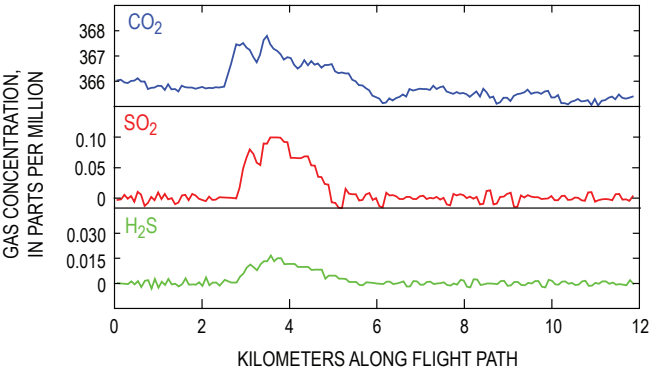

Figure 12. Concentrations of CO_2, SO_2, and H_2S measured along a helicopter flight path in Mount St. Helens crater on October 11, 2004. Concentrations of CO_2 show a broad anomaly above ambient atmospheric levels; concentrations of SO_2 and H_2S show coincident anomalies. Note that concentration levels of the SO_2 anomaly now are clearly greater than those of H_2S.

dent anomalies of roughly equivalent concentration levels (fig. 11). Wet degassing prevailed at this time as large gas bubbles were seen streaming through and ejecting from pools of water, which often contained chunks of floating ice that calved in from the adjacent melting glacier. By October 11, SO_2 clearly dominated H_2S as temperatures rose, pools of water dried up, and steaming increased greatly (fig. 12). Coherent plumes began to form regularly on or about October 7 and spilled over the crater rim (fig. 4), permitting acquisition of reliable emission rates by remote SO_2 column-abundance measurements and direct measurements of CO_2, SO_2, and H_2S gas concentrations (fig. 13).

Composite Degassing Sources

Mount St. Helens continued to produce buoyant plumes throughout the remainder of 2004 and all of 2005. In addition to the principal degassing site from the vent area on the north side of the new dome, several additional sites degassing both CO_2 and SO_2 were present at various locations on both old and new lobes of the growing new dome. By summer 2005, gas emissions were declining, and airborne gas measurements began to be conducted closer to the gas sources. These measurements provided more spatial resolution of gas concentrations within the proximal plume and revealed a minor source of the CO_2 within the plume coming from the 1980s dome. Since 2005, we have consistently detected CO_2 coming from the southwest side of the 1980s dome, just north of the vent area for the new dome. In addition, the older dome hosts a smaller CO_2 source on its east shoulder and several scattered point sources of CO_2. The spatial separation of new-dome and old-dome gas sources is best developed when winds are from the east or west. The degassing from the 1980s dome involves little or no SO_2. Nearly all of the SO_2 in the plume, and the majority of CO_2, originates from the hotter vents associated with the new dome. Under appropriate wind conditions, airborne traverses through the plume show CO_2 clearly degassing from both domes, whereas SO_2 is virtually absent from the

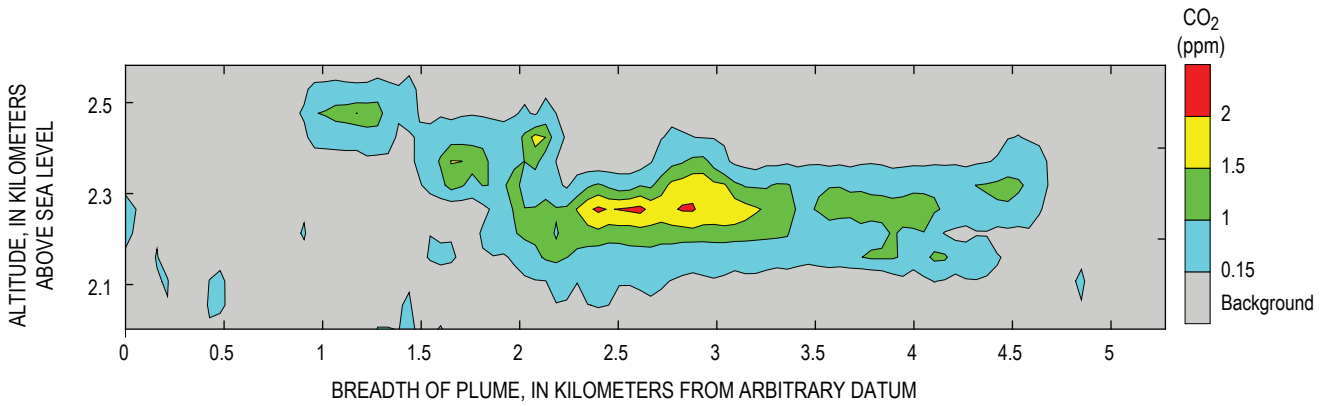

Figure 13. Concentrations of CO_2 in a vertical cross section of a coherent gas plume from Mount St. Helens on November 12, 2004, 1.7 km downwind of source. Bar on right shows scale for concentration of CO_2 above local atmospheric background. Plume cross section gives a CO_2 emission rate of 980 t/d.

1980s dome (fig. 14). Figure 14 shows CO_2 concentrations on a single plume traverse; most plume traverses show CO_2 concentrations are much higher over the new dome.

CO_2 Plume from Loowit Springs

During some of the airborne gas-measurement flights, a small CO_2 plume was observed that did not emanate from the new or the old dome. The source of this plume proved to be the Loowit springs area (Thompson, 1990), north of the 1980s dome and near the mouth of the crater, as determined by a series of low helicopter traverses on June 9, 2005, when winds from the north or northwest were favorable for distinguishing it. Orbital profiling around the upper part of the Loowit drainage defined the extent of the plume and quantified the CO_2 emission rate at 27 t/d (fig. 15), although the exact spring or springs involved could not be distinguished; neither SO_2 nor H_2S were detected. The spring discharge of magmatic CO_2 as inorganic carbon (aqueous CO_2 and HCO_3^- in about equal amounts) dissolved in Loowit waters and other thermal features draining the crater is ~22 t/d, which is similar to the emission rate of CO_2 gas around Loowit (Bergfeld and others, this volume, chap. 25). It is not known if the Loowit springs plume is a result of the current eruption or a longer-term feature.

Discussion

The key fact about the CO_2 and SO_2 emission rates is that they are generally low. This fact was evident early on and motivated our hypothesis that the CO_2 and SO_2 emissions of the 2004–5 eruption were derived from source dacite depleted in excess (that is, exsolved) volatiles at depth (Gerlach and others, 2005), herein termed "flat" magma. The corollary hypothesis—that gas emissions from flat dacite are expressly vulnerable to scrubbing, particularly during the unrest and early stages of the eruption—follows from the depletion in excess volatiles. The flat magma and gas scrubbing hypotheses underlie much of the discussion that follows.

Comparisons with 1980s Emission Rates

Comparisons of the 1980s and 2004–5 passive emission rates of SO_2 and CO_2 support the interpretation that the current eruption involves flat magma, possibly left over in the reservoir since the last lava-dome eruption in 1986. The 2004–5 SO_2 emission rates (fig. 7; table 2) are not significantly different from 1980s SO_2 emission rates during the period from October 18, 1980, to December 9, 1986 (fig. 16), according to the MWRST ($P \geq 0.05$). This time interval matches closely

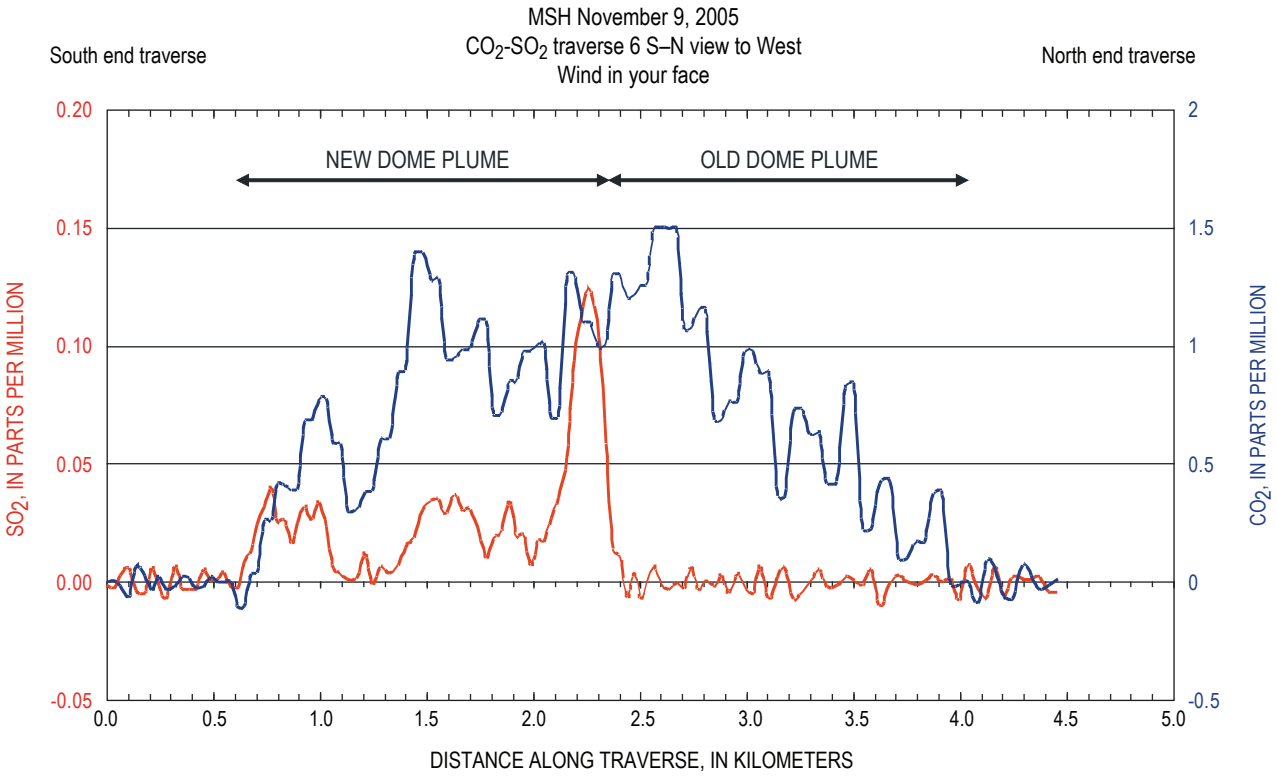

Figure 14. Airborne traverse of plume on November 9, 2005, showing above-background CO_2 concentration (blue) and SO_2 concentration (red). Wind direction from nearly due west allows comparison of plume data from the new dome complex with the older 1980–1986 dome. Traverse flown approximately 2.3 km downwind of central source area. The older dome is discharging CO_2 but little or no SO_2.

the period of 17 lava-dome eruptions and stable dome growth that produced the 1980s dome. October 18, 1980, is the date of the first SO_2 emission-rate measurement after the start of a lava-dome eruption on October 16, 1980—the first lava-dome eruption of the 1980s to produce a dome that survived. The last lava-dome eruption of the 1980s was on October 21, 1986, and the last significant SO_2 emission rate at the end of this eruption was 80 t/d on December 9, 1986. Of the 113 SO_2 emission-rate measurements made after this date, until measurements ceased on September 6, 1988, 95 percent were <25 t/d and 70 percent were <3 t/d—barely above detection limits. We did not include these data in the MWRST analysis in order to avoid confounding the emission rates associated with the 1980s lava-dome eruptions with emission rates of the protracted period of residual degassing at the end of the 1980s eruption cycle. The1980s dataset for the calculations started with the data from December 9, 1986, and was extended back in time by incrementally adding earlier SO_2 emission rates. Along this time line, the probability level decreased steadily from P >0.05 and converged on the critical significance level (P = 0.05) when the October 18, 1980, data were added to the dataset. When still earlier 1980 data were included, P dropped abruptly below 0.05, indicating that the difference between the two groups of data became robustly significant. Thus, between October 18, 1980, and December 9, 1986, the two groups of data sample a similar population, and the differences between them—for example, median SO_2 emission rates of 72 t/d versus 100 t/d—can be explained by random sampling variations. However, we stress that the MWRST analysis operates only on the rates of the two groups of data without regard for the associated dates. This is important because if the dates are considered, it is evident that although the 10/18/1980–12/9/1986 SO_2 emission rates may share a common population with 2004–5 SO_2 emission rates, they are not randomly distributed in time, as indicated by the conspicuous skewing of their higher rates to earlier dates (fig. 16).

Plotting the SO_2 emission rates of the 1980s and 2004–5 together as time series on the same scale reveals that the emission rates of the 2004–5 eruption appear similar to those of the 1980s lava-dome eruptions back to at least late 1981 (fig. 16). MWRST comparisons back to late 1981 produce large P values indicating virtually no likelihood of a significant difference in the SO_2 emission rates of the 1980s and 2004–5 lava-dome eruptions; for example, comparisons back to October 1, 1981, give a P value of 0.7. Such differences as exist in the patterns of the two time-series plots are readily explained. The generally lower peak values of the 2004–5 eruption probably are related to the more-crystalline magma and steadier character of the present eruption; these properties act to curb extrusive surges that frequently caused SO_2 emission-rate peaks during the 1980s lava-dome eruptions. The 2004–5 emission rates appear blockier and less spiky on the graph, partly because of the steadier nature of the present eruption, but also because the steadier activity itself (along with tighter funding) led to less frequent monitoring flights—four to five times less frequent than in the 1980s. The fact that the current eruption has lasted considerably longer than the 1980s lava-dome eruptions also contributes to the blockier pattern of its SO_2 emission rates. The annualized 2004–5 SO_2 outputs also bear a noteworthy similarity to annual SO_2 outputs that occurred during the later years of the 1980s lava-dome eruptions. The 14-month, 30,000-t SO_2 output of the 2004–5 eruption (table 2) indicates an annualized output of 26,000 t, which is equivalent to the total Mount St. Helens SO_2 output for 1984 (Gerlach and McGee, 1994)—a year in which there were three lava-dome eruptions over a 6-month period. The 11-month output for 2005 of 18,000 t (computed from table 2 data) annualizes to an output of 19,600 t—comparable with the 1986 SO_2 output of 17,000 t (Gerlach and McGee, 1994). Thus, the MWRST analyses, the time-series patterns of SO_2 emission rates, and the annualized SO_2 outputs strongly suggest that the 2004–5 SO_2 emissions are similar to those of the 1980s lava-dome eruptions, possibly back as far as late 1981 or late 1980.

The CO_2 emission-rate measurements of the 1980s are restricted to the period between July 1980 and August 1981 (fig. 17; McGee and Casadevall, 1994); the measurements were terminated after August 1981 because the detection limit of the older measurement technique was reached. Applications of the MWRST to these data and the 2004–5 CO_2 emission-rate data (fig. 7, table 2), following the procedure described

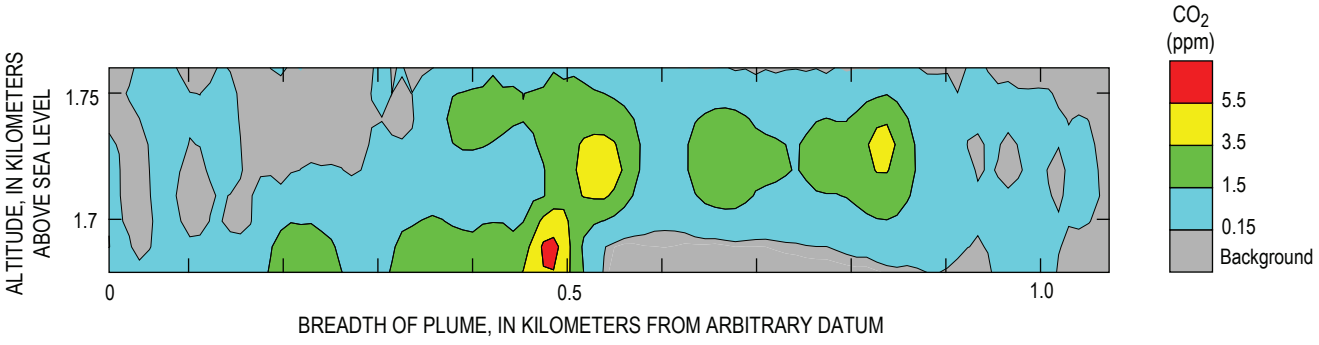

Figure 15. Vertical cross section of CO_2 gas plume 250 m downwind of Loowit springs area on June 9, 2005. The CO_2 emission rate computed from these data was 27 t/d. Scale bar on right shows CO_2 concentration above local atmospheric background.

above for comparing SO_2 emission rates, indicates that the 2004–5 data are significantly different from the July 1980–May 1981 data ($P \leq 0.05$). However, the 2004–5 data and the June–August 1981 data are not different and appear to be sampling the same population ($P > 0.05$). The similarity probably would have persisted beyond August 1981 had measurements been made by a more sensitive technique. Plotting the CO_2 emission rates of 1980–81 and 2004–5 together as time series on the same scale reinforces the MWRST analysis by revealing a pattern in which the latter CO_2 emission rates appear as an extension of the lower CO_2 emission rates of June–August 1981 (fig. 17). As in the case of the SO_2 emission rates, differences in magma physical properties and frequency of measurement account for the blockier, less spiky, and generally lower peak values of the 2004–5 CO_2 emission rates.

Thus, the time-series comparisons and MWRST results for CO_2 and SO_2 emission rates support a flat 2004–5 magma depleted in excess volatiles and producing generally low CO_2 and SO_2 emissions like those of the 1980s lava-dome eruptions. The flat magma is distinctly different from the gas-rich magma that produced the much higher CO_2 and SO_2 emissions earlier in 1980 (figs. 16, 17; Gerlach and McGee, 1994). The similarity to the gas emissions of the 1980s lava-dome eruptions suggests that the flat magma of the current eruption could involve leftover reservoir magma from 1986.

Comparison with 1980s CO_2/SO_2 Ratios

Contemporaneous measurements of CO_2 and SO_2 emission rates in the 1980s allow calculation of CO_2/SO_2 ratios on 117 days during a 418-day period from July 6, 1980, to August 28, 1981. The median CO_2/SO_2 ratio is 8, but there is considerable variation—25 percent of the ratios are ≤5 and 25 percent are ≥11. As noted earlier, measured and weighted CO_2 and SO_2 emission rates and total emissions of the current eruption imply a somewhat higher grand median CO_2/SO_2 ratio of 11±1. The MWRST indicates that the 117 1980–1981 CO_2/SO_2 ratios and the 24 2004–5 CO_2/SO_2 ratios—whether calculated from measured or weighted emission rates—are associated with significantly different populations ($P < 0.05$). Taking these results at face value would imply a real difference in CO_2/SO_2 ratios of the older and current gases, but we show below that the higher CO_2/SO_2 ratios of the current gases are caused by scrubbing.

Scrubbing in the 2004–2005 Eruption

Doukas and Gerlach (1995) drew attention to the unusually weak SO_2 emission rates that both preceded and followed eruptions at Crater Peak on Mount Spurr volcano, Alaska, in 1992 and noted the exceptionally strong and persistent H_2S odor in the Crater Peak plume during repose periods. They argued that liquid water present at or beneath the surface interacted with ascending magmatic gases, scrubbing SO_2 and other strongly acidic gases (HCl, HF) but impacting the weakly and moderately acidic gases (CO_2 and H_2S) less severely. The principal mechanisms for SO_2 scrubbing by liquid water are the hydrolysis reactions:

$$4SO_{2(g)} + 4H_2O_{(l)} = H_2S_{(g)} + 6H^+_{(aq)} + 3SO_4^{-2}{}_{(aq)}, \text{ and}$$

$$3SO_{2(g)} + 2H_2O_{(l)} = S_{(l,s)} + 4H^+_{(aq)} + 2SO_4^{-2}{}_{(aq)}.$$

These equilibria shift strongly to the right below 400°C, mainly converting SO_2 into dissolved sulfate as sulfuric acid. Some H_2S gas and native sulfur also are generated, which explained the intense H_2S odor at Crater Peak. Detailed thermochemical modeling (Symonds and others, 2001) confirms the significant scrubbing of magmatic SO_2, HCl, and HF by contact with surface, ground, and hydrothermal waters of volcanoes and indicates that scrubbing of CO_2 and H_2S also becomes significant at low gas-to-water ratios (<0.01, mass basis).

Carbon isotopes of dissolved inorganic carbon in hydrothermal, ground, spring, and stream waters reveal the scrubbing of magmatic CO_2 in the vicinity of several Cascade Range volcanoes: Lassen Peak, Mount Shasta, Crater Lake, Mount Bachelor, Broken Top, Three Sisters, Belknap Crater, and Mount Jefferson (Rose and Davisson, 1996; James and others, 1999; Evans and others, 2004). Scrubbing of potentially coexisting, more acidic magmatic gases (SO_2, H_2S, HCl, and HF) also probably occurs. Copious ground-water recharge in the High Cascades and subsequent downward and lateral flow (Ingebritsen and others, 1989, 1992, 1994) is probably chiefly responsible for the scrubbing and provides a basis for a conceptual model of scrubbing throughout much of the Cascade Range. Scrubbing processes may, therefore, be responsible for the currently absent to negligible emission rates of CO_2, SO_2, and H_2S at several Cascade Range volcanoes we have investigated with airborne measurements since the late 1990s (table 1). Although some of these volcanoes (for example, Mount Adams and Mount Jefferson) may simply be dormant, it is likely that much of the CO_2, SO_2, H_2S, HCl, and HF degassed from magmas at most of these volcanoes is captured by hydrothermal systems or ground water and is thus unavailable to form gas emissions at volcanic centers. Boiling of hydrothermal fluid containing captured magmatic gases may give rise to persistent degassing of CO_2 and H_2S (but not SO_2 because of hydrolysis to dissolved sulfate) at some volcanoes—Mount Baker and Lassen Peak being likely examples (table 1).

Symonds and others (2001) applied their thermochemical scrubbing models to several eruptions, including the 1980 eruption of Mount St. Helens, which they say illustrates SO_2 scrubbing in the early stage of an eruption. Low SO_2 emission rates—from less than 10 t/d to 48 t/d—during the period of phreatic eruptions and nonexplosive degassing that began on March 27, 1980, continued for 52 days up to the May 18 climactic explosion. Observations supporting early scrubbing of SO_2 include reports by COSPEC investigators of persistent H_2S odor in the crater at times when SO_2 emissions rarely exceeded 10 t/d (Stoiber and others, 1980). Emission rates of

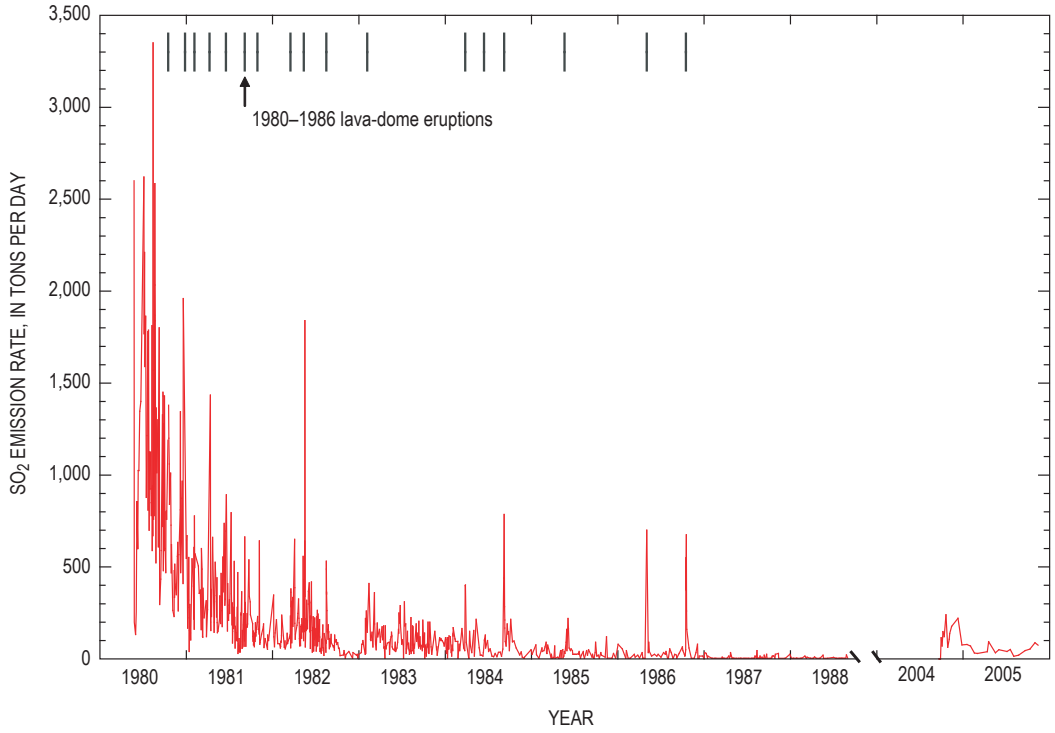

Figure 16. Time-series plots of all SO_2 emission rates measured during the 1980s (McGee and Casadevall, 1994) and during the 2004–2005 eruption. Scale break after last 1980s measurements in 1988 separates the two time series. Vertical lines indicate the starting dates of the 1980–1986 lava-dome eruptions. All 1980s and 2004–2005 time-series data are passive emission rates, except for the first 1980 data point—2,600 t/d measured in the May 25, 1980, explosive eruption. The May 18, 1980, explosive emission rate of 4,000,000 t/d is not included (Gerlach and McGee, 1994; Symonds and others, 2001).

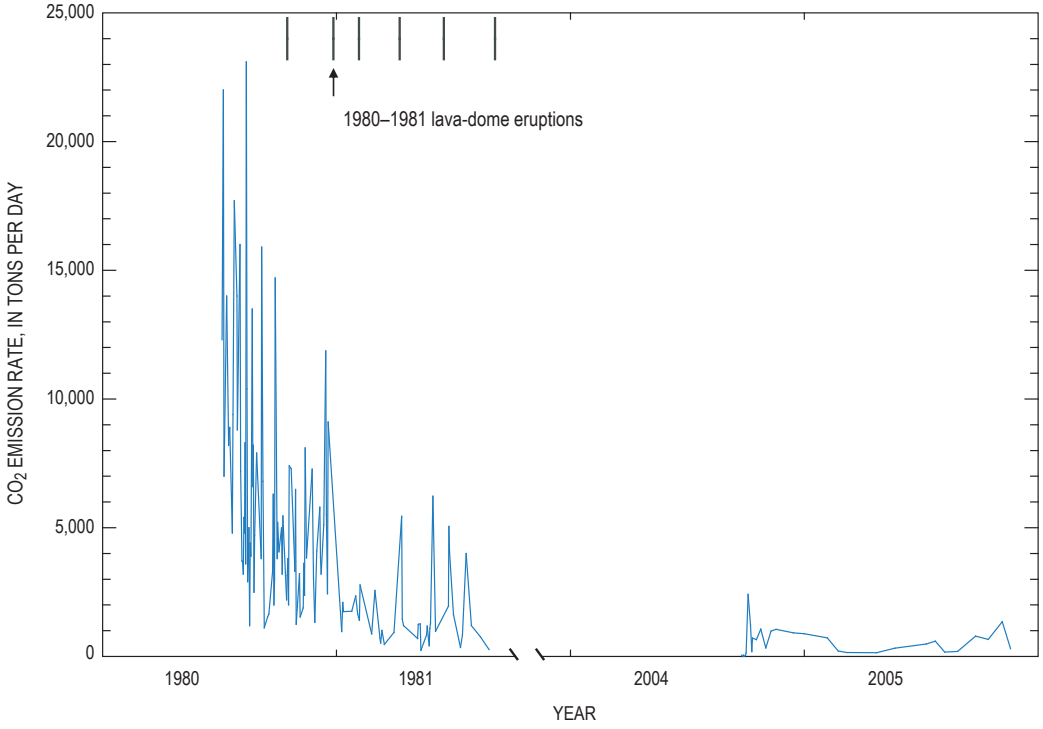

Figure 17. Time-series plots of all CO_2 emission rates measured during the 1980s (McGee and Casadevall, 1994) and during the 2004–2005 eruption. Scale break after the last measurements in 1981 separates the two time series. Vertical lines indicate starting dates of the 1980–1981 lava-dome eruptions. All 1980s and 2004–2005 time-series data are passive emission rates. The 1980 data begin with the 12,300 t/d CO_2 emission rate measured on July 6.

passively degassed SO_2 increased after the May 18 eruption and after the second explosion on May 25 but still remained relatively low (130–260 t/d). Twenty days later, on June 6, SO_2 emission rates jumped to 860 t/d and remained high (>600 t/d) until the end of October 1980 (fig. 16), finally attaining levels comparable to those of other erupting arc volcanoes and signaling the end of significant scrubbing. Note that the July 6, 1980, to August 28, 1981, CO_2/SO_2 ratios discussed above represent postscrubbing values.

Symonds and others (2001) also inferred that SO_2 scrubbing was active again during the period of seismic unrest at Mount St. Helens in the summer of 1998 when, as described above, an airborne survey on June 22 measured a CO_2 emission rate of 1,900 t/d (table 1), while concurrent COSPEC measurements failed to detect SO_2. These results are consistent with the degassing and scrubbing of SO_2 from an intrusion at a time when melting of snow from a permanent snowfield growing in the crater since 1986 (Anderson and others, 1998) helped create a wet edifice. Thus, an unknown amount of degassed CO_2 may also have been scrubbed at this time.

Scrubbing played a major role in the period of unrest and the early stages of the current eruption. We interpret the measurements during the September 27–30, 2004, period of insignificant gas emission with little or no detectable SO_2 or H_2S and with CO_2 largely at atmospheric levels (fig. 9) to be the result of fairly complete gas scrubbing at low gas-to-water mass ratios <0.01 (Symonds and others, 2001). Sealing of rock permeability in the old dome and the upper part of the 1980s conduit may also have played a role (Moran, 1994). It is likely, however, that scrubbing would soon have dominated sealing as a deterrent to gas emission. The concurrent shallow seismicity and deformation would tend to reestablish permeability. High seismicity was well established by September 26 and increased significantly on September 28 at shallow levels in and below the old lava dome (Moran and others, this volume, chap. 2). Radial fractures were visible in Crater Glacier adjacent to the old dome by September 26, and an area of deformation south of the dome was clearly evident on oblique photos on September 30 (Schilling and others, this volume, chap. 8). Furthermore, the 2004 unrest and eruption followed a period with an unusually large potential for ground-water recharge by surface water. No August–September interval since the cessation of dome-building eruptions in 1986 has had heavier rainfall than in 2004 (http://www.wcc.nrcs.usda.gov/snotel, last accessed March 15, 2008). The growth of Crater Glacier since 1986 provided increased storage of water available for release and ground-water recharge into late summer. Moreover, the earlier detection of sharp CO_2 concentration spikes on October 1 and 2, while SO_2 and H_2S remained at detection limits (fig. 10), strongly suggests scrubbing, rather than sealing, as the main cause restricting earlier gas emissions, since water does not scrub CO_2 as effectively as it scrubs SO_2 and H_2S. The subsequent appearance of wet degassing with large gas bubbles ejecting through pools of water obviously involved scrubbing. However, the subequal concentrations of SO_2 and H_2S at this time (fig. 11) reflected incomplete scrubbing of SO_2, which is likely because rapid transport in large bubbles restricted its interaction with water, thus allowing some of it to escape the pools. Wet degassing increasingly gave way to dry degassing, and SO_2 became the major sulfur gas (fig. 12). As temperatures rose and steaming increased, rock adjacent to the invading magma progressively dried out in the days before the initial emergence of a lava spine from the deforming area south of the 1980s dome on October 11. This date probably marks the end of significant scrubbing in the early stages of the eruption.

The composite degassing sources from the 1980s and 2004–5 domes bear the mark of gas scrubbing (fig. 14). Nearly all of the SO_2 in the plume comes from the hotter new dome. Degassing from the colder old dome involves minor CO_2 but little or no SO_2. We speculate that the source of gas at depth is the same for both domes but that the gas feeding the vents on the old dome is scrubbed of its SO_2 since water is more likely to be present within and beneath this colder dome. Edmonds and others (this volume, chap. 27) measured several gases, including SO_2 and HCl, in hot vent emissions on the new dome by remote Fourier-transform infrared spectroscopy from high on the east rim of Mount St. Helens. If our hypothesis is correct, both SO_2 and HCl—being strong acids—should be scrubbed in emissions from the old dome. Unfortunately, confirmation of concurrent scrubbing of both SO_2 and HCl at the old dome by similar measurements was not possible, owing to the absence of hot infrared sources.

The 24 CO_2/SO_2 ratios calculated from cumulative CO_2 and SO_2 emissions (fig. 8; table 2) show a striking pattern when plotted as a time series (fig. 18). The ratios decrease regularly and precipitously from October 7 until October 27, 2004, when they make a abrupt transition to nearly constant CO_2/SO_2 values of 9±1, close to the median value of 8 noted above for the 1980–81 CO_2/SO_2. They remain in this range (9±1) until September 28, 2005, after which subsequent 2005 values drift to CO_2/SO_2 values as high as 11.3.

We interpret the sharp decline in CO_2/SO_2 (fig. 18) to reflect the drying out of the shallow conduit and crater-floor rock adjacent to the invading dacite and the reduction of SO_2 scrubbing that dominated the early part of the 2004–5 eruption. However, cumulative emissions, although smoothing out short-term variations, can lag in their response to significant changes. In this case, measurements suggest early SO_2 scrubbing largely ceased on or about October 11, 2004, as discussed above, approximately two weeks before the October 27 date suggested by the cumulative emission data (fig. 18). After October 27, the CO_2/SO_2 ratio of cumulative emissions stabilized within the range of 9±1 for many months, grazing the median 1980–81 CO_2/SO_2 value of 8 (fig. 18). We interpret this range of values to represent the CO_2/SO_2 of nonscrubbed gas emissions of the current eruption, although it may be slightly high because of SO_2 scrubbing of gases from the old dome. The CO_2/SO_2 of the cumulative emissions rises above this range again after September 28, 2005 (fig. 18), presumably in response to renewed scrubbing. Because of the lag effect, the return to scrubbing may have started somewhat earlier. We have no data suggesting

a specific cause of this return to scrubbing, but plausible factors may include the cracking and development of fracture permeability within the cooling and thickening carapace of the new dome and (or) seasonal changes affecting rainfall and groundwater recharge in the crater.

The CO_2/SO_2 time-series pattern in figure 18 illustrates the role of scrubbing in the early part of the current eruption and the close similarity of CO_2/SO_2 values in the nonscrubbed gas emissions of the 2004–5 eruption to those in the early 1980s. We contend, moreover, that scrubbing is the cause of the significant difference in CO_2/SO_2 indicated between the 1980–81 and 2004–5 gases by the MWRST analysis. The striking pattern of CO_2/SO_2 ratios (fig. 18) with their approach to the median 1980–81 CO_2/SO_2 ratio, hardly seems the result of chance, and it is consistent with flat magma remaining from 1986 that, although depleted in excess volatiles, still retains a similar CO_2/SO_2 ratio. However, the depletion of excess volatiles causes the emissions from the flat magma upon ascent and eruption to be generally weak and susceptible to scrubbing if water is present.

Fluid Content of the 2004–2005 Dacite at Depth

Recent studies indicate that the dacite erupted explosively at Mount St. Helens on May 18, 1980, had a fluid content (that is, excess volatiles) prior to ascent and eruption of ≥15 volume percent (vol. percent), which corresponds to ≥3 weight percent (wt. percent) (Wallace, 2001, 2003; P.J. Wallace, written commun., 2005). The May 18, 1980, dacite was decidedly not flat magma. We have tested the flat-magma hypothesis for the 2004–5 dacite by using the current CO_2 emission data to quantify the fluid content of the 2004–5 dacite at depth. If the flat-magma hypothesis is valid for the current dacite, its fluid content at depth should be significantly lower than that determined for the May 18, 1980, dacite.

Fluid Content of the 2004–2005 Dacite and the May 18, 1980, Dacite at 900°C and 220 MPa (8.6 km Depth)

The May 18, 1980, dacite last equilibrated prior to eruption at a temperature of 900°C and a pressure of 220 MPa (Rutherford, 1993), corresponding to 8.6 km depth (from crustal density model B-B' of Williams and others, 1987, used in this study to convert lithostatic pressures to depths beneath the crater). The rhyolitic melt of the May 18 dacite was relatively H_2O rich prior to eruption. Microprobe studies of melt inclusions give water-by-difference concentrations of 4.6±1 wt. percent (Rutherford, 1993), and recent ion-microprobe studies of melt inclusions in the May 18 white pumice show a clustering of H_2O concentrations around 5 wt. percent (Blundy and Cashman, 2005).

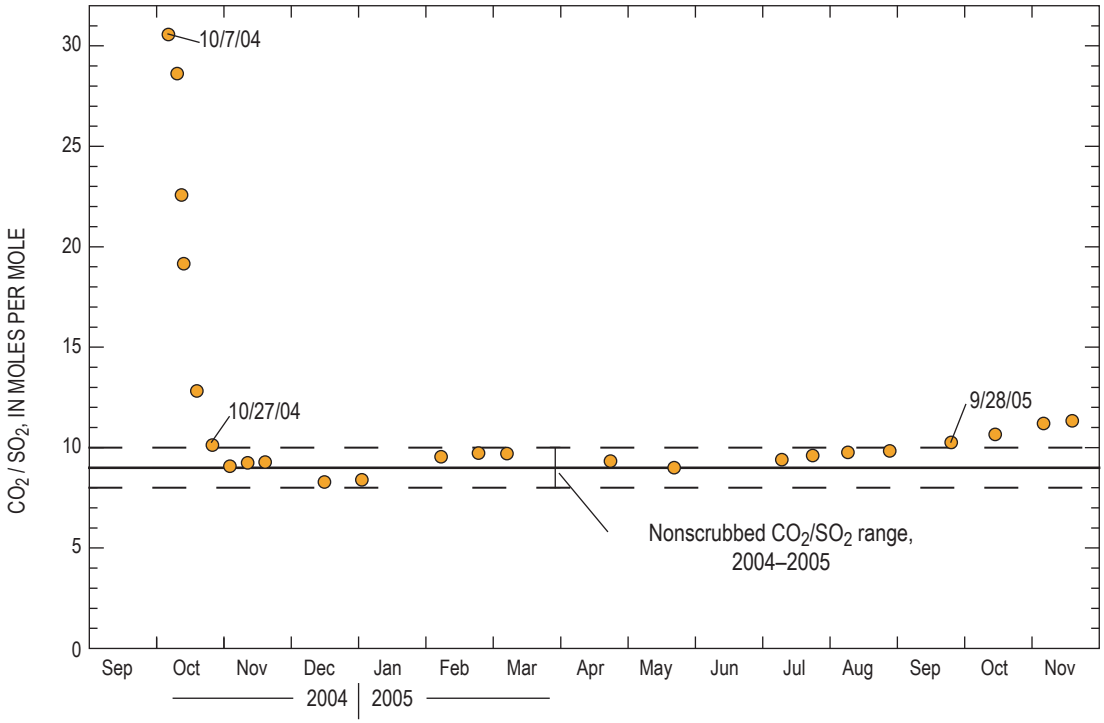

Figure 18. Time-series plot of molar CO_2/SO_2 ratios (dots) calculated from cumulative 2004–2005 emissions (fig. 8; table 2). Solid and dashed lines indicate nonscrubbed CO_2/SO_2 median and range of 9±1 for the 2004–5 gases. Lower dashed line also represents the median value (8) of the 1980–81 CO_2/SO_2 ratios as discussed in the text.

To maintain comparability with the May 18 dacite, we have used the constraints 900°C, 220 MPa, and a rhyolitic melt H_2O concentration of 5 wt. percent to estimate the fluid content of the 2004–5 dacite at 8.6 km depth. Several observations and experimental results support the use of these constraints. The current dacite contains phenocrysts of plagioclase, hypersthene, amphibole, and oxides—the same as the 1980–86 dacite, except for an absence of minor clinopyroxene (Pallister and others, this volume, chap. 30; Rutherford and Devine, this volume, chap. 31). The current dacite also is similar in bulk composition to the 1980–86 dacite, being only slightly more evolved (65 vs. 63 wt. percent SiO_2) and distinct in U-series isotopic ratios of plagioclases (Cooper and Donnelly, this volume, chap. 36) and in bulk-composition ratios of Ti and Cr to SiO_2 (Pallister and others, this volume, chap. 30)—differences that are most readily explained by addition of a minor fraction of new magma to the reservoir between 1986 and 2004 (Pallister and others, this volume, chap. 30). Melt inclusions provide no data on the H_2O concentration of preeruption melt in the current dacite (Pallister and others, this volume, chap. 30; Rutherford and Devine, this volume, chap. 31; Blundy and others, this volume, chap. 33). However, on the basis of phase equilibria experiments, Rutherford and Devine (this volume, chap. 31) propose that the new magma entered the storage reservoir as dacite with a melt concentration >4 wt. percent—implied by the amphiboles—and at a temperature of ~900°C—suggested by high-TiO_2 magnetite phenocrysts and the maximum anorthite content of cyclically zoned feldspar phenocrysts. These conditions are similar to those determined for the 1980 magma. To explain the cyclic zoning of the magma's phenocrysts, Rutherford and Devine invoke convective circulation of injected dacite, which would have involved exposure to pressures of 220 MPa at various times before rising to the shallower part of the reservoir, where they infer it last equilibrated at about 850°C and 120–140 MPa prior to final ascent and eruption.

We used VolatileCalc (Newman and H_2O Lowenstern, 2002) to model CO_2 solubility in hydrous rhyolitic melt at 900°C and 220 MPa to estimate the fluid content of the 2004–5 dacite for comparison with the May 18 dacite at 8.6 km depth. At these conditions, rhyolitic melt with 5 wt. percent H_2O would contain associated dissolved CO_2 at a concentration of ~350 ppm (fig. 19*A*). The mole fraction composition of the coexisting fluid would be ~0.76 for X_{H_2O} and ~0.24 for X_{CO_2} (fig. 19*B*), which is consistent with hydrothermal phase equilibria experiments on the current dacite that indicate X_{H_2O} would be ≥0.7 in the presence of a CO_2-bearing coexisting fluid (Rutherford and Devine, this volume, chap. 31). The fluid also would contain a small amount of sulfur, but since CO_2/SO_2 is ~9 in the nonscrubbed gas emissions—and CO_2/S would likely have been higher in the fluid at elevated pressure—we ignore sulfur in the present analysis.

We calculated the fluid content of the dacite at 8.6 km and the conditions delineated above for 14 dates in 2004–5 corresponding to the dates of digital elevation models (DEMs; Schilling and others, this volume, chap. 8). Table 3 lists values keyed to DEM dates for several parameters (defined in table 3 headnotes) used in the calculations. The last 2005 DEM date (12/15/2005) could not be used because weather conditions prevented measurement of CO_2 emission rates during December 2005, as noted above.

Table 3 contains values for two melt mass parameters: one for dacite like the 2004–5 dacite that contained 53.5 vol. percent melt prior to eruption (Pallister and others, this volume, chap. 30), which we discuss later, and the other for preeruption dacite with 70 vol. percent melt. The 70-vol. percent case for melt masses is based on the groundmass abundances of 65–80 vol. percent reported for the somewhat less evolved May 18, 1980, white pumice (Cashman and Taggert, 1983; Rutherford and others, 1985; Cashman, 1992) and a

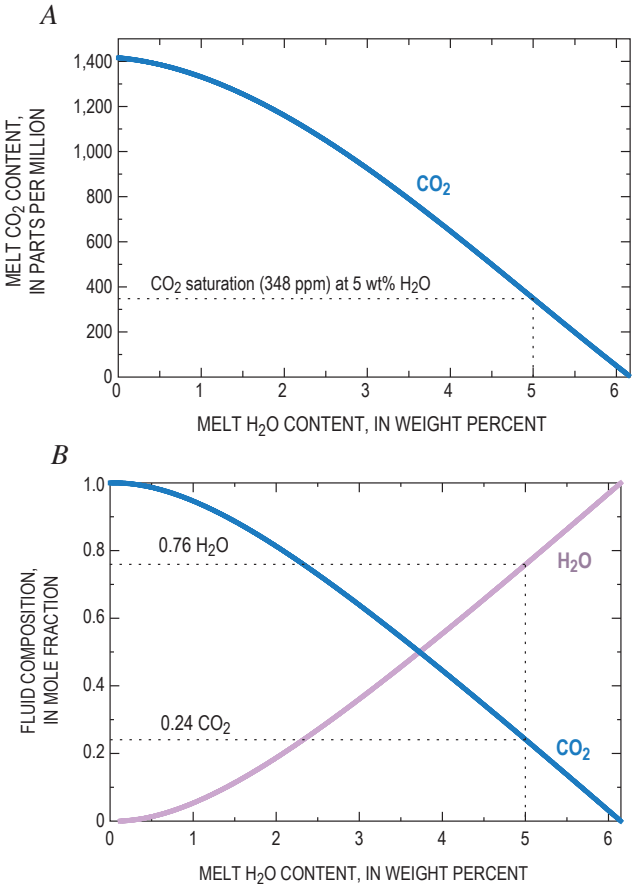

Figure 19. Concentration of CO_2 in hydrous rhyolitic melt and coexisting fluid composition at 220 MPa and 900°C (Newman and Lowenstern, 2002). *A*, Solubility of CO_2 (solid blue curve) in hydrous rhyolitic melts with a range of water concentrations. Dotted lines indicate a CO_2 saturation limit of 348 ppm for rhyolitic melt containing 5 wt. percent H_2O. Melt H_2O content is total H_2O—that is, OH and molecular H_2O. *B*, Mole fraction concentrations of H_2O and CO_2 (solid curves) in fluids coexisting with hydrous rhyolitic melts over a range of water concentrations. Dotted lines indicate fluid composition of 0.76 X_{H_2O} and 0.24 X_{CO_2} coexisting with rhyolitic melt containing 5 wt. percent water.

Table 3. Parameters for calculation of fluid content of the 2004–2005 dacite, Mount St. Helens, Washington.

[Digital elevation model (DEM) dates are the dates of DEMs of Schilling and others (this volume, chap. 8). Dacite volumes are estimated cumulative volumes of the newly extruded lava dome (Schilling and others, this volume, chap. 8). Dense rock equivalent (DRE) volumes are cumulative dacite volumes adjusted for an average porosity of 10 vol. percent (Cashman and others, this volume, chap. 19; Pallister and others, this volume, chap. 30; C. Thornber, written commun., 2006). Dacite masses are cumulative masses in metric tons (t) of dacite derived from the DRE volumes and the dacite DRE density of 2.62 g/cm^3 (K. Russell, written commun., 2006). Melt masses (t) are cumulative masses of melt estimated from DRE volumes and preeruption melt fractions of 53.5 vol. percent and 70 vol. percent, as described in the text. CO_2 masses (t) are cumulative masses of CO_2 output as of each DEM date, calculated from a curve fit to the cumulative CO_2 emissions (fig. 8). Significant figures were exaggerated to reduce roundoff errors.]

DEM date	Dacite volume (10^6 m^3)	DRE volume (10^6 m^3)	Dacite mass (10^6 t)	Melt mass for 53.5 vol. percent melt (10^6 t)	Melt mass for 70 vol. percent melt (10^6 t)	CO_2 mass (t)
11/04/2004	11.8	10.62	27.82	13.07	17.10	23,482
11/20/2004	18.4	16.56	43.39	20.38	26.66	39,380
11/29/2004	21.3	19.17	50.23	23.59	30.86	48,800
12/11/2004	25.5	22.95	60.13	28.24	36.95	61,162
01/03/2005	30.5	27.45	71.92	33.78	44.19	82,459
02/01/2005	35.1	31.59	82.77	38.87	50.86	102,639
02/21/2005	39.2	35.28	92.43	43.41	56.80	112,188
03/10/2005	41.9	37.71	98.80	46.40	60.71	118,092
04/19/2005	47.5	42.75	112.01	52.60	68.83	127,630
06/15/2005	53.9	48.51	127.10	59.69	78.10	141,901
07/14/2005	57.1	51.39	134.64	63.24	82.74	152,123
08/10/2005	61.7	55.53	145.49	68.33	89.40	163,184
09/20/2005	67.3	60.57	158.69	74.53	97.52	182,139
10/24/2005	70.0	63.00	165.06	77.52	101.43	202,885

melt density of 2.3 g/cm^3 reported for experimental investigations of rhyolite densities at elevated temperature and water pressure (Silver and others, 1990). The 70-vol. percent case maintains comparability with 1980 conditions of 900°C, 220 MPa, and rhyolitic melt containing 5 wt. percent dissolved H_2O at 8.6 km depth.

For each DEM date, the amount of dissolved CO_2 was calculated from the concentration of CO_2 in the melt (fig. 19*A*) and the mass of melt for the DEM date (table 3), as estimated from the 70-vol. percent melt fraction discussed above. In all cases, the amount of dissolved CO_2 was a minor fraction (<20 percent) of the cumulative (total) CO_2 output as of the DEM date (table 3), indicating that 2004–5 dacite containing 70 vol. percent rhyolitic melt with 5 wt. percent dissolved H_2O would indeed have been fluid saturated in the magma reservoir at 900°C and 220 MPa (8.6 km depth). We determined the amount of CO_2 in the fluid phase by subtracting the amount of CO_2 dissolved in the melt from the cumulative CO_2 emitted as of the DEM date (table 3). Having determined the amount of fluid CO_2, we calculated the amount of fluid H_2O from the H_2O-CO_2 fluid compositional relation (fig. 19*B*). We converted the amounts of fluid CO_2 and H_2O into a fluid volume by assuming ideal mixing and by using the modified Redlich-Kwong (MRK) equation of state (Holloway, 1977, 1981) to calculate molar volumes of CO_2 and H_2O at 900°C and 220 MPa. The volume of fluid and the DEM-based dacite volume (table 3), corrected to dense rock equivalent (DRE) basis (table 3), gave the fluid content as a volume percent of the dacite. The dacite masses (table 3) and the amounts of fluid CO_2 and H_2O also allowed expression of the fluid content as a weight percent of the dacite.

Figure 20 shows the fluid content of the dacite for the 14 DEM dates at 900°C and 220 MPa (8.6 km depth). The results, ranging from 0.82 to 1.32 vol. percent (0.15–0.24 wt. percent), indicate steady fluid content for the dacite at 8.6 km depth after a brief period of regularly increasing values involving the points for the first four DEM dates (November–December 2004). Steady fluid content begins with the January 3, 2005, DEM date and continues thereafter; it ranges from 1.16 to 1.32 vol. percent (0.21–0.24 wt. percent) and averages 1.23 vol. percent (0.22 wt. percent). These results are consistent with those of Mastin and others (this volume, chap. 22), who also inferred a low reservoir fluid content of <1.5 vol. percent from the relation between erupted-dacite volume and the volume shrinkage of the reservoir obtained from geodetic data (Lisowski and others, this volume, chap. 15).

It is noteworthy that the results are steady throughout 2005 despite the disparate datasets involved. Several factors may be at work during the brief period involving the four points of lower but steadily rising fluid content during November–December 2004 (fig. 20). These factors probably reflect the declining influence with time of CO_2 lost in scrubbing prior to November 2004 (or missed if airborne measurements were too infrequent) on the cumulative CO_2 output. Increasing the cumulative CO_2 outputs by 38 percent (11/4/2004) to 15 percent (12/11/2004) would bring the four points into the steady range of values. Alternatively, the lower fluid content may reflect a higher porosity of the earlier dacite—somewhere in the range 11–32 vol. percent (K. Russell, written commun., 2006)—compared to the eruption average of 10 vol. percent (table 3) used in the calculations, although there is presently no evidence that porosity declined in a steady way early in the eruption. A higher porosity decreases the DRE volume and mass of dacite in proportion to the cumulative amount of CO_2 and causes the volume percent fluid for the four 2004 DEM dates to increase—porosities of 35 vol. percent (11/4/2004) to 22 vol. percent (12/11/2004) would cause the fluid content of these dates to fall within the range of steady 2005 results. Involvement of shallower, more degassed magma early in the eruption might also account for the lower 2004 fluid content, but it is not obvious from the CO_2 emissions that the earlier magma was more degassed (figs. 7, 17). Lastly, the procedures used to estimate dacite volumes from DEMs may overestimate the smaller dacite volumes of the eruption-startup period, causing erroneously low calculated fluid content. Significant underestimation of early dacite volumes seems more likely, however, because of unaccounted for dacite residing in the conduit. Apparently, the volume of conduit dacite became a negligible fraction of the measurable dacite volume fairly early—sometime prior to the first DEM on 11/4/2004 (table 3).

The sensitivity of the modeling to the volume percent melt-fraction parameter is an important concern that is easily addressed. Recalculating the model for a melt fraction of 53.5 vol. percent (table 3), compared to the 70-vol. percent melt fraction used above, illustrates the low sensitivity of the results to a plausible range of values for the volume percent melt parameter. The resulting steady 2005 fluid content ranges from 1.23 to 1.39 vol. percent and averages 1.29 vol. percent—hardly different from the above results for 70 vol. percent melt.

Recently, Liu and others (2005) derived a new empirical model of CO_2 and H_2O solubility in fluid-saturated rhyolitic melt and recommended it over VolatileCalc (Newman and Lowenstern, 2002) for eruptive degassing and magma-chamber dynamics calculations because it gives better fits to experimental solubility data, especially at pressures above 200 MPa. At the conditions considered here, though, the two models agree closely on the dacite fluid content. For example, during the period of steady 2005 DEM dates, the model of Liu and others (2005) gives 1.17–1.33 vol. percent and a 1.24-vol. percent average versus 1.16–1.32 vol. percent and a 1.23-vol. percent average by VolatileCalc. The agreement becomes virtually exact in calculations at the lower pressures considered below. For these reasons, and because of VolatileCalc's user-friendly software, we have used it throughout this study.

We conclude that the average steady 2005 fluid content of 1.23 vol. percent (0.22 wt. percent; fig. 20) is the best estimate of the fluid content of the current dacite at a reservoir depth of 8.6 km, 900°C, and 220 MPa. This result and, indeed, all the results obtained above are significantly less than the ≥15-vol. percent (≥3 wt. percent) fluid determined for the May 18 dac-

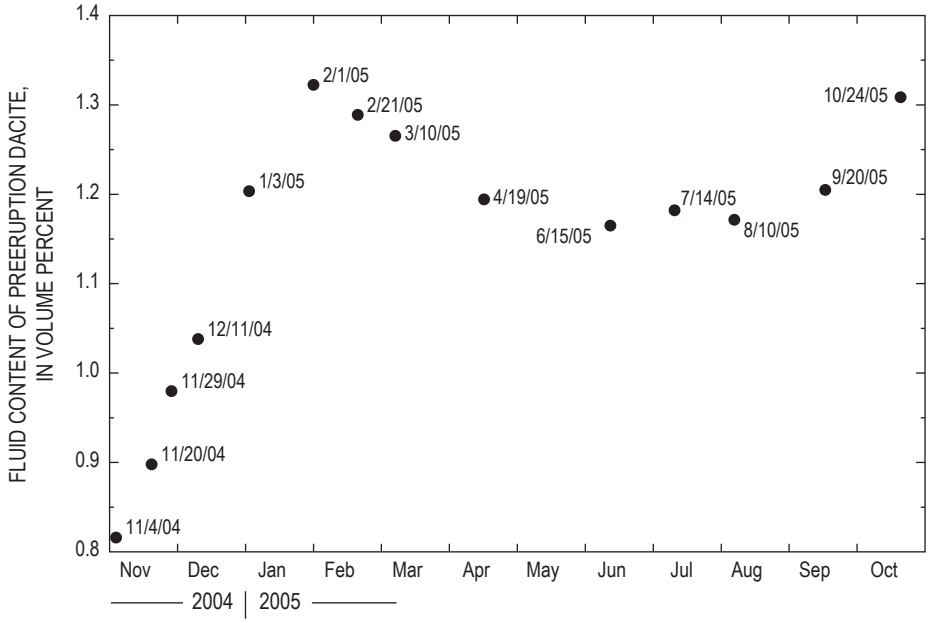

Figure 20. Fluid content of dacite at 900°C and 220 MPa (8.6 km) calculated as described in the text for 14 DEM dates in 2004–5.

ite; furthermore, they are much less than the 5–30-vol. percent (1–6 wt. percent) fluid indicated for several other explosive eruptions of silicic and intermediate magma (Wallace, 2001, 2003). The present analysis, therefore, indicates depletion of excess volatiles and thus confirms the flat-magma hypothesis for the dacite of the 2004–5 eruption.

Fluid Content of the 2004–2005 Dacite Prior to Ascent at 850°C and 130 MPa (5.2 km Depth)

As the dacite migrates to reservoir depths shallower than 8.6 km, its fluid content increases. Of particular interest is the fluid content where the dacite last equilibrated at about 850°C and 120–140 MPa in the presence of an H_2O-rich fluid ($X_{H_2O} \approx 1$) prior to ascent and eruption (Rutherford and Devine, this volume, chap. 31). The corresponding depth range of 4.8–5.6 km (Williams and others, 1987) places the preeruption dacite in the shallowest part of the ellipsoidal-cylindrical magma reservoir extending from 4.5–5 km to ≥12 km, as indicated by deformation data from the current eruption (Lisowski and others, this volume, chap. 15). The average volume percent groundmass of the 2004–5 dacite is 53.5 (Pallister and others, this volume, chap. 30; Rutherford and Devine, this volume, chap. 31). As such, it is a reasonable approximation of the rhyolitic melt fraction of the current dacite before its ascent and eruption from a shallow reservoir depth of 5.2 km (130 MPa)—the median of the 4.8–5.6-km depth range (120–140 MPa) where the dacite last equilibrated. This is the basis for the melt mass case corresponding to a melt fraction of 53.5 vol. percent in table 3. Accordingly, we have taken our results for all DEM dates obtained above (fig. 20) for dacite containing 70 vol. percent melt at 900°C, 220 MPa, and 8.6 km depth and repartitioned CO_2 and H_2O from melt to fluid to obtain a dacite with 53.5 vol. percent melt. To bring this dacite to the last equilibrium conditions within the shallow reservoir at 5.2 km (assuming a closed system), we used VolatileCalc to find the dissolved melt H_2O and CO_2 concentrations at 850°C and 130 MPa (fig. 21*A*) that—after further adjusting of H_2O and CO_2 partitioning between fluid and the 53.5-vol. percent melt phase—gave a fluid composition consistent with the X_{H_2O} and X_{CO_2} predicted by the model (fig. 21*B*). This iterative process consistently gave a melt H_2O concentration of ~4.4 wt. percent and an associated melt CO_2 concentration of ~37 ppm (fig. 21*A*) for each DEM date. The coexisting fluid composition is X_{H_2O} = ~0.96 and X_{CO_2} = ~0.04 (fig. 21*B*), consistent with experimental results of Rutherford and Devine (this volume, chap. 31) that indicate the X_{H_2O} of coexisting fluid would be close to 1.0 in the shallower part of the reservoir. These results also constrain the bulk dacite concentrations of CO_2 and H_2O—that is, fluid plus melt amounts of CO_2 and H_2O as mass fractions of the dacite—at average values of 1,167 ppm and 3.1 wt. percent, respectively, for the ten 2005 DEM dates. The corresponding average bulk dacite S concentration calculated from the cumulative SO_2 emissions (fig. 8; table 2) is 90 ppm for the 10 DEM dates.

The fluid content results for all the DEM dates range from 10.11 to 10.85 vol. percent (fig. 22); again, there is a tight grouping of steady fluid content for the ten 2005 DEM dates—10.63 to 10.85 vol. percent with an average 10.72 vol. percent. The large increase in the average volume percent fluid content from 1.23 to 10.72 vol. percent in going from 8.6 km to 5.2 km depth reflects the crystallization of melt (from 70 vol. percent melt to 53.5 vol. percent melt) and the decreased solubility of H_2O and CO_2 in rhyolite melt at lower pressure; it also includes the effect of fluid expansion as the pressure drops from 220 MPa to 130 MPa. The fluid expansion factor confounds comparisons of fluid content of magmas from different depths. This confusion is avoided by using mass units, which do

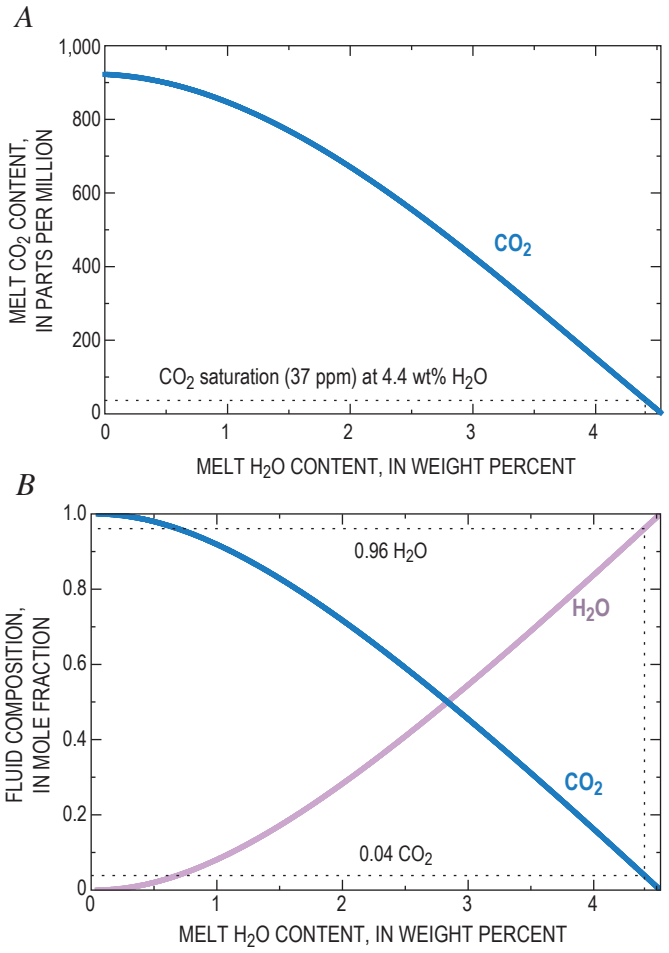

Figure 21. Concentration of CO_2 in hydrous rhyolitic melt and coexisting fluid composition at 130 MPa and 850°C (Newman and Lowenstern, 2002). *A*, Solubility of CO_2 (solid blue curve) in hydrous rhyolite melt with a range of water concentrations. Dotted lines indicate a CO_2 saturation limit of 37 ppm for rhyolitic melt containing 4.4 wt. percent H_2O. Melt H_2O content is total H_2O—that is, OH and molecular H_2O. *B*, Mole fraction concentrations of H_2O and CO_2 (solid curves) in fluids coexisting with hydrous rhyolitic melts over a range of water concentrations. Dotted lines indicate fluid composition of 0.96 X_{H_2O} and 0.04 X_{CO_2} coexisting with rhyolitic melt containing 4.4 wt. percent water.

not reflect fluid expansion; in the present case, the steady fluid content at 5.2 km depth ranges from 1.22 to 1.25 wt. percent and averages 1.23 wt. percent. Despite the relatively shallow depth, these results are still significantly smaller than Wallace's ≥3 wt. percent fluid content for the May 18 dacite at 8.6 km depth and on the low end of his 1–6 wt. percent range for deeper intermediate to silicic magmas involved in explosive volcanism (Wallace, 2001, 2003). These results further confirm the flat-magma hypothesis for the 2004–5 dacite.

We have assumed closed-system degassing with respect to the excess-volatile fluid phase's mobility in magma at depth. The steady excess-volatile fluid content of ~1.23 wt. percent calculated for the dacite at 5.2 km throughout 2005 is consistent with this assumption. Equilibrium (^{210}Pb)/(^{226}Ra) values reported for dacite erupted in 2004–5 (Reagan and others, this volume, chap. 37) also support closed-system degassing. Unlike those of the 1980 lava and tephra (Berlo and others, 2004), (^{210}Pb)/(^{226}Ra) values of the 2004–5 dacite were not affected by continuous open flow of fluid carrying ^{222}Rn from depth in sufficient amount or for sufficient duration to disturb secular equilibrium and generate ^{210}Pb deficits or excesses (Reagan and others, this volume, chap. 37); in our view, this reflects the depletion of excess volatiles compared to 1980 dacite. However, to explain the Li enrichment unique to plagioclase phenocrysts of the October 2004 dacite, Kent and others (2007) propose preferential partitioning of Li from deep melt into aqueous fluid migrating to the uppermost part of the magma chamber at 4.5 km, about 1 year before eruption; they argue that at this depth, which corresponds to 110 MPa (Williams and others, 1987), the fluid unmixed into a low-density vapor and a Li-rich brine that fostered the enrichment of Li in what became the October 2004 dacite's plagioclase phenocrysts. We suggest that Li in the dacite magma is partitioned preferentially into the accompanying excess-volatile fluid and that the Li-enriched plagioclase phenocrysts resulted when that fluid unmixed a Li-rich brine as the dacite ascended from 5.2 km to 4.5 km, where the magma stalled for several months before final ascent to the surface at the start of the eruption.

Ascent Degassing

We carried out calculations like those described above for the current dacite to model its closed-system degassing at 850°C during ascent from shallow reservoir depths. The calculations began at 5.2 km (130 MPa) and terminated at 0.47–0.95 km (10–20 MPa) where melt of the 1980s lava-dome eruptions crystallized extensively to groundmass (Blundy and Cashman, 2001). Figure 23 shows the fluid content, fluid composition, and melt H_2O and CO_2 concentrations of the dacite with ascent depth. We evaluated these variables for all DEM dates at each pressure of calculation and then correlated results to appropriate depths (Williams and others, 1987). The curves of figure 23 employ the average values of the ten 2005 DEM dates, which agreed within 5 percent.

Figure 23*A* shows the fluid content of the 2004–5 dacite during ascent; the fluid content of current dacite at 8.6 km and that of the May 18, 1980, dacite (Wallace, 2003) are included for comparison. The fluid content of the ascending 2004–5 dacite ranges from 10.7 vol. percent at the last equili-

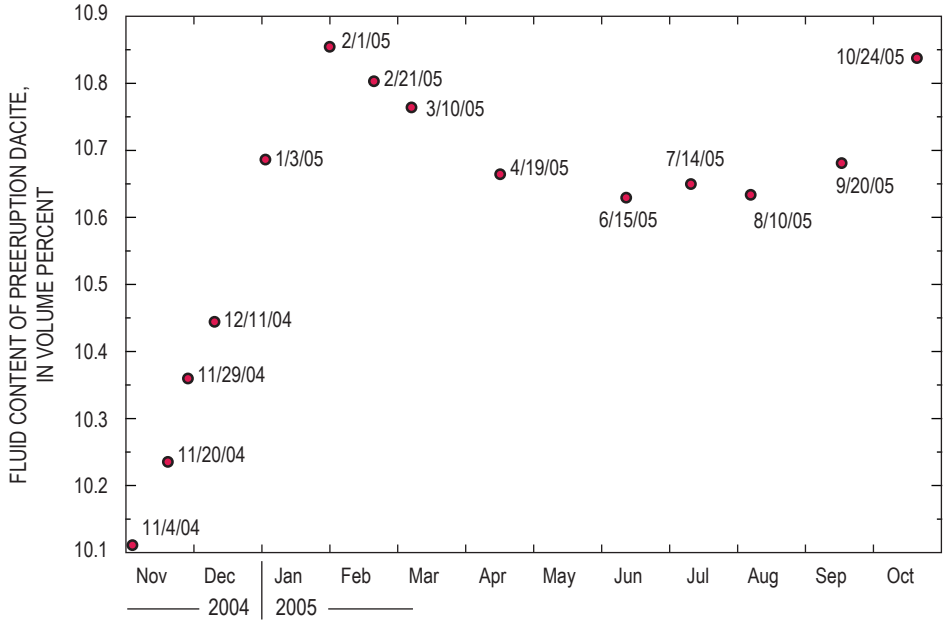

Figure 22. Fluid content of dacite at 850°C and 130 MPa (5.2 km) calculated as described in the text for 14 DEM dates in 2004–5.

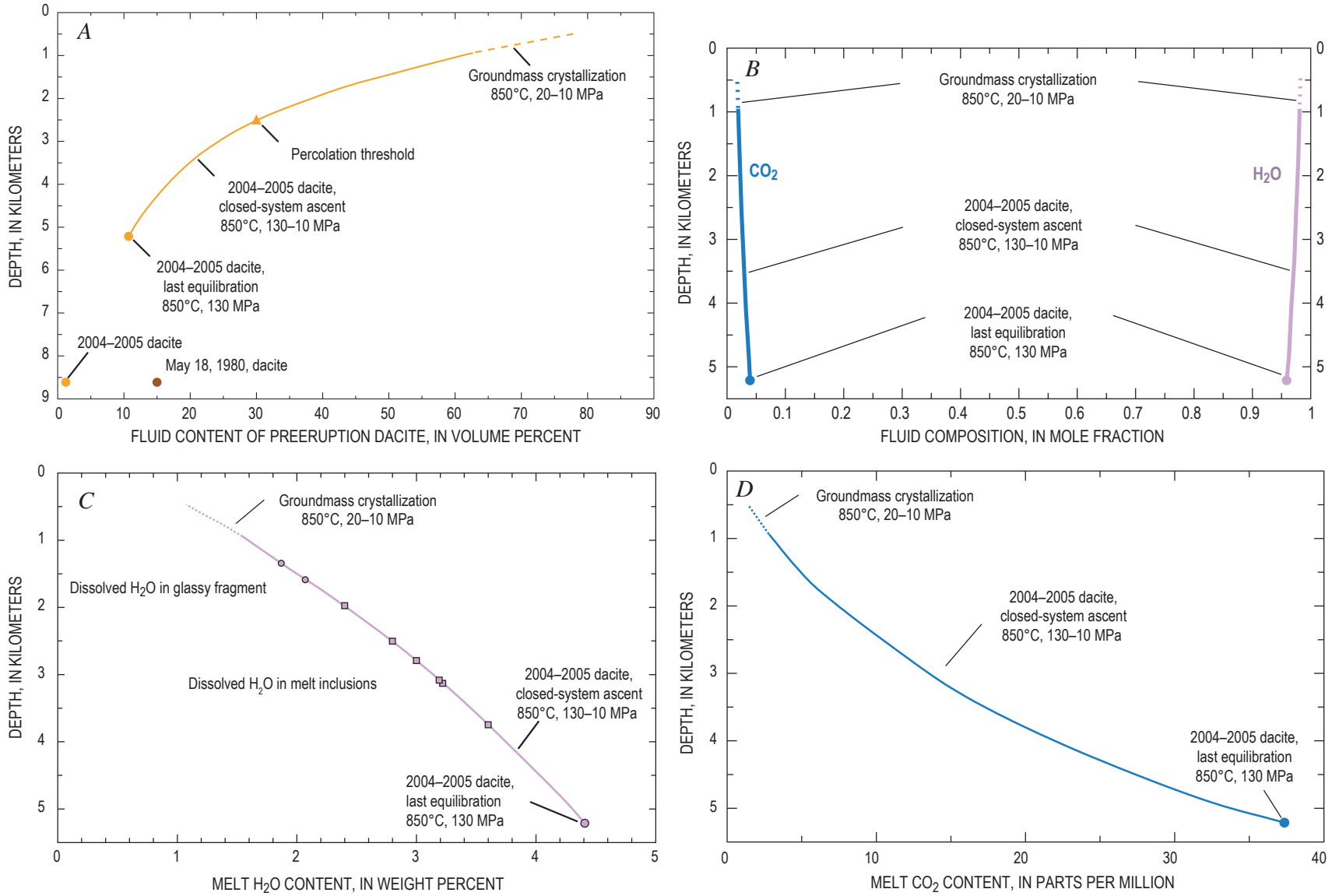

Figure 23. Closed-system ascent of 2004–2005 dacite from 5.2-km depth of last equilibration at 850°C and 130 MPa before eruption (Rutherford and Devine, this volume, chap. 31) to 0.47–0.95-km depth range of groundmass crystallization at 10–20 MPa (Blundy and Cashman, 2001). *A*, Fluid content (exolved fluid phase) of 2004–2005 dacite during ascent, and fluid content of 2004–2005 dacite and May 18, 1980, dacite (Wallace, 2003) at 8.6 km as discussed in the text. *B*, H_2O-CO_2 fluid composition of 2004–2005 dacite during ascent. *C*, Dissolved H_2O in melt of 2004–2005 dacite during ascent; dissolved H_2O in six melt inclusions (filled squares) with highest observed H_2O concentrations (Pallister and others, this volume, chap. 30; Blundy and others, this volume, chap. 33); and dissolved H_2O in a rare glassy fragment (filled circles) of October 2004 dacite sample SH304 (Pallister and others, 2005). *D*, Dissolved melt CO_2 concentration of 2004–2005 dacite during ascent.

bration depth to 60–80 vol. percent at depths of groundmass crystallization. The corresponding fluid composition of 2004–5 dacite during ascent (fig. 23*B*) is H_2O rich with X_{H_2O} always >0.96 and reaching 0.98 at the stage of groundmass crystallization. Extrapolating the compositional trends to near-surface conditions indicates that H_2O forms about 99 percent (molar basis) of the magmatic gases emitted to the atmosphere, whereas the monitored gases CO_2 and SO_2 account for only about 1 percent of the emitted magmatic gases. The implied magmatic $H_2O/(CO_2+SO_2)$ of ~99 is consistent with the value of 113 measured by open-path Fourier-transform infrared spectroscopy (Edmonds and others, this volume, chap. 27) on gas emissions from the new dome on August 31, 2005, considering that dome gases are likely to contain a meteoric component in addition to the magmatic component of water. Our CO_2 and SO_2 emission-rate data thus allow calculation of expected magmatic H_2O emission rates during 2004–5; the expected magmatic H_2O emission rates range from ~7 kt/d to ~100 kt/d with an estimated median of ~30 kt/d. We estimate cumulative H_2O production through 2005 at ~10 Mt from the cumulative production of CO_2 and SO_2.

The concentration of H_2O—that is, total OH and molecular H_2O—dissolved in the melt of the 2004–5 dacite ranges during ascent from the 4.4 wt. percent of last equilibration in the reservoir at 5.2 km to about 1.1–1.5 wt. percent at the conditions of groundmass crystallization (fig. 23*C*). The ascent curve for H_2O dissolved in melt indicates last equilibration depths of about 1.3–1.6 km for two measurements of H_2O concentration by Fourier-transform infrared spectrometry on a rare glassy fragment found in the October 2004 dacite sample SH304 (Pallister and others, 2005). Melt inclusions in the current dacite contain 0.0–3.6 wt. percent H_2O (Pallister and others, this volume, chap. 30; Blundy and others, this volume, chap. 33). The six highest melt-inclusion H_2O concentrations range from 2.4 to 3.6 wt. percent, corresponding to depths of only 2.0–3.7 km on the ascent curve for H_2O (fig. 23*C*). These results corroborate petrologic findings indicating that the melt inclusions provide no data on the volatile content of preeruption melt, apparently because slow ascent and eruption caused rupturing and (or) crystallization of virtually all melt inclusions, as suggested by their frequent mafic-mineral hosts, high crystallinity (≥70 percent), and variable SiO_2 concentrations (in this volume: Pallister and others, chap. 30; Rutherford and Devine, chap. 31; Blundy and others, chap. 33). Alternative explanations of the low melt-inclusion H_2O concentrations—for example, that they formed during ascent from 5.2 km, or that the source magma at 5.2 km depth was relatively dry (<4 wt. percent H_2O, which would imply X_{H_2O} <0.84)—are implausible in view of petrologic evidence. The concentration of CO_2 dissolved in the melt during ascent ranges from 37 ppm at the last equilibration in the reservoir at 5.2 km to about 1.3–2.9 ppm at the conditions of groundmass crystallization (fig. 23*D*).

The percolation threshold of 30 vol. percent indicated at ~2.5 km (fig. 23*A*) is a first-order approximation of the depth beyond which further ascent causes interconnected bubbles to increasingly dominate in overall degassing, ultimately transitioning to open-system degassing (Mueller and others, 2005). Melt concentrations of H_2O and CO_2 at the percolation threshold are about 2.8 wt. percent and 10 ppm, respectively, and the associated fluid composition is H_2O rich (X_{H_2O} = 0.975). The transition to open-system degassing during ascent at some depth shallower than ~2.5 km is an important step in the mobilization and flow of the H_2O-rich volcanic gases. Measured H_2O/HCl ratios of gas emissions on August 31, 2005, are consistent with a transition to open-system degassing at depths of ~1 km and prevailing to the surface (Edmonds and others, this volume, chap. 27). Open flow of H_2O-rich volcanic gases during ascent and dome emplacement purged shallow dacite of other volatile elements, including the entrainment of 210Po (Reagan and others, this volume, chap. 37) and the loss of Li from melt and the margins of plagioclase phenocrysts in the October 2004 dacite (Kent and others, 2007).

Fluid H_2S/SO_2 During Ascent

The gas-emission data show that SO_2 is the main sulfur species emitted to the atmosphere during the 2004–5 eruption. However, SO_2 may not be the dominant sulfur gas species at depth, where increased pressure can strongly affect sulfur speciation. Gerlach and Casadevall (1986) proposed from thermodynamic calculations constrained by fumarole gas compositions that H_2S was the dominant sulfur gas in the 1980s dacite at depth, whereas SO_2 dominated at pressures less than 4 MPa (depths less than 0.2 km). They cited reports of high H_2S/SO_2 in Mount St. Helens plumes from explosive eruptions of 1980–1981 in which 35–100 percent of the sulfur was present as H_2S (Hobbs and others, 1982) and suggested that rapid release of gas from depth prevented full equilibration to low pressure and allowed high H_2S/SO_2 to persist. They further suggested that rapid unloading during explosive eruptions of magma with oxygen fugacity as much as 1 order of magnitude above the Ni-NiO (NNO) buffer could burden the atmosphere with significant H_2S, as well as SO_2, and that SO_2 might increase as the H_2S oxidized, because the lifetime of H_2S in the atmosphere is only ~1 day (Graedel, 1977). Subsequent examination of TOMS satellite measurements made once a day on stratospheric volcanic clouds showed higher SO_2 masses for the May 18, 1980, cloud from Mount St. Helens on the second day than on the first day after eruption (Bluth and others, 1995).

We have taken a different approach to that of Gerlach and Casadevall (1986) and used the reaction

$$SO_2 + H_2O = H_2S + 1.5\ O_2$$

to estimate the H_2S/SO_2 ratio of the fluid phase during ascent of the current dacite from its last equilibration depth to the surface. For this reaction, the molar H_2S/SO_2 ratio is given by

$$H_2S/SO_2 = (pX_{H_2O}/Kf_{O_2}^{1.5})(\gamma_{H_2O}\gamma_{SO_2}/\gamma_{H_2S}), \quad (2)$$

where p is the total pressure in bars (1,300 bars to 1 bar), X_{H_2O} is the mole fraction of H_2O in the fluid (0.96 to 0.99, fig. 23*C*), K is the reaction equilibrium constant of $10^{20.03}$ at 850°C (HSC Chemistry for Windows v. 5.1), f_{O_2} is the current dacite's oxygen fugacity of $10^{-12.29}$ bar at 850°C (Pallister and others, this volume, chap. 30), and γ_i terms are dimensionless fugacity coefficients correcting for the nonideality of H_2O, SO_2, and H_2S. Fugacity coefficients from the MRK equation of state (Holloway, 1977, 1981), the corresponding state equation of Shi and Saxena (1992), and the ideal gas assumption ($\gamma_i = 1$) give H_2S/SO_2 results that agree within 10 percent, consistent with the relatively low-pressure, high-temperature conditions. The results confirm that H_2S is the dominant sulfur gas at depths >0.2 km (fig. 24), as in the 1980s (Gerlach and Casadevall, 1986); the H_2S/SO_2 ratio is >40 at the last equilibration depth in the shallow reservoir (5.2 km) and 3.3–6.5 in the depth range of groundmass crystallization (0.47 to 0.95 km). Compared to the explosive eruptions of the early 1980s, the slow ascent of magma from depth in the present eruption favors a closer approach to equilibrium with more complete conversion of H_2S to SO_2—consistent with the generally low H_2S emissions of the current eruption. Nevertheless, field crews often reported strong intermittent H_2S odor, especially after the early steam-and-ash events, and H_2S odor was reported by an airborne observer downwind of the volcano during and immediately after the first explosion of the eruption on October 1, 2004. These reports may be the result of rapid release of H_2S from depth. However, we cannot rule out an alternative H_2S origin by scrubbing and hydrolysis of SO_2, as discussed above, for the early days of the eruption in 2004.

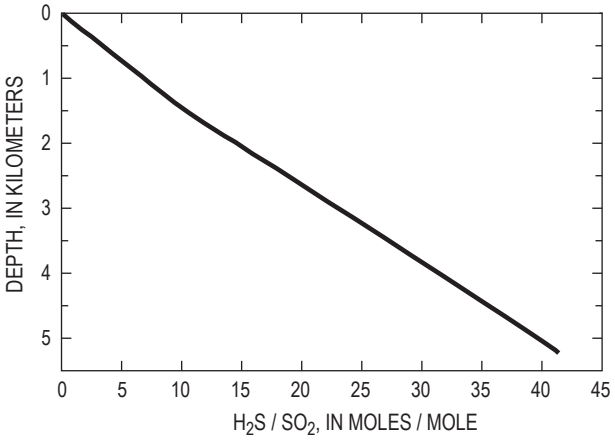

Figure 24. Calculated fluid H_2S/SO_2 of 2004–2005 dacite at 850°C ascending from the 5.2-km depth (130 MPa) of last equilibration in the shallow reservoir to the surface (0.1 MPa), as described in the text.

Excess Sulfur

The existence of an excess sulfur problem, although clear in the 1980s cycle of volcanism at Mount St. Helens (Gerlach and McGee, 1994), is problematic in the 2004–5 eruption. Assuming that the cumulative SO_2 emissions (table 2; fig. 8) for the DEM dates derived entirely from the melt fraction of the dacite prior to ascent implies a melt S concentration of 192 ppm at 5.2 km depth. The rupturing and high crystallinity of virtually all melt inclusions and the below-detection-limit sulfur concentrations of most melt inclusions and matrix glasses (Pallister and others, this volume, chap. 30), however, prevent the use of glass measurements to constrain the preeruption melt sulfur concentration of the current dacite prior to ascent from 5.2 km, thus precluding comparisons with the 192-ppm figure. Whether or not the preeruption melt sulfur concentration at 5.2 km depth accounts for the 2004–5 SO_2 emissions is therefore presently irresolvable, as is the question of excess sulfur for the 2004–5 eruption. The alternative source of the SO_2 emissions—that is, the fluid fraction of the dacite at 5.2 km—thus remains viable; this option would require a mole-fraction S concentration in the fluid (X_S) of only 0.004 prior to ascent (recall that the fluid X_{H_2O} and X_{CO_2} at 5.2 km are about 0.96 and 0.04, respectively). Moreover, experimental studies (Keppler, 1999) on haplogranitic melt at 850°C, 200 MPa, and f_{O_2} of 0.5 log units above the Ni-NiO buffer (NNO + 0.5)—close to the current dacite's f_{O_2} of NNO + ~1 (Pallister and others, this volume, chap. 30)—give fluid/melt partition coefficients for S of 47±4. These results strongly favor excess sulfur in the fluid fraction of the dacite at 5.2 km as the main source of the SO_2 emissions.

Concluding Remarks

The gas emissions of the 2004–5 eruption of Mount St. Helens provide no compelling evidence that gas-rich "new" magma was introduced into the reservoir during the months just prior to or since the onset of activity in September 2004, although additions of gas-poor new magma cannot be ruled out. The gas emissions are instead indicative of a flat source magma markedly depleted in excess volatiles compared to the May 18, 1980, dacite and the intermediate and silicic magmas commonly involved in explosive volcanism. However, the flat dacite of this eruption contains rhyolitic melt with appreciable dissolved water (4.4 wt. percent) despite its depletion in excess volatiles. It remains unclear whether flat dacite of this sort can give rise to large and violent explosive eruptions. The flat dacite has not done so in the present case, but this fact begs the question of how dependent explosive volcanism involving intermediate and silicic magma is on the magnitude of the excess-volatile load.

The 2004–5 gas emissions are plausibly compatible with 1980–86 dome-building magma left over in the reservoir and (or) with gas-poor new magma that entered the reservoir since 1986. Petrologic evidence favors the introduction of new magma (Pallister and others, this volume, chap. 30), but why is this new magma so gas poor compared to the May 18, 1980, magma? Perhaps the new magma was initially depleted in excess volatiles, or it may have mixed with a large amount of leftover 1980–86 magma already greatly depleted in exsolved volatiles. Alternatively, the new magma may simply have lost most of its excess-volatile load by fluid escape while stored at shallow reservoir depths long before the events of September 2004. The degassing of CO_2 measured on June 22, 1998, may represent the product of such fluid escape during a short period of seismicity accompanying recharge of the shallow reservoir. Although this is the strongest evidence of post-1986 fluid escaping and reaching the surface, we cannot rule out the possibility that fluid escaped from the shallow reservoir at other times since 1986 and was captured by hydrothermal fluid at depth or scrubbed by surficial water (Shevenell and Goff, 1993); the large increase of HCO_3^- in the waters of thermal springs at Loowit and Step canyons since 1994 (Bergfeld and others, this volume, chap. 25) may be the result of these processes.

The small load of excess volatiles in the 2004–5 dacite was an important factor in making it possible for scrubbing to shut down and strongly reduce gas emissions to the atmosphere in the period of unrest and the early stage of the eruption. The 2004–5 eruption affirms several implications of scrubbing for assessment of volcano hazards by volcanic gas monitoring: scrubbing can mask shallow magmatic degassing and thus severely restrict gas-emission monitoring as a volcano hazards assessment tool; scrubbing and its masking effects are most effective in the early stages of unrest; no great solace should be taken from low SO_2 emission rates during periods of unrest; early monitoring of CO_2 should accompany early SO_2 monitoring; the monitoring of CO_2, SO_2, and H_2S can track the drying out of a volcano and help distinguish the effects of gas scrubbing and permeability sealing on emissions; and emissions of CO_2 and H_2S in the early stages of unrest, when SO_2 and emissions are absent or trivial, should not be regarded as merely the degassing of hydrothermal fluid, as they can reflect significant shallow magmatic degassing combined with the effects of scrubbing.

Acknowledgments

We are indebted to the following, all of whom made valuable contributions to this paper by sharing ideas, observations and data: Roger Denlinger, Dan Dzurisin, Marie Edmonds, Mike Lisowski, Larry Mastin, John Pallister, Kelly Russell, Steve Schilling, Carl Thornber, and Paul Wallace. Our special thanks to Jeff Sutton for help with instrumentation and early monitoring flights, and to Larry Mastin and John Pallister for technical reviews. Finally, we acknowledge the support of the U.S. Geological Survey Volcano Hazards Program.

References Cited

Anderson, C.H., Jr., Behrens, C.J., Floyd, G.A., and Vining, M.R., 1998, Crater firn of Mount St. Helens, Washington: Journal of Cave Karst Studies, v. 60, p. 44–50.

Bergfeld, D., Evans, W.C., McGee, K.A., and Spicer, K.R., 2008, Pre- and post-eruptive investigations of gas and water samples from Mount St. Helens, Washington, 2002 to 2005, chap. 25 *of* Sherrod, D.R., Scott, W.E., and Stauffer, P.H., eds., A volcano rekindled; the renewed eruption of Mount St. Helens, 2004–2006: U.S. Geological Survey Professional Paper 1750 (this volume).

Berlo, K., Blundy, J., Turner, S., Cashman, K., Hawkesworth, C., and Black, S., 2004, Geochemical precursors to volcanic activity at Mount St. Helens, USA: Science, v. 306, p. 1167–1169.

Blundy, J., and Cashman, K., 2001, Ascent-driven crystallisation of dacite magmas at Mount St. Helens, 1980–1986: Contributions to Mineralogy and Petrology, v. 140, no. 6, p. 631–650, doi:10.1007/s004100000219.

Blundy, J., and Cashman, K., 2005, Rapid decompression-driven crystallization recorded by melt inclusions from Mount St. Helens volcano: Geology, v. 33, no. 10, p. 793–796, doi:10.1130/G21668.1.

Blundy, J., Cashman, K.V., and Berlo, K., 2008, Evolving magma storage conditions beneath Mount St. Helens inferred from chemical variations in melt inclusions from the 1980–1986 and current (2004–2006) eruptions, chap. 33 *of* Sherrod, D.R., Scott, W.E., and Stauffer, P.H., eds., A volcano rekindled; the renewed eruption of Mount St. Helens, 2004–2006: U.S. Geological Survey Professional Paper 1750 (this volume).

Bluth, G.J.S., Scott, C.J., Sprod, I.E., Schnetzler, C.C., Krueger, A.J., and Walter, L.S., 1995, Explosive emissions of sulfur dioxide from the 1992 Crater Peak eruptions, Mount Spurr volcano, Alaska, *in* Keith, T., ed., The 1992 eruptions of Crater Peak vent, Mount Spurr volcano, Alaska: U.S. Geological Survey Bulletin 2139, p. 37–45.

Caltabiano, T., Guiduzzi, G., Leuzzi, S., and Romano, R., 1992, Helicopter borne COSPEC SO_2 flux measurement: Acta Vulcanologica, v. 2, p. 95–98.

Casadevall, T.J., Johnston, D.A., Harris, D.M., Rose, W.I., Malinconico, L.L., Stoiber, R.E., Bornhorst, T.J., Williams, S.N., Woodruff, L., and Thompson, J.M., 1981, SO_2 emission rates at Mount St. Helens from March 29 through December, 1980, *in* Lipman, P.W., and Mullineaux, D.L., eds., The 1980 eruptions of Mount St. Helens, Washington: U.S. Geological Survey Professional Paper 1250, p. 193–200.

Casadevall, T.J., Johnston, D.A., Rose, W.I., Gerlach, T.M., Ewert, J., Wunderman, R., and Symonds, R., 1983, Gas

emissions and the eruptions of Mount St. Helens through 1982: Science, v. 221, p. 1383–1385.

Cashman, K.V., 1992, Groundmass crystallization of Mount St. Helens dacite, 1980–1986—a tool for interpreting shallow magmatic processes: Contributions to Mineralogy and Petrology, v. 109, no. 4, p. 431–449, doi:10.1007/BF00306547.

Cashman, K.V., and Taggert, J.E., 1983, Petrologic monitoring of 1981 and 1982 eruptive products from Mount St. Helens: Science, v. 221, no. 4618, p. 1385–1387.

Cashman, K.V., Thornber, C.R., and Pallister, J.S., 2008, From dome to dust; shallow crystallization and fragmentation of conduit magma during the 2004–2006 dome extrusion of Mount St. Helens, Washington, chap. 19 *of* Sherrod, D.R., Scott, W.E., and Stauffer, P.H., eds., A volcano rekindled; the renewed eruption of Mount St. Helens, 2004–2006: U.S. Geological Survey Professional Paper 1750 (this volume).

Cooper, K.M., and Donnelly, C.T., 2008, ^{238}U-^{230}Th-^{226}Ra disequilibria in dacite and plagioclase from the 2004–2005 eruption of Mount St. Helens, chap. 36 *of* Sherrod, D.R., Scott, W.E., and Stauffer, P.H., eds., A volcano rekindled; the renewed eruption of Mount St. Helens, 2004–2006: U.S. Geological Survey Professional Paper 1750 (this volume).

Crafford, T.C., 1975, SO_2 emission of the 1974 eruption of Volcán Fuego, Guatemala: Bulletin Volcanologique, v. 39, p. 536–556.

Doukas, M.P., 2002, A new method for GPS-based wind speed determinations during airborne volcanic plume measurements: U.S. Geological Survey Open-File Report 02–395, 13 p.

Doukas, M.P., and Gerlach, T.M., 1995, Sulfur dioxide scrubbing during the 1992 eruption of Crater Peak, Mount Spurr, Alaska, *in* Keith, T., ed., The 1992 eruptions of Crater Peak vent, Mount Spurr volcano, Alaska: U.S. Geological Survey Bulletin 2139, p. 47–57.

Edmonds, M., McGee, K.A., and Doukas, M.P., 2008, Chlorine degassing during the lava dome-building eruption of Mount St. Helens, 2004–2005, chap. 27 *of* Sherrod, D.R., Scott, W.E., and Stauffer, P.H., eds., A volcano rekindled; the renewed eruption of Mount St. Helens, 2004–2006: U.S. Geological Survey Professional Paper 1750 (this volume).

Elias, T., Sutton, A.J., Oppenheimer, C., Horton, K.A., Garbeil, H., Tsanev, V., McGonigle, A.J.S., and Williams-Jones, G., 2006, Comparison of COSPEC and two miniature ultraviolet spectrometer systems for SO_2 measurements using scattered sunlight: Bulletin of Volcanology, v. 68, p. 313–322.

Evans, W.C., van Soest, M.C., Mariner, R.H., Hurwitz, S., Wicks, C.W., Jr., and Schmidt, M.E., 2004, Magmatic intrusion west of Three Sisters, central Oregon, USA: The perspective from spring geochemistry: Geology, v. 32, no. 1, p. 69–72.

Galle, B., Oppenheimer, C., Geyer, A., McGonigle, A.J.S., Edmonds, M., and Horrocks, L., 2002, A miniaturized ultraviolet spectrometer for remote sensing of SO_2 fluxes—a new tool for volcano surveillance: Journal of Volcanology and Geothermal Research, v. 119, p. 241–254.

Gerlach, T.M., and Casadevall, T.J., 1986, Fumarole emissions at Mount St. Helens volcano, June 1980 to October 1981—degassing of a magma-hydrothermal system: Journal of Volcanology and Geothermal Research, v. 28, nos. 1–2, p. 141–160, doi:10.1016/0377-0273(86)90009-0.

Gerlach, T.M., and McGee, K.A., 1994, Total sulfur dioxide emissions and pre-eruption vapor-saturated magma at Mount St. Helens, 1980–88: Geophysical Research Letters, v. 21, no. 25, p. 2833–2836, doi:10.1029/94GL02761.

Gerlach, T.M., Delgado, H., McGee, K.A., Doukas, M.P., Venegas, J.J., and Cardenas, L., 1997, Application of the LI-COR CO_2 analyzer to volcanic plumes—a case study, Volcán Popocateptl, Mexico, June 7 and 10, 1995: Journal of Geophysical Research, v. 102, p. 8005–8019.

Gerlach, T.M., Doukas, M.P., McGee, K.A., and Kessler, R., 1999, Airborne detection of diffuse carbon dioxide at Mammoth Mountain, California: Geophysical Research Letters, v. 26, 3661–3664.

Gerlach, T.M., McGee, K.A., and Doukas, M.P., 2005, Emission rates, pre-eruption gas saturation and ascent degassing during the 2004–2005 eruption of Mount St. Helens [abs.]: Eos (American Geophysical Union Transactions), v. 86, no. 52, Fall Meet. Suppl., Abstract V52B–07.

Glantz, S.A., 2005, Primer of biostatistics (5th ed.): New York, McGraw-Hill, 489 p.

Graedel, T.E., 1977, The homogeneous chemistry of atmospheric sulfur: Reviews of Geophysics and Space Physics, v. 15, p. 421–428.

Harris, D.M., Sato, M., Casadevall, T.J., Rose, W.I., and Bornhorst, T.J., 1981, Emission rates of CO_2 from plume measurements, *in* Lipman, P.W., and Mullineaux, D.L., eds., The 1980 eruptions of Mount St. Helens, Washington: U.S. Geological Survey Professional Paper 1250, p. 201–207.

Hobbs, P.V., Tuell, J.P., Hegg, D.A., Radke, L.F., and Eltgroth, M.W., 1982, Particles and gases in the emissions from the 1980–1981 volcanic eruptions of Mount St. Helens: Journal of Geophysical Research, v. 87, no. C12, p. 11062–11086.

Holloway, J.R., 1977, Fugacity and activity of molecular species in supercritical fluids, *in* Fraser, D., ed., Thermodynamics in Geology: Boston, D. Reidel, p. 161–181.

Holloway, J.R., 1981, Volatile interactions in magmas, *in* Newton, R.C., Navrotsky, A., and Wood, B.J., eds., Thermodynamics of Minerals and Melts: New York, Springer-Verlag, p. 273–293.

Horton, K.A., Williams-Jones, G., Garbeil, H., Elias, T., Sutton, A.J., Mouginis-Mark, P., Porter, J.N., and Clegg, S., 2006, Real-time measurement of volcanic SO_2 emissions: validation of a new UV correlation spectrometer (FLYSPEC): Bulletin of Volcanology, v. 68, p. 323–327.

Ingebritsen, S.E., Sherrod, D.R., and Mariner, R.H., 1989, Heat flow and hydrothermal circulation in the Cascade Range, north-central Oregon: Science, v. 243, p. 1458–1462.

Ingebritsen, S.E., Sherrod, D.R., and Mariner, R.H., 1992, Rate and patterns of groundwater flow in the Cascade Range volcanic arc, and the effect on subsurface temperatures: Journal of Geophysical Research, v. 97, no. B4, p. 4599–4627.

Ingebritsen, S.E., Mariner, R.H., and Sherrod, D.R., 1994, Hydrothermal systems of the Cascade Range, north-central Oregon: U.S. Geological Survey Professional Paper 1044L, 86 p.

James, E.R., Manga, M., and Rose, T.P., 1999, CO_2 degassing in the Oregon Cascades: Geology, v. 27, no. 9, p. 823–826.

Kent, A.J.R., Blundy, J., Cashman, K.V., Cooper, K.M., Donnelly, C., Pallister, J.S., Reagan, M., Rowe, M.C., and Thornber, C.R., 2007, Vapor transfer prior to the October 2004 eruption of Mount St. Helens, Washington: Geology, v. 35, no. 3, p. 231–234, doi:10.1130/G22809A.1.

Keppler, H., 1999, Experimental evidence for the source of excess sulfur in explosive volcanic eruptions: Science, v. 284, p. 1652–1654.

Lisowski, M., Dzurisin, D., Denlinger, R.P., and Iwatsubo, E.Y., 2008, Analysis of GPS-measured deformation associated with the 2004–2006 dome-building eruption of Mount St. Helens, Washington, chap. 15 *of* Sherrod, D.R., Scott, W.E., and Stauffer, P.H., eds., A volcano rekindled; the renewed eruption of Mount St. Helens, 2004–2006: U.S. Geological Survey Professional Paper 1750 (this volume).

Liu, Y., Zhang, Y., and Behrens, H., 2005, Solubility of H_2O in rhyolite melts at low pressures and a new empirical model for mixed H_2O-CO_2 solubility in rhyolitic melts: Journal of Volcanology and Geothermal Research, v. 143, p. 219–235.

Malinconico, L.L., 1979, Fluctuations in SO_2 emission during recent eruptions of Etna: Nature, v. 278, p. 43–45.

Mastin, L.G., Roeloffs, E., Beeler, N.M., and Quick, J.E., 2008, Constraints on the size, overpressure, and volatile content of the Mount St. Helens magma system from geodetic and dome-growth measurements during the 2004–2006+ eruption, chap. 22 *of* Sherrod, D.R., Scott, W.E., and Stauffer, P.H., eds., A volcano rekindled; the renewed eruption of Mount St. Helens, 2004–2006: U.S. Geological Survey Professional Paper 1750 (this volume).

McGee, K.A., 1992, The structure, dynamics, and chemical composition of noneruptive plumes from Mount St. Helens, 1980–88: Journal of Volcanology and Geothermal Research, v. 51, p. 269–282.

McGee, K.A., and Casadevall, T.J., 1994, A compilation of sulfur dioxide and carbon dioxide emission-rate data from Mount St. Helens during 1980–88: U.S. Geological Survey Open-File Report 94–212, 24 p.

McGee, K.A., and Sutton, A.J., 1994, Eruptive activity at Mount St. Helens, Washington, USA, 1984–1988—a gas geochemistry perspective: Bulletin of Volcanology, v. 56, nos. 6–7, p. 435–446.

McGee, K.A., Doukas, M.P., and Gerlach, T.M., 2001, Quiescent hydrogen sulfide and carbon dioxide degassing from Mount Baker, Washington: Geophysical Research Letters, v. 28, p. 4479–4483.

Moran, S.C., 1994, Seismicity at Mount St. Helens, 1987–1992—evidence for repressurization of an active magmatic system: Journal of Geophysical Research, v. 99, no. B3, p. 4341–4354, doi:10.1029/93JB02993.

Moran, S.C., Malone, S.D., Qamar, A.I., Thelen, W.A., Wright, A.K., and Caplan-Auerbach, J., 2008, Seismicity associated with renewed dome building at Mount St. Helens, 2004–2005, chap. 2 *of* Sherrod, D.R., Scott, W.E., and Stauffer, P.H., eds., A volcano rekindled; the renewed eruption of Mount St. Helens, 2004–2006: U.S. Geological Survey Professional Paper 1750 (this volume).

Mueller, S., Melnik, O., Spieler, O., Scheu, B., and Dingwell, D.B., 2005, Permeability and degassing of dome lavas undergoing rapid decompression—an experimental determination: Bulletin of Volcanology, v. 67, no. 6, p. 526–538.

Newman, S., and Lowenstern, J.A., 2002, VolatileCalc—a silicate melt-H_2O-CO_2 solution model written in Visual Basic for excel®: Computers and Geosciences, v. 28, no. 5, p. 597–604, doi:10.1016/S0098-3004(01)00081-4.

Pallister, J.S., Reagan, M., and Cashman, K., 2005, A new eruptive cycle at Mount St. Helens?: Eos (American Geophysical Union Transactions), v. 86, no. 48, p. 499–500, doi:10.1029/2005EO480006.

Pallister, J.S., Thornber, C.R., Cashman, K.V., Clynne, M.A., Lowers, H.A., Mandeville, C.W., Brownfield, I.K., and Meeker, G.P., 2008, Petrology of the 2004–2006 Mount St. Helens lava dome—implications for magmatic plumbing and eruption triggering, chap. 30 *of* Sherrod, D.R., Scott, W.E., and Stauffer, P.H., eds., A volcano rekindled; the renewed eruption of Mount St. Helens, 2004–2006: U.S. Geological Survey Professional Paper 1750 (this volume).

Reagan, M.K., Cooper, K.M., Pallister, J.S., Thornber, C.R., and Wortel, M., 2008, Timing of degassing and plagioclase

growth in lavas erupted from Mount St. Helens, 2004–2005, from ^{210}Po-^{210}Pb-^{226}Ra disequilibria, chap. 37 *of* Sherrod, D.R., Scott, W.E., and Stauffer, P.H., eds., A volcano rekindled; the renewed eruption of Mount St. Helens, 2004–2006: U.S. Geological Survey Professional Paper 1750 (this volume).

Rose, T.P., and Davisson, M.L., 1996, Radiocarbon in hydrologic systems containing dissolved magmatic carbon dioxide: Science, v. 273, p. 1367–1370.

Rutherford, M.J., 1993, Experimental petrology applied to volcanic processes: Eos (American Geophysical Union Transactions), v. 74, no. 5, p. 49 and 55.

Rutherford, M.J., and Devine, J.D., III, 2008, Magmatic conditions and processes in the storage zone of the 2004–2006 Mount St. Helens dacite, chap. 31 *of* Sherrod, D.R., Scott, W.E., and Stauffer, P.H., eds., A volcano rekindled; the renewed eruption of Mount St. Helens, 2004–2006: U.S. Geological Survey Professional Paper 1750 (this volume).

Rutherford, M.J., Sigurdsson, H., Carey, S., and Davis, A., 1985, The May 18, 1980, eruption of Mount St. Helens, 1. Melt composition and experimental phase equilibria: Journal of Geophysical Research, v. 90, no. B4, p. 2929–2947.

Schilling, S.P., Thompson, R.A., Messerich, J.A., and Iwatsubo, E.Y., 2008, Use of digital aerophotogrammetry to determine rates of lava dome growth, Mount St. Helens, Washington, 2004–2005, chap. 8 *of* Sherrod, D.R., Scott, W.E., and Stauffer, P.H., eds., A volcano rekindled; the renewed eruption of Mount St. Helens, 2004–2006: U.S. Geological Survey Professional Paper 1750 (this volume).

Scott, W.E., Sherrod, D.R., and Gardner, C.A., 2008, Overview of 2004 to 2006, and continuing, eruption of Mount St. Helens, Washington, chap. 1 *of* Sherrod, D.R., Scott, W.E., and Stauffer, P.H., eds., A volcano rekindled; the renewed eruption of Mount St. Helens, 2004–2006: U.S. Geological Survey Professional Paper 1750 (this volume).

Shevenell, L., and Goff, F., 1993, Addition of magmatic volatiles into the hot spring waters of Loowit Canyon, Mount St. Helens, Washington, USA: Bulletin of Volcanology, v. 55, no. 7, p. 489–503, doi:10.1007/BF00304592.

Shi, P., and Saxena, S.K., 1992, Thermodynamic modeling of the C-H-O-S fluid system: American Mineralogist, v. 77, p. 1038–1049.

Silver, L.A., Ihinger, P.D., and Stolper, E., 1990, The influence of bulk composition on the speciation of water in silicate glasses: Contributions to Mineralogy and Petrology, v. 104, p. 142–162.

Stoiber, R.E., and Jepsen, A., 1973, Sulfur dioxide contribution to the atmosphere by volcanoes: Science, v. 182, p. 577–578.

Stoiber, R.E., Williams, S.N., and Malinconico, L.L., 1980, Mount St. Helens, Washington, 1980, volcanic eruption—magmatic gas component during the first 16 days: Science, v. 208, p. 1258–1259.

Stoiber, R.E., Malinconico, L.L., and Williams, S.N., 1983, Use of the correlation spectrometer at volcanoes, *in* Tazieff, H., and Sabroux, J.C., eds., Forecasting volcanic events: Amsterdam, Elsevier, p. 425–444.

Symonds, R.B., Gerlach, T.M., and Reed, M.H., 2001, Magmatic gas scrubbing—implications for volcanic monitoring: Journal of Volcanology and Geothermal Research, v. 108, nos. 1–4, p. 303–341, doi:10.1016/S0377-0273(00)00292-4.

Thompson, J.M., 1990, Chemical data from thermal and nonthermal springs in Mount St. Helens National Monument, Washington: U.S. Geological Survey Open-File Report 90–690A, 16 p.

Wallace, P.J., 2001, Volcanic SO_2 emissions and the abundance and distribution of exsolved gas in magma bodies: Journal of Volcanology and Geothermal Research, v. 108, nos. 1–4, p. 85–106, doi:10.1016/S0377-0273(00)00279-1.

Wallace, P.J., 2003, From mantle to atmosphere—magma degassing, explosive eruptions, and volcanic volatile budgets, *in* De Vivo, B., and Bodnar, R.J., eds., Melt inclusions in volcanic systems—methods, applications and problems: Amsterdam, Elsevier, p. 105–128.

Williams, D.L., Abrams, G., Finn, C., Dzurisin, D., Johnson, D.J., and Denlinger, R., 1987, Evidence from gravity data for an intrusive complex beneath Mount St. Helens: Journal of Geophysical Research, v. 92, no. B10, p. 10207–10222.

This page intentionally left blank

A Volcano Rekindled: The Renewed Eruption of Mount St. Helens, 2004–2006
Edited by David R. Sherrod, William E. Scott, and Peter H. Stauffer
U.S. Geological Survey Professional Paper 1750, 2008

Chapter 27

Chlorine Degassing During the Lava Dome-Building Eruption of Mount St. Helens, 2004–2005

By Marie Edmonds[1], Kenneth A. McGee[2], and Michael P. Doukas[2]

Abstract

Remote measurements of volcanic gases from the Mount St. Helens lava dome were carried out using Open-Path Fourier-Transform Infrared spectroscopy on August 31, 2005. Measurements were performed at a site ~1 km from the lava dome, which was used as a source of IR radiation. On average, during the period of measurement, the volcanic gas contained 99 mol percent H_2O, 0.78 percent CO_2, 0.095 percent HCl, 0.085 percent SO_2, 0.027 percent HF, 4.8×10^{-4} percent CO, and 2.5×10^{-4} percent COS close to the active vent. The fluxes of these species, constrained by synchronous measurements of SO_2 flux, were 7,200 t/d H_2O, 140 t/d CO_2, 22 t/d SO_2, 14 t/d HCl, 2.0 t/d HF, 54 kg/d CO, and 59 kg/d COS, ±20 percent. Observations of H_2O/Cl in the vapor and melt are compared to models of closed- and open-system degassing and to models where a closed system dominates to depths as shallow as ~1 km, and gases are then allowed to escape through a permeable bubble network. Although several features are consistent with this model—for example, (1) H_2O/Cl in the gases emitted from stagnant parts of the lava dome, (2) the concentration of Cl in the matrix glass of erupted dacite, and (3) the glass H_2O/Cl—the gases emitted from the active part of the lava dome have much higher H_2O/Cl than expected. These higher H_2O/Cl levels result from a combination of two factors (1) the addition of substantial amounts of ground water or glacier-derived H_2O to the gases at shallow depths, such that only ~10 mol percent of the measured H_2O is magmatic, and (or) (2) some Cl present as alkali chloride (NaCl and KCl) in the gas phase. The mean molar Cl/S is similar to gases measured at other silicic subduction-zone volcanoes during effusive activity; this may be due to the influence of Cl in the vapor on S solubility in the melt, which produces a solubility maximum for S at vapor Cl/S ~1.

Introduction

Volcanic gases comprise water (H_2O), carbon dioxide (CO_2), sulfur dioxide (SO_2), hydrogen sulfide (H_2S), hydrogen chloride (HCl), and, to a lesser extent, hydrogen fluoride (HF), carbon monoxide (CO), and a host of trace species (for example, Symonds and others, 1994). Volatiles (mainly H_2O and CO_2) exsolve from magma during decompression, generating vesicularity and buoyancy relative to the surrounding rocks, thereby driving eruptions. The rate and style of degassing controls the rheological development of magma and governs eruptive style (for example, Sparks and others, 2000). Preeruptive dissolved H_2O, CO_2, S, and Cl contents in silicic magmas typically range from 1 to 6 weight percent and 0–400, 30–200 and 900–3,000 ppm, respectively, after having undergone ~60–70 percent vapor-saturated fractional crystallization at 2–5 kb in the crust to evolve from mafic magma compositions (Wallace, 2005).

Chlorine is a significant volatile component of magmas associated with subduction zones and is derived from devolatilization of the subducting lithospheric slab (Manning, 2004). Recent analysis of volatile fluxes at subduction zones indicates that the flux of subducted Cl in the form of seawater and sediments approximately balances the output from arc volcanism (~$4–7\times10^{12}$ g/yr), consistent with the low abundance of Cl in mantle plume-derived basalt tapping the deep mantle (Wallace, 2005). Along with other volatiles, Cl dissolves in the partial melt and, thereafter, behaves as an incompatible element during crystallization, although small amounts may be taken up by amphibole phases. Cl is finally removed from the melt by partitioning into a vapor phase during magma ascent through the crust. A high partition coefficient (vapor/melt) for Cl was first recognized by Kilinc and Burnham (1972). The release

[1]U.S. Geological Survey, P.O. Box 51, Hawaii National Park, HI 96718; now at University of Cambridge, Downing Street, Cambridge CB2 3EQ, U.K.

[2] U.S. Geological Survey, 1300 SE Cardinal Court, Vancouver, WA 98683

of Cl with H_2O and other volatiles from magma is important for the transport and concentration of ore metals, such as gold, copper, and iron, which may eventually form mineral deposits in large magmatic systems (Lowenstern and others, 1991). The acidic nature of HCl-containing gases may leach and alter volcanic rocks and contribute to instability in volcanic edifices (Le Friant and others, 2002).

Hydrogen chloride is the dominant chloride species in volcanic gases (Webster and Holloway, 1988); significant amounts of NaCl and KCl have also been detected (Le Guern and others, 1975). Gaseous HCl enters the atmosphere during volcanic eruptions; tropospheric emissions can cause local acid rain, and stratospheric injection of HCl gas can lead to degradation of the ozone layer (Tabazedeh and Turco, 1993). The rate of emission of HCl from volcanoes, compared to that of SO_2, has been linked to eruptive processes and has applications for volcano monitoring. Stoiber and Rose (1974) noted that gas Cl/S tends to increase throughout an eruptive episode, owing to the lower solubility of S. At Augustine Volcano, Symonds and others (1990) noted that older volcanic deposits exsolved gas with higher Cl/S than the main eruptive vents, suggesting that Cl continues to degas from melt after emplacement at the surface. At Soufrière Hills volcano[3], Montserrat, S-rich basaltic magma is supplied to the base of a porphyritic, Cl-rich andesite body. Volcanic gases with high levels of Cl/S are emitted during eruptive periods and gases with low levels of Cl/S are emitted during noneruptive periods. These emissions are caused by the degassing of negligible Cl but extensive S from the basalt to a vapor phase at 5–7 km; and the degassing of Cl but negligible S from the andesite during eruption (Edmonds and others, 2002).

During the current eruption of Mount St. Helens (ongoing in August 2006), CO_2, SO_2, and H_2S emission rates have been measured regularly and are well constrained (Gerlach and others, this volume, chap. 26); H_2O, HCl, and other minor species had not been quantified until this study. HCl is an important constituent of volcanic gases, yet fewer measurements of HCl than of SO_2 are carried out during volcanic eruptions. This paper presents new data on the composition of the volcanic gas plume emitted from the lava dome at Mount St. Helens in August 2005. Remote spectroscopic measurements of the volcanic plume made by using Open-Path Fourier-Transform Infrared spectroscopy (OP–FTIR) yield the relative proportions of magmatic H_2O, CO_2, HCl, SO_2, HF, CO, and COS of the gas phase. Synchronous measurements of SO_2 emission rates are used to calculate emission rates for the other six species.

The emission of Cl in the form of HCl gas is the focus of the analysis. In order to interpret the rate and mechanism of HCl emission from volcanoes, an understanding of how magmatic vapor evolves chemically with changes in pressure, temperature, and melt composition is necessary; this is reasonably constrained for H_2O, CO_2, and H_2O-CO_2 melt-vapor systems at shallow to intermediate pressures (for example, for basaltic melts, Dixon and others, 1995) but less well understood for systems containing S and Cl. The measured molar H_2O/Cl of the gases is compared to models describing different degassing regimes in order to evaluate the evolution of the vapor phase with magma ascent. The gas composition is compared to the compositions of volcanic gases at other silicic volcanoes and to observations made during 1980–86 at Mount St. Helens. The Cl/S molar ratio is evaluated with reference to the solubility of S and Cl in silicic melts.

Method

Open-path Fourier-transform infrared spectroscopy (OP–FTIR) is a spectroscopic technique that utilizes the absorptivity of specific gas molecules in order to quantify them accurately (fig. 1*A*). A spectrometer acquires infrared (IR) radiation from a source that has passed through volcanic gas. Di-atomic and monatomic compounds (for example, H_2, He) do not have an IR signature and, thus, cannot be measured by this technique. Absorption due to the gases is isolated and calibrated. OP–FTIR has been used successfully at several volcanoes, including Unzen, Japan (Mori and others, 1993); Vulcano, Italy (Francis and others, 1995); Etna, Italy (Burton and others, 2003); Soufrière Hills, Montserrat (Edmonds and others, 2002); and Kīlauea, USA (Edmonds and others, 2005). The OP–FTIR technique has advantages over direct methods of sampling, the most important of which is the remote aspect of the measurements and, hence, the higher level of safety, because it is not necessary to approach the fumaroles or vents closely. This technique is particularly useful for measuring gases at lava dome-building volcanoes, where explosions can occur with little warning; measurements can be collected throughout eruptive and noneruptive periods. For example, during the 1980–86 Mount St. Helens eruption, gas sampling was possible only from peripheral fumaroles, and when the lava dome was particularly active, no gas samples were collected at all (Gerlach and Casadevall, 1986). OP–FTIR also allows rapid measurements; several hundred spectra may be collected every hour, each containing information about the amount of various major and minor gas species in the pathlength.

The OP–FTIR data presented in this paper were collected on August 31, 2005, using the 2004–5 Mount St. Helens lava dome as a source of IR radiation (fig. 1). A digital elevation model formulated from photographs taken on September 1, 2005, (S.P. Schilling, written commun., 2008) is shown in figure 2. The massive parts of the dome were broken whaleback-shaped spines, each surrounded by a thick layer of blocky talus material. The measurements were taken in three sets; pathlengths ranged from 1,040 to 1,150 m (fig. 2). Temperatures on the surface of the lava dome were highly variable,

[3]Capitalization of "Volcano" indicates adoption of the word as part of the formal geographic name by the host country, as listed in the Geographic Names Information System, a database maintained by the U.S. Board on Geographic Names. Noncapitalized "volcano" is applied informally—eds.

ranging from ~10°C to >200°C (fig. 3). For the OP–FTIR measurements, cracks in the spine surfaces were used as IR sources and had temperatures as high as 600°C (Schneider and others, this volume, chap. 17). Volcanic gas rose from the lava dome (fig. 1*B*) and passed through the spectrometer's field of view.

A MIDAC IR spectrometer with a resolution of 0.5 cm^{-1} was mounted onto a 20-inch Newtonian telescope on a heavy-weight tripod (fig. 1*A*). The spectrometer design incorporates a Michelson interferometer, laser optics, CaF_2 optical windows, and an InSb Stirling-cycle cooled detector with a range of 5,000–1,800 cm^{-1}. The field of view of the instrument is 2–3 m at 800 m. A laptop computer and PCMCIA interface enable real-time data acquisition and processing, using Autoquant4 software (MIDAC Corp.). Analysis is based on a linear model of the sample absorbance known as Beer's Law, which can be written as:

$$A_i = \sum_{j=1}^{M} a_{ij} LC_j \qquad i = 1, 2 \ldots N, \tag{1}$$

where M is the number of compounds assumed to absorb in the spectral region analyzed; A_i is the observed sample absorbance at the ith frequency, C_j is the (unknown) concentration of the jth component of the mixture, L is the absorption pathlength used in recording the sample spectrum and a_{ij} is the absorptivity of the jth compound at the ith IR frequency. A_i, the absorbance spectrum, is obtained from the measured spectrum by normalizing the measured spectrum, S_i, by a background spectrum B, which is free of, or contains less, absorption due to volcanic gases:

$$A_i = -\log\left(S_i / B\right). \tag{2}$$

The absorbance spectra, therefore, contain information pertaining only to the volcanic gas phase; all other background gases are canceled out by this procedure. The absorbance spectra, A_i, are baseline corrected (in each fitting region) before analysis, using a second-order polynomial, and they also are corrected for their temperature and pressure relative to the reference spectra. A calibration set of spectra of pure components at known concentrations are used to calculate the absorptivities a_{ij}.

The uncertainty in the measurements is calculated from the residual spectrum, which should have a mean of zero in the fitted region and is proportional to the square root of the sum of the squares of the residual:

$$\sigma^2 = \sum_i R_i^2 \Big/ (n-1), \tag{3}$$

where σ^2 is the error variance, R is the residual spectrum, and n is the number of observations. The standard error of the estimated concentration, ε, is equal to:

$$\varepsilon = \sigma C \Big/ \sqrt{\sum_i A_i^2}. \tag{4}$$

This technique allows the evaluation of precise concentration-pathlengths (LCj from equation 1) for each species, which have units of parts per million meters (ppm·m). The ratios of the concentration-pathlengths for different species in the plume typically are accurate to within a few percent, given appropriate analysis. The absolute values, however, are a minimum because the background spectrum, B, is not a clear-

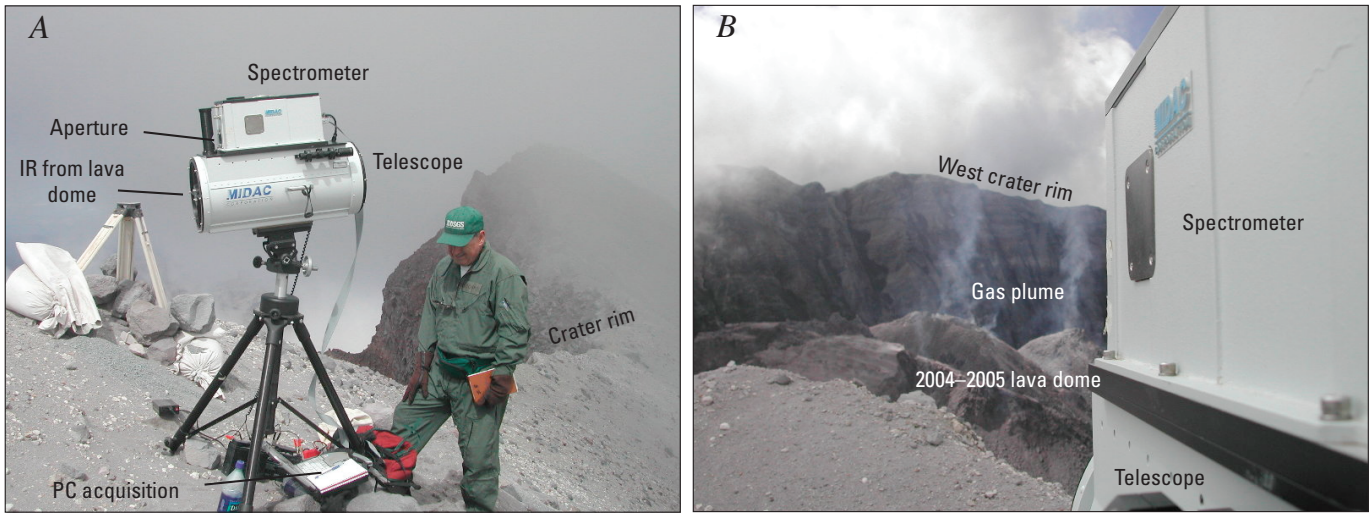

Figure 1. Fourier-transform infrared (FTIR) spectrometer in field settings. *A*, At FTIR measurement site (Brutus), on east crater rim of Mount St. Helens. *B*, Collecting radiation from hot cracks in the dacitic lava dome of Mount St. Helens, 2005. Volcanic gas is passing into the path in front of the infrared source.

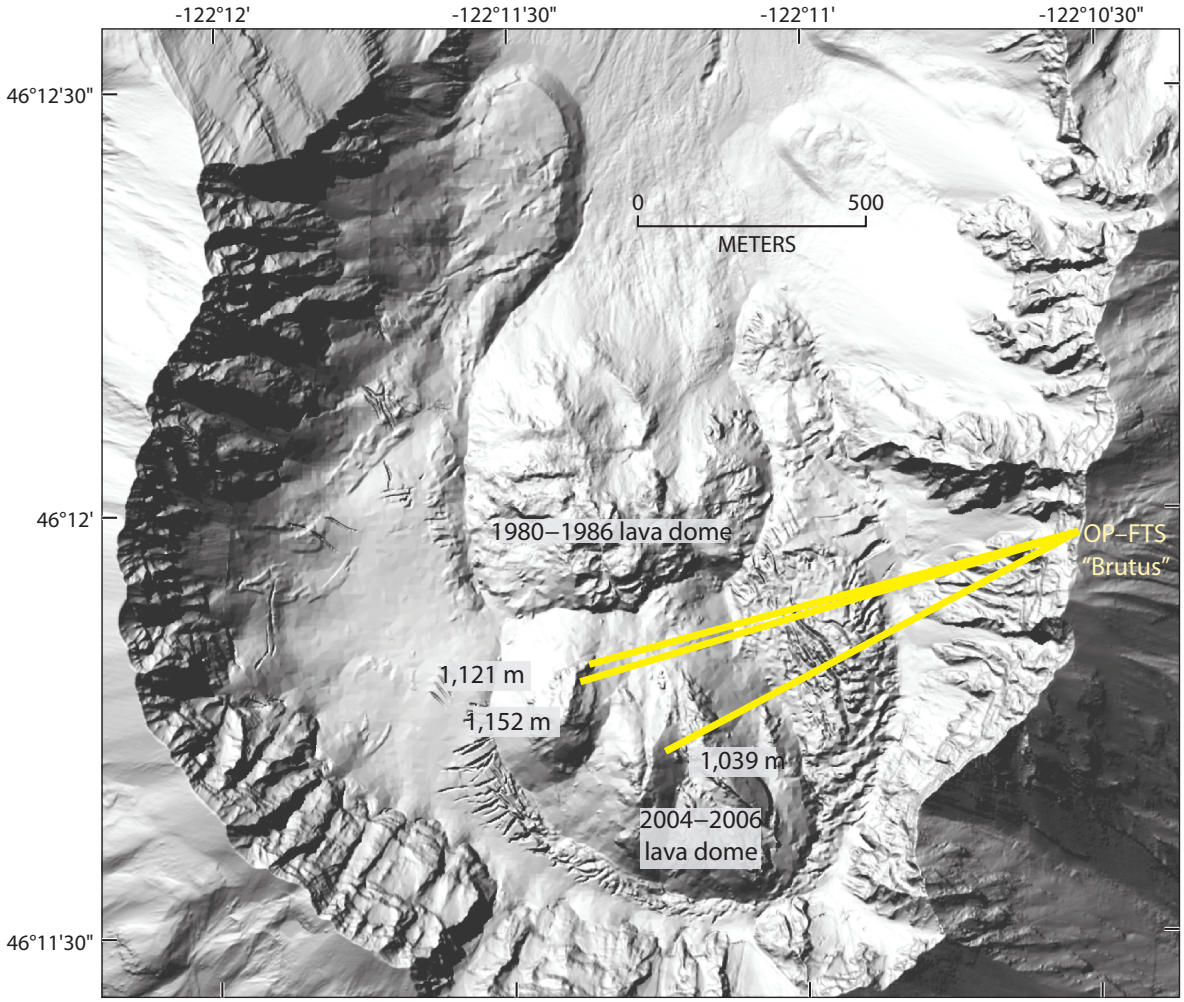

Figure 2. Shaded-relief digital elevation model of September 1, 2005, showing three paths used for OP–FTIR measurements in this study (courtesy of S.P. Schilling, USGS). Lengths of paths are labeled. Datum and projection are NAD83, UTM zone 10.

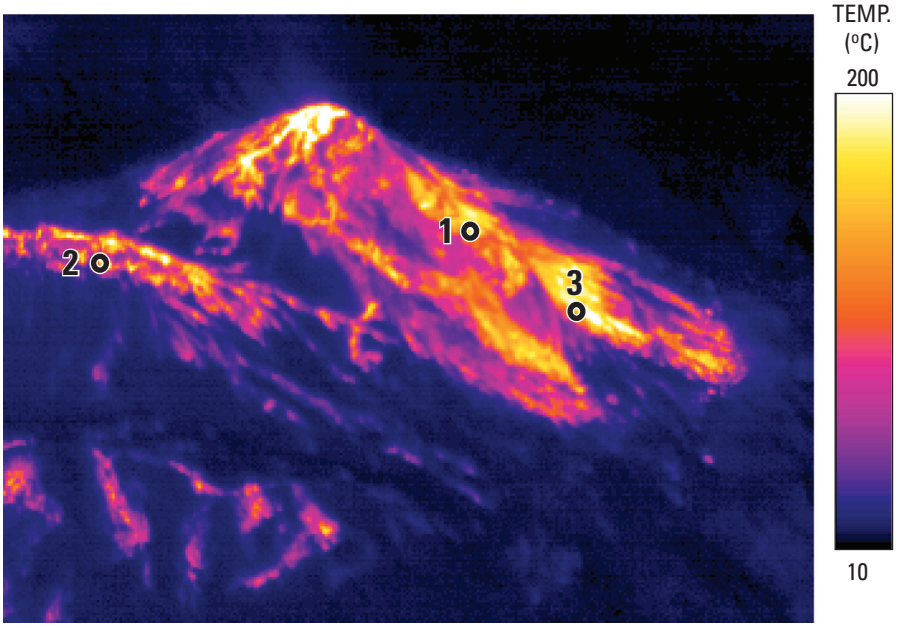

Figure 3. Thermal image, taken by forward-looking infrared radiometer (FLIR), showing lava dome from a helicopter near OP–FTIR measurement site (Brutus) on September 2, 2005 (courtesy of M. Logan, USGS). Numbers mark the parts of the lava dome used as infrared sources for measurement sets 1 to 3. Temperature scale on right.

Table 1. Summary of wavenumber windows used in analysis, detection limits, and mean errors for volcanic gas species detected by OP–FTIR in this study, Mount St. Helens, Washington, 2005.

Species	Wavenumber window (cm^{-1})	Detection limit (ppm·m)	Mean error (%)
H_2O	2134.80–2140.51	4,000	13.2
CO_2	2264.26–2273.20	2,000	15.3
HCl	2744.18–2848.38	3	7.6
SO_2	2447.36–2532.96	15	17.4
HF	4062.31–4089.16	20	14.1
CO	2089.29–2199.87	0.8	8.2
COS	2093.60–2020.87	0.7	7.6

sky spectrum for these measurements; rather, it is the spectrum containing the fewest molecules of volcanic gas in the series of measured spectra, S_i. A background spectrum under the exact conditions of the measurements containing no volcanic gas often is impossible to obtain in practice in this mode. Spectra were acquired once per second, and eight spectra were averaged, a procedure which typically took about 8 s.

In this study, retrievals for seven major volcanic gas species were carried out: H_2O, CO_2, HCl, SO_2, HF, CO, and COS. Retrievals for HCl and CO are relatively low in error, owing to their strong and fast absorption features; COS is detectable owing to its high absorptivity. Measured SO_2 exceeds detection limits, but the errors are larger owing to its weak absorption signature (at around 2,500 cm^{-1}). H_2O has a moderately high error owing to its high and variable background concentration derived from nonmagmatic, highly variable local sources, such as evaporating ground water, ice, and meteoric water. At these long pathlengths, background CO_2 is around 280,000 ppm·m, and, in order to be detected, volcanic CO_2 must be present at levels >5 percent above background levels. The errors and detection limits on the measurements are shown in table 1.

The results of the measurements take the form of molar ratios and gas compositions. The molar ratios are calculated by plotting the abundance (in concentration-pathlength units) of one gas species against another. The gas species will plot in a straight line if they are derived from a common origin (the volcanic vent) and a gas of constant composition is being emitted. All background gases, including random amounts of nonvolcanic H_2O, are eliminated from the results, owing to the normalization by background spectra. Any mixing of the volcanic gas with ambient air should, therefore, not affect the results unless chemical reactions are taking place, or unless there is significant heterogeneity in the atmospheric air composition in the pathlength (which is significant here for H_2O). The mean slope of the plots of gas abundances is equal to the molar ratio between the two species. Changes in the concentration-pathlength of a species with time are controlled by source effects (variations in the emission rate of gases), combined with fluctuating wind speeds and directions, which blow the plume gases out of the pathlength. Pairs of species concentration-pathlengths are used to calculate molar ratios, thereby eliminating these source and wind effects, as they will affect all gases similarly.

Emission rates for SO_2 were measured by absorption spectroscopy with a miniature spectrometer manufactured by Ocean Optics and an instrumental housing (incorporating calibration cells; FLYSPEC) and software developed by Horton and others (2006). Horizontal traverses were made beneath the plume, approximately 1.5 km downwind of the lava dome. Integrated concentration-pathlength across the plume width was multiplied by the plume speed (measured by using methodology developed by Doukas, 2002) to generate SO_2 emission rates. Three measurements of SO_2 emission rates were carried out, and errors are less than 10 percent.

Results

The spectra measured on August 31, 2005, record seven volcanic gas species: H_2O, CO_2, HCl, SO_2, HF, CO, and COS, in typical order of abundance for the three sets of measurements (fig. 2). The first set of measurements contained 109 spectra. The IR source for the measurements was part of spine 6, and the pathlength was 1,150 m (figs. 2, 3). These spectra recorded absorptions due to H_2O, HCl, CO, and COS gases; CO_2, SO_2, and HF were below detection, possibly due to a relatively low source temperature and (or) the long pathlength, both of which tend to decrease the signal-to-noise ratio. Figure 4 shows the characteristic absorption signature due to HCl gas in the measured spectra compared to a reference spectrum, the concentration-pathlength of H_2O and HCl, and the concentration-pathlengths of CO and COS with time for this set of measurements. Table 2 shows a summary of the data (labeled set 1) and includes mean and maximum concentrations measured for each species and the mean H_2O/Cl ratio. The relatively low abundances of all the detected gases (HCl, as much as 147 ppm·m, and H_2O, as much as 21,000 ppm·m) suggest that the

abundances of CO_2 and SO_2 were probably below detection for this set of measurements. The mean H_2O/Cl molar ratio was 120 (table 2).

The second set of measurements were taken using a shorter pathlength of 1,040 m and a remnant of spine 5 as an IR source (figs. 2, 3). Figure 5 shows that HCl, HF, CO, and COS are detectable during the entire time period, whereas H_2O, CO_2, and SO_2 are detectable in only some of the spectra. Nondetection in some parts of the time series might be due to a weakening of the IR source or a decrease in gas-column abundance. The abundance of HCl ranged from 0 to 624 ppm·m over the pathlength, whereas SO_2 reached 251 ppm·m (table 2, set 2). Carbon monoxide reached a maximum concentration-pathlength of 15 ppm·m, and COS reached 2.6 ppm·m. The mean Cl/S ratio was 2.1, and H_2O/Cl was 85 (table 2).

The third set of measurements was taken using an IR source on spine 6, with a pathlength of 1,120 m (figs. 2, 3). This set of measurements imaged gases emitted from the

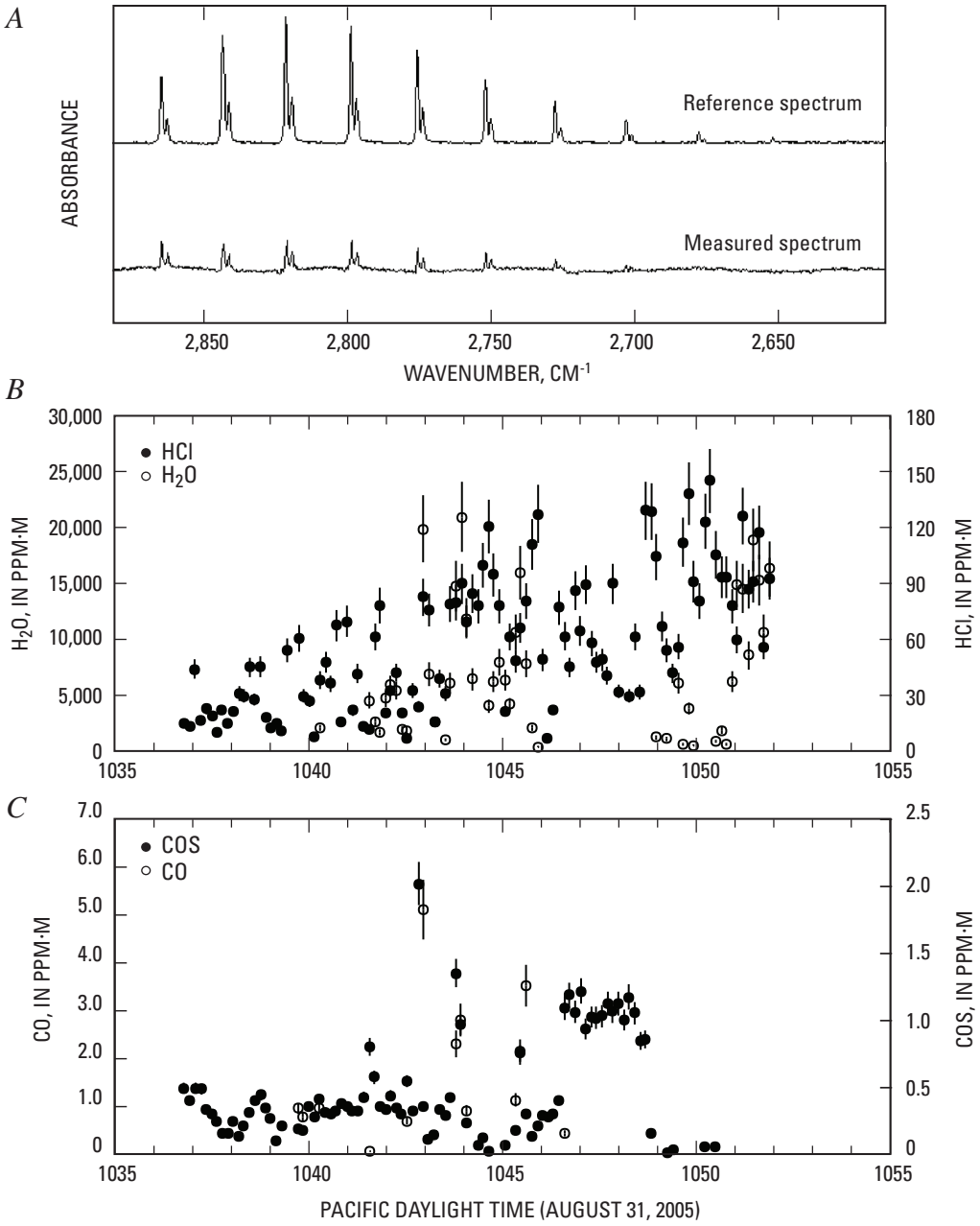

Figure 4. Data for measurement set 1, Mount St. Helens, Washington, 2005. *A*, Measured absorbance spectrum and reference spectrum for HCl gas for spectra collected along path 1. *B*, HCl and H_2O concentration pathlengths. *C*, CO and COS concentration pathlengths with time for measurement set 1.

Table 2. Summary of OP–FTIR measurements (sets 1, 2, and 3), Mount St. Helens, Washington, 2005.

[N is number of spectra in each set. Maximum $(LC)_{max}$ and mean $(LC)_{mean}$ are concentration pathlengths (in ppm·m) for the seven gas species detected; bd, below detection. Mean molar ratios are given with estimates of errors. Dashes show ratios not calculated where sulfur data are lacking.]

Set	HCl	SO_2	CO	CO_2	COS	H_2O	HF	Cl/S	Cl/F	H_2O/Cl	SO_2/COS	CO/CO_2
1 *N*=109												
$(LC)_{max}$	147	bd	5.1	bd	2.0	21,000	bd					
$(LC)_{mean}$	57.0	bd	1.7	bd	0.47	7,000	bd	--	--	120±25	--	--
2 *N*=479												
$(LC)_{max}$	624	251	15	10,300	2.6	51,000	310					
$(LC)_{mean}$	279	145	5.0	5,870	1.2	28,900	74	2.1±0.4	8.8±2.0	85±15	120±15	0.00086±0.0002
3 Active vent *N*=97												
$(LC)_{max}$	261	155	1.3	4,400	0.84	310,000	86					
$(LC)_{mean}$	110	121	0.42	1,300	0.35	64,000	40	1.1±0.3	3.5±2.0	1040±200	350±60	0.00032±0.00006

area closest to the active vent at the base of the most recently erupted spine. H_2O, CO_2, HCl, SO_2, HF, CO, and COS were detected in the absorption spectra (fig. 6 and table 2). The abundances of the gases were generally less than for measurement set 2; HCl concentration pathlengths reached 261 ppm·m, and SO_2 reached 155 ppm·m (table 2, set 3). The mean molar H_2O/Cl was 1,040 and Cl/S was 1.1. The molar ratios can be used to formulate a gas composition (table 3, column A). The gas was composed mainly of H_2O (99 mol percent), with 0.78 mol percent CO_2, 0.095 mol percent HCl, 0.085 mol percent SO_2, and minor amounts of HF, CO, and COS. For comparison, a gas sample collected in September 1981 (Gerlach and Casadevall, 1986) is shown in column D. Columns B and E show the same gas compositions recalculated to H_2O-free compositions, and columns C and F show them recalculated to H_2O- and CO_2-free compositions. The gas composition measured in 2005 is similar to that measured in 1981, albeit with less CO and more COS.

The ultraviolet spectrometer traverses carried out at 1400 PDT on August 31, 2005, yielded a mean SO_2 flux of 22 t/d. By converting the molar gas composition into the mass composition (table 4) for measurement set 3, the SO_2 emission rate (bold, table 4) can be used to calculate emission rates for the six other species. On August 31, 2005, H_2O was emitted at rates of about 83 kg/s (7,200 t/d), CO_2 at 1.6 kg/s (140 t/d), HCl at 0.16 kg/s (14 t/d), and HF at 0.024 kg/s (2.0 t/d). CO and COS were emitted at rates of 0.63 and 0.69 g/s, respectively; these fluxes are associated with errors of ~±20 percent. CO_2 emission rates were measured independently by using LICOR and were found to be 198 t/d (Gerlach and others, this volume, chap. 26). The excess can be attributed to a small amount of CO_2 degassing from the 1980–86 lava dome (Gerlach and others, this volume, chap. 26), which was not captured by the OP–FTIR measurements.

Discussion

Partitioning of Cl into Aqueous Vapor

Experimental work on Cl behavior in silicic magmas demonstrates the strong affinity that Cl has for a H_2O-rich vapor phase (Kilinc and Burnham, 1972; Webster and Holloway, 1988). The fluid-melt partition coefficient increases with decreasing temperature and with increasing dissolved melt Cl content; and decreases with decreasing pressure (Shinohara and others, 1989), although the latter is not well constrained. The partition coefficient is high for subaluminous melts and decreases with increasing aluminous or peralkaline character (Webster, 1992). Increasing the Cl molality of the vapor phase to high levels causes the formation of an immiscible Cl-rich liquid, as observed in the H_2O-NaCl system (Shinohara and others, 1989). Signorelli and Carroll (2002) determined Cl solubility limits of 4,800–6,800 ppm for the hydrous rhyolite melt of recent Soufrière Hills volcano eruptions, which has a (Na+K)/Al ~0.6. These concentrations are much higher than those observed in melt-inclusion glasses (Edmonds and others,

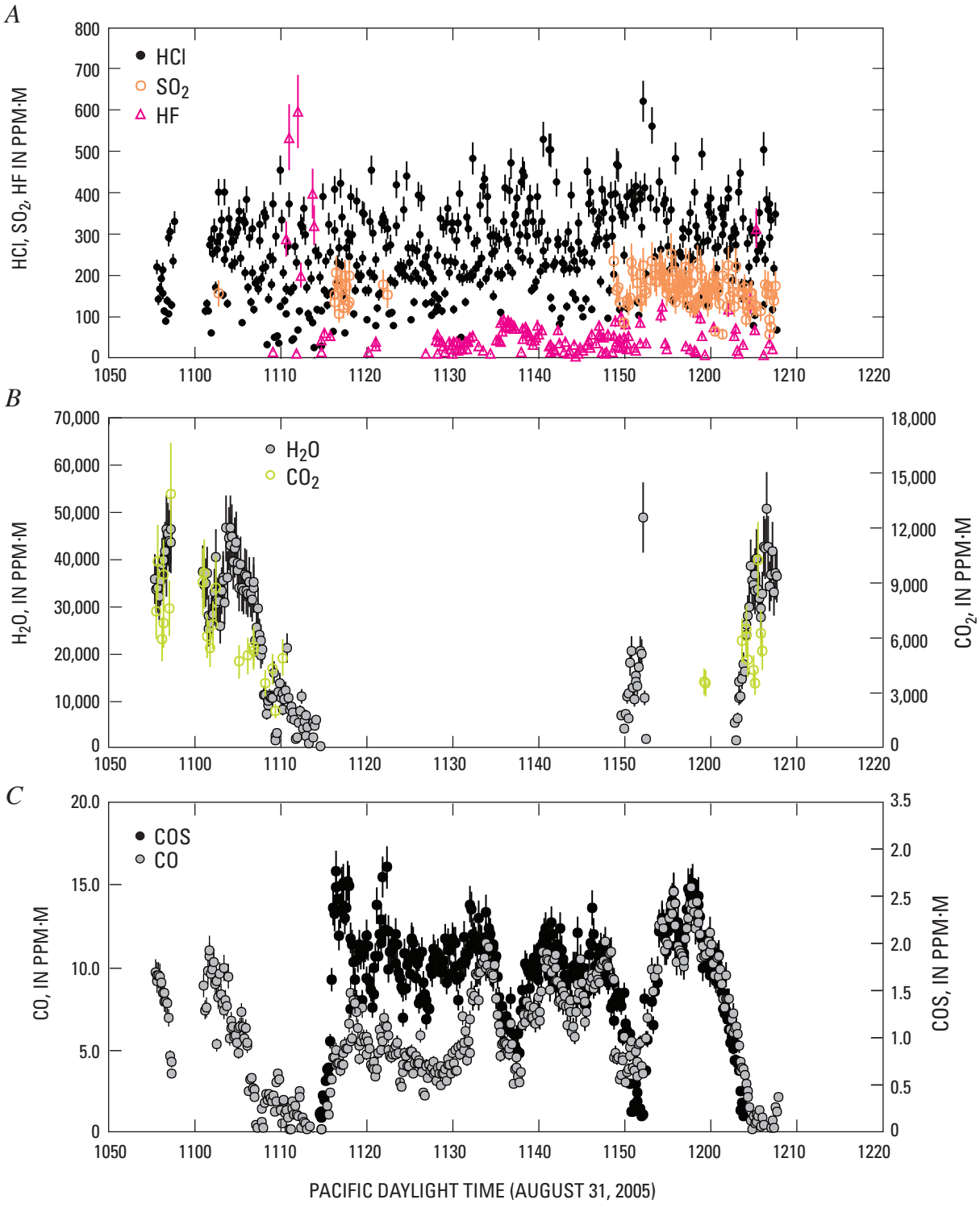

Figure 5. Data for measurement set 2, Mount St. Helens, Washington, 2005, as concentration pathlengths with time. *A*, HCl, HF, and SO_2. *B*, H_2O and CO_2. *C*, CO and COS.

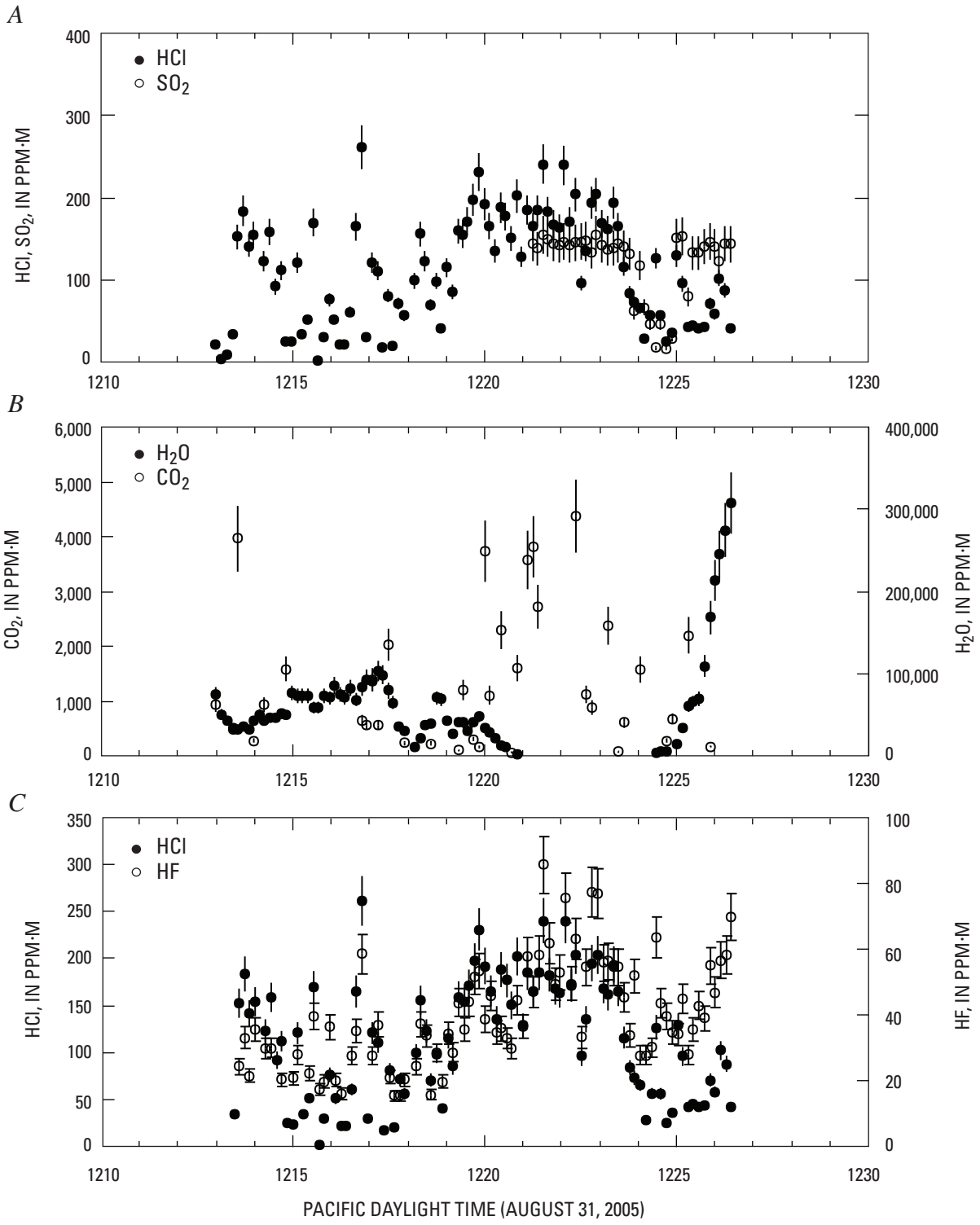

Figure 6. Data for measurement set 3, Mount St. Helens, Washington, 2005, as concentration pathlengths with time. *A*, HCl and SO_2. *B*, H_2O and CO_2. *C*, HCl and HF.

Table 3. Gas compositions at Mount St. Helens, 1981 and 2005.

[Compositions (in molar percent) derived from this study (column A) are compared with a representative gas composition derived from sampling of gases by using caustic soda in May 1981 (column D; Gerlach and Casadevall, 1986). Columns B and E show the gas compositions recalculated to H_2O-free compositions. Columns C and F show the gas compositions recalculated to H_2O- and CO_2-free compositions.]

	This study (set 3)			September 17, 1981		
	A	B	C	D	E	F
H_2O	99			99		
CO_2	0.78	79		0.89	83	
HCl	0.095	9.7	46	0.076	7.2	43
SO_2	0.085	8.6	41	0.067	6.3	38
HF	0.027	2.8	13	0.030	2.8	17
CO	0.00048	0.049	0.23	0.0023	0.22	1.3
COS	0.00025	0.025	0.12	1.8×10^{-5}	0.0017	0.010

Table 4. Gas composition derived from this study (from measurement set 3), Mount St. Helens, Washington, 2005, in molar percent and mass percent.

[Flux of each species is calculated using the flux of SO_2 gas measured with ultraviolet spectrometers (22 t/d; in bold). Fluxes expressed both in kg/s and in t/d.]

Species	Molar %	Mass %	Flux (kg/s)	Flux (t/d)
H_2O	99	98	83	7,200
CO_2	0.78	1.9	1.6	140
HCl	0.095	0.19	0.16	14
SO_2	0.085	0.30	0.25	**22**
HF	0.027	0.028	0.024	2.0
CO	0.00048	0.00073	0.00063	0.054
COS	0.00025	0.00080	0.00069	0.059

2002) and suggest that the aqueous vapor phase was relatively Cl poor. In the case of Mount St. Helens, melt-inclusion data for the erupted products of 1980–86 indicate that the maximum Cl content of the preeruptive melt was around 1,000 ppm (Rutherford and others, 1985), which is within the range of Cl concentrations in melt inclusions from the 2004–5 eruption of Mount St. Helens (Pallister and others, this volume, chap. 30) and is much lower than the solubility for Cl in a melt with (Na+K)/Al ~1 at 850–900°C and 200 MPa (around 2,000–2,500 ppm; Metrich and Rutherford, 1992). If the 2004–5 Mount St. Helens melt had an initial H_2O content of ~4.6 weight percent, similar to that obtained from melt-inclusion analysis for the 1980s erupted products (Rutherford and others, 1985), and if P_{total} is equal to P_{H_2O}, then the melt was in equilibrium with a H_2O-rich vapor at a depth of around 6 km (assuming lithostatic pressure with depth). The preeruption dissolved Cl content of the melt at about 6 km is assumed to be close to 1,000 ppm, on the basis of the maximum Cl concentration measured in melt inclusions (Pallister and others, this volume, chap. 30), which is within range of typical silicic arc magmas (Wallace, 2005).

The H_2O/HCl molar ratio of the vapor varies during melt ascent and eruption and is controlled by water solubility and degassing, partitioning of Cl into the vapor, the degassing regime (whether open- or closed-system degassing or some combination of the two is in operation), and microlite crystallization on ascent (which will tend to increase the concentration of volatiles in the melt and promote further degassing). These factors can be incorporated into models describing the evolution of the vapor phase on ascent and compared with the

observations presented here. This analysis assumes there is no breakdown of hydrous phases (for example, amphibole), which would tend to increase the bulk H_2O of the system on magma ascent.

Closed-system degassing occurs when volatiles exsolve and remain in contact and in equilibrium with the host melt. The vesicularity of the melt is related to the amount of volatiles exsolved and the total pressure. Closed-system degassing can occur (1) during rapid ascent of magma from depth, resulting in fragmentation when the overpressure inside the expanding bubbles exceeds the strength of the magma, (2) in static magma bodies as a result of second boiling, and (3) during slow ascent of magma at depths of greater than a few kilometers, where gas fractions will typically be too low for fragmentation to occur. The partitioning of Cl between melt and aqueous vapor can be used to describe closed-system degassing:

$$\left(X^0_{H_2O} - X_{H_2O}\right) = \left(\frac{X^0_{Cl}}{X_{Cl}} - 1\right) \Big/ D_{Cl}^{fluid-melt}, \quad (5)$$

where $X^0_{H_2O}$ and X^0_{Cl} are the original H_2O and Cl mass fractions, X_{H_2O} and X_{Cl} are the melt H_2O and Cl mass fractions, and $D_{Cl}^{fluid-melt}$ is the vapor-melt coefficient for Cl (assumed here to be constant). X_{H_2O} varies with pressure according to its solubility, which is calculated using VolatileCalc for a rhyolite melt at 920°C and with a $X^0_{H_2O}$ of 4.6 weight percent (Newman and Lowenstern, 2002).

Open-system degassing involves increments of vapor being removed from the host melt after exsolution. For volatiles that partition strongly into a vapor phase, this style of degassing results in efficient removal of the species from the melt. This style of degassing may occur (1) along conduit sidewalls, where exsolved volatiles can escape by migrating upward or through the conduit walls, or (2) during shallow, slow ascent of magma, when sufficient porosity develops to allow permeability and vapor escape through a three-dimensional bubble network (for example, Blower, 2001); significant gas loss through bubble ascent would be suppressed by the high viscosity of the magma and crystals. Open-system degassing can be modeled using a Rayleigh fractionation equation (for example, Villemant and Boudon, 1999):

$$X_{Cl} = X^0_{Cl} f^{\alpha}, \quad (6)$$

$$\text{where } \alpha = \left(D_{Cl}^{fluid-melt} - 1\right), \quad (7)$$

$$\text{and } f = 1 - \left[\left(X^0_{H_2O} - X_{H_2O}\right) \Big/ X^0_{H_2O}\right], \quad (8)$$

where f is the fraction of water remaining in the melt. X_{Cl} is calculated for 5-MPa increments in pressure and converted to depth (km) assuming lithostatic pressures and a mean crustal density of 2,500 kg/m^3.

In order to account for microlite crystallization on ascent, which decreases the melt volume and causes increased exsolution of water, a factor q was introduced to the equation for the open-system degassing case, whereby

$$q = q^0 - q^0\left(\left(X^0_{H_2O} - X_{H_2O}\right) \Big/ X^0_{H_2O}\right), \quad (9)$$

where q^0 is the initial melt fraction (taken to be 0.6). The expression for f, the fraction of H_2O remaining in the melt, is modified thus:

$$f = 1 - \left[\left(X^0_{H_2O} - X_{H_2O}\right) \Big/ X^0_{H_2O}\right] - \left[\left(\frac{q_n}{q_{n-1}}\right) X_{H_2O} - X_{H_2O}\right], \quad (10)$$

where q_n is the melt fraction for the previous step and q_{n-1} is the melt fraction for the current step and $q_{n-1} < q_n$. This has the effect of decreasing f to a slightly greater degree at each step to account for the effects of microphenocryst and microlite crystallization.

Figure 7 shows the results for closed- and open-system degassing for three partition coefficients (D). These results show the large dependence of the vapor composition at the surface on degassing regime. The plots show the depletion of Cl in the melt, the ratio of dissolved H_2O/Cl, and the H_2O/Cl ratio in the vapor phase, with depth. Three measured parameters are marked on the plots to compare to the model data: (1) the mass fraction of dissolved Cl, (2) the H_2O/Cl in the matrix glass of the erupted products (for microcrystalline and flow-banded dacite; from Pallister and others, this volume, chap. 30; summarized in table 5), and (3) the mass ratio H_2O/Cl in the volcanic gases (converted from molar ratios given in table 2). The H_2O/Cl in gases from measurement sets 1 and 2 range from 35 to 70 and are labeled stagnant dome (SD), and those from measurement set 3 range from 430 to 630 and are labeled active dome (AD).

The mass fraction of Cl in the melt, dissolved melt H_2O/Cl, and vapor H_2O/Cl from the stagnant dome are consistent with closed-system degassing, with a large partition coefficient (D~50) for Cl, from depths of ~ 6 km. The active dome gases are richer in H_2O and are closer to the modeled H_2O/Cl for an open-system degassing regime. Open-system degassing from depth would deplete the melt almost entirely of Cl, however, which is not the case (figs. 7*A*, *B*); open-system degassing from depth is therefore inconsistent with observation. Closed-system degassing from depth with constant D is consistent with observation but unrealistic on two counts: (1) closed-system degassing could not physically lead to lava dome building, owing to the inevitably large gas fractions that would result at shallow depths, and (2) a constant partition coefficient for Cl is improbable, based on the experiments of Shinohara and others (1989), which suggests that D is strongly dependent on both dissolved melt Cl and on pressure.

Recent studies of degassing during the lava dome building of Soufrière Hills volcano, Montserrat, have shown that the degassing of H_2O in the upper conduit leads to cooling,

crystallization, and an increase in viscosity of the magma (for example, Sparks and others, 2000). The development of permeability during degassing in the top ~1 km of the conduit leads to gas loss and effusive eruption. In order to investigate whether this mechanism is consistent with the proportions of H_2O and Cl in the melt and in volcanic gases at Mount St. Helens, the model is adjusted by using equation 5 in order to incorporate the effects of closed-system degassing at depths greater than 1 km with the same mean fluid-melt partition coefficients for Cl (3, 10, and 50), followed by open-system degassing along the top 1 km of the conduit (fig. 8), using equations 6–10 with fluid-melt partition coefficients of 1, 2, and 3 ($X^0_{H_2O}$ and $X^0{}_{Cl}$ are set equal to the final X_{H_2O} and X_{Cl} given by the closed-system degassing model at 1-km depth; fig. 8). A partition coefficient of 1 represents the case whereby no further degassing of Cl occurs. The plots in figures 7 and 8 are, therefore, identical up to 1-km depth; at shallower depths, the effects of open-system degassing are shown in figure 8. Observations of the melt and gases are marked on figure 8 to compare to the models. The mass fraction of Cl remaining dissolved in the melt, the melt H_2O/Cl, and the H_2O/Cl for gases emitted from the stagnant part of the lava dome are consistent with deep, closed-system degassing (D~10), followed by open-system degassing with D~2–3 (fig. 8). A decrease in D to <5 was noted by Shinohara and others (1989) for lithostatic pressures corresponding to depths less than 2 km.

Table 5. Mean concentrations of Cl and H_2O in erupted matrix glasses of microcrystalline (from 5 measurements) and flow-banded (from 12 measurements) dacite, Mount St. Helens, Washington, 2004—2005.

[From Pallister and others, this volume, chap. 30.]

Matrix glass	Cl (ppm)	H_2O (wt%)	H_2O/Cl
Microcrystalline dacite			
Mean concentration	278	1.40	41
1σ deviation	53	0.98	24
Flow-banded dacite			
Mean concentration	853	2.40	28
1σ deviation	47	0.29	4.5

The H_2O/Cl of gases emitted from the active part of the lava dome, however, are not consistent with any of the theoretical models formulated here. This may be due to one or all of three factors: (1) a cessation of Cl degassing in the top 1 km of the conduit, (2) addition of substantial amounts of meteoric, ground-water, and glacier-derived H_2O to the gases at shallow

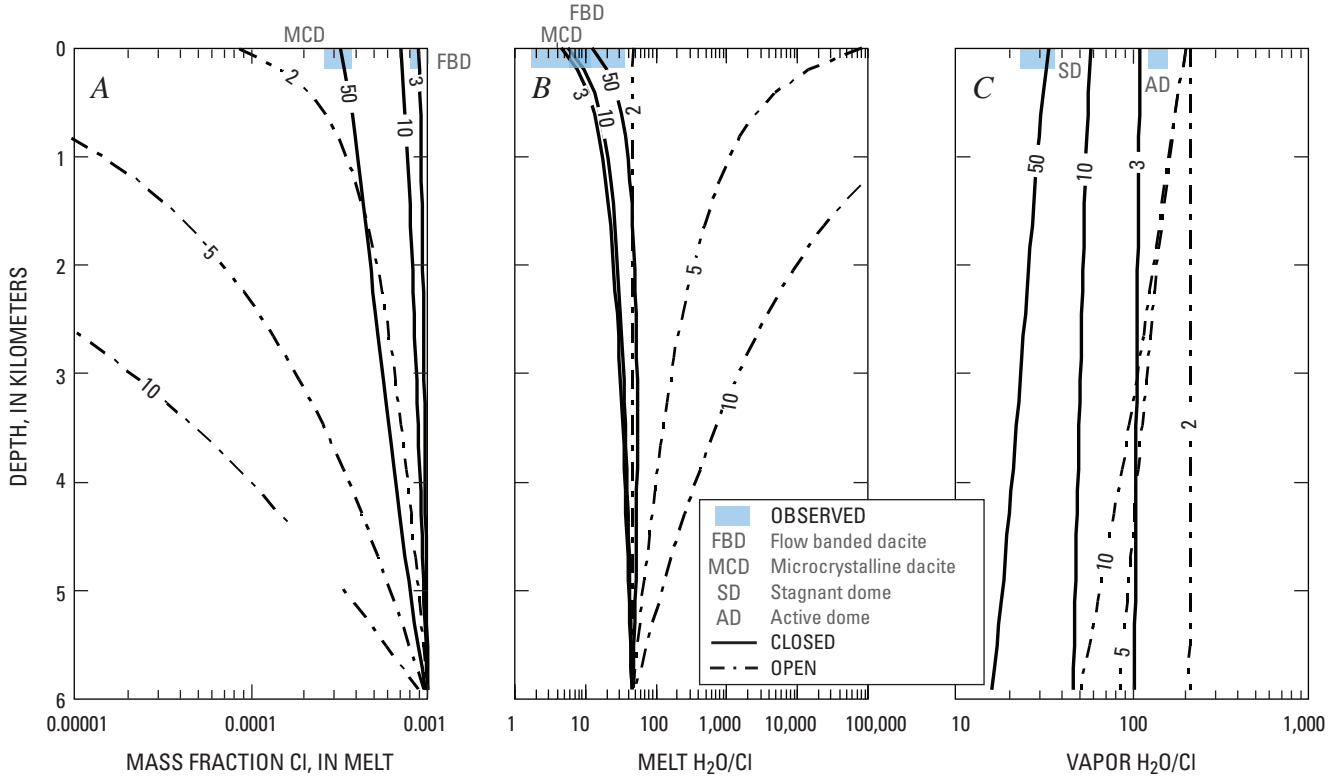

Figure 7. Effect on evolution of gases with depth for various models of degassing regime. Solid lines indicate closed-system degassing models and are labeled with the fluid-melt partition coefficient, D. Dot-dash lines indicate open-system degassing models and are labeled with the fluid-melt partition coefficient. Blue boxes indicate observed melt Cl, melt H_2O/Cl, and vapor H_2O/Cl. *A*, Fraction of Cl in melt. *B*, Dissolved melt H_2O/Cl. *C*, vapor H_2O/Cl.

depths, or (3) some Cl present as alkali chloride (NaCl and KCl) in the gas phase, as observed by Le Guern and Shinohara (1985) and studied experimentally by Shinohara and others (1989). The proportions of dissolved H_2O and Cl remaining in the erupted glasses suggests that there is no cessation of Cl degassing in the top 1 km of the conduit (fig. 8; compare observations to solid line presenting D=1), so this factor is discounted. Shevenell and Goff (1999) used oxygen- and hydrogen-isotope data from hot springs to show that only 30–70 mol percent of the H_2O in the fumaroles around the lava dome in 1981–86 was magmatic. In this case, the discrepancy between models and observations requires that only ~10 mol percent of the measured H_2O be magmatic. Modification of the gas composition is shown in table 3, column A; using this factor yields 91 mol percent H_2O and 7 mol percent CO_2, which might be more representative of the magmatic gas composition. The presence of alkali chlorides in the gas phase is consistent with the presence of chloride encrustations on the lava dome (possibly halite and (or) sylvite) observed during 2004–5 (C.R. Thornber, oral comm. 2005). Yellow encrustations on the September 1980 lava dome were noncrystalline and composed of Al, Cl, Fe, Ca, S, and H_2O. A sublimate film near fumaroles <250°C produced a yellow-brown stain on crack walls, which had a high Cl content (Keith and others, 1981).

Comparison and Significance of Molar Cl/S

The behavior of S in silicic melts differs significantly from both Cl and H_2O. The partitioning of sulfur into a vapor phase is controlled by several factors, the most significant being the fugacities of oxygen and sulfur in the vapor phase and melt composition (Carroll and Webster, 1994). The solubility of sulfur is much lower than that of Cl for a given set of magmatic conditions. Table 6 shows molar Cl/S measured using a variety of techniques during eruptions at a range of dacitic and andesitic subduction-zone volcanoes, including the 1980–86 Mount St. Helens lava-dome eruption. The molar ratio measured during this study is similar (within error) to ratios measured at most other volcanoes and to ratios measured during the 1980–86 Mount St. Helens eruption, with the notable exception of Soufrière Hills volcano, which shows considerably higher Cl/S during lava dome-building activity. A molar Cl/S of ~1 appears to be a dominant feature of most reported gas compositions measured during eruptions in subduction-zone settings.

Botcharnikov and others (2004) reported solubility data for melts coexisting with mixed H_2O-Cl-S gases to illustrate the effect of multiple volatile components on their solubility. The total Cl content of the melt-vapor system can affect the

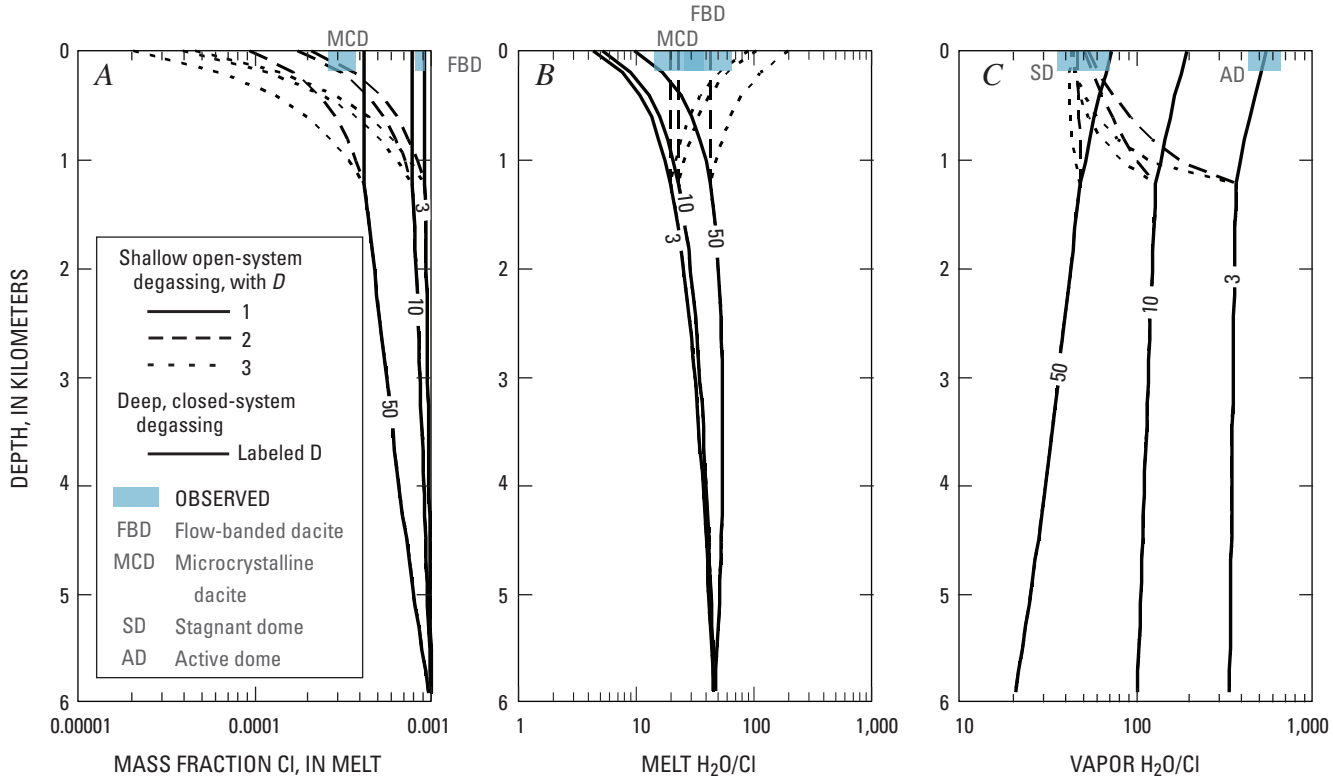

Figure 8. Effect of closed, then open-system (in the upper 1 km of the conduit) degassing on the composition of volcanic gases at the surface. The evolution of (*A*) the fraction of Cl in the melt, (*B*) dissolved melt H_2O/Cl, and (*C*) vapor H_2O/Cl with depth (km) for various models of degassing regime are shown. Closed-system degassing regimes are indicated by solid lines up to 1 km depth, labeled with values of D. Above 1 km depth, open-system degassing regimes are shown as dashed-dotted lines for three different values of D (see key). Observed melt Cl, melt H_2O/Cl, and vapor H_2O/Cl are shown as blue boxes.

Table 6. Molar Cl/S ratios in volcanic gases measured at other silicic subduction-zone volcanoes and at Mount St. Helens, Washington, 2005.

[Errors are estimated as ranging from 5 to 10 percent. OP–FTIR, open-path Fourier-transform IR spectroscopy; EBS, evacuated bottle sampling.]

Volcano	Type	Method	Cl/S
Usu-san, Japan[1]	Basaltic andesite	OP–FTIR	0.8
Mount St. Helens, USA[2]	Dacite	EBS	1.2
Mount St. Helens, USA[3]	Dacite	OP–FTIR	1.1
Augustine Volcano, USA[4]	Dacite	EBS	1.0
Unzen-dake, Japan[5]	Dacite	OP–FTIR	0.9
Soufrière Hills, Montserrat[6]	Andesite	OP–FTIR	2.0

[1]Mori and others, 1997.

[2]Gerlach and Casadevall, 1986.

[3]This study.

[4]Symonds and others, 1990.

[5]Mori and others, 1993.

[6]Edmonds and others, 2002.

solubility of S (Botcharnikov and others, 2004). The addition of 1 weight percent Cl increased S solubility by two times at 850°C and 200 MPa for a dacite-composition melt, with all other conditions constant. For a given H_2O vapor concentration, over a range of total S content and solubility, a maximum S solubility occurred corresponding to a vapor Cl/S of ~1. A vapor Cl/S of ~1 may, therefore, be a direct consequence of the presence of moderate amounts of Cl in the melt, which is typical for arc magmas; vapor Cl/S might further be buffered by the addition or depletion of small amounts of Cl to the system. The maximum in S solubility might be explained by two main factors (Botcharnikov and others, 2004): (1) S is dissolved as sulphate (SO_4^{2-}) in hydrous melts, where oxygen fugacity is relatively high, and as sulfide (S^{2-}) at low oxygen fugacities (Carroll and Webster, 1994); the transition occurs at oxygen fugacities close to NNO. The addition of Cl to an S-bearing system might shift the redox conditions to slightly more oxidized conditions. The other possibility is (2) that S-Cl-bearing complexes may form in the melt, which would increase the solubilities of both components.

The Abundance of Minor Gaseous Components (HF, CO, COS)

The solubility of fluorine (F) in silicic melts is generally much higher than that of Cl and, hence, does not degas to the same extent (Carroll and Webster, 1994). The vapor-melt partition coefficient for F is usually less than unity (Webster, 1990). Table 2 shows that the molar ratio of Cl/F in the volcanic gases is around 3.5. A similar molar Cl/F has been reported at a number of other silicic volcanoes in subduction-zone settings (Symonds and others, 1994) and compares well with the abundance of HF emitted from fumaroles at Mount St. Helens in September 1981 (table 3; Gerlach and Casadevall, 1986).

The mean CO/CO_2 ratio of the gases of around 3.2×10^{-4} (table 2) implies that the gases equilibrated at a temperature of about 570°C, on the basis of the relation:

$$\log\left(CO/CO_2\right) = 1.76 - 4417/T, \qquad (11)$$

where T is the temperature in Kelvin (Mori and Notsu, 1997). Collection temperatures derived from similar relations in gases sampled in 1981 ranged from 620°C to 762°C (Gerlach and Casadevall, 1986).

COS has been detected previously in volcanic plumes (for example, Le Guern and others, 1975), although measurements are few. Rasmussen and others (1982) reported abundances of 5 ppm by volume in the Mount St Helens gas plume of May 18, 1980, and suggested that injection of COS contributes to the stratospheric S burden during large silicic eruptions. Gerlach and Casadevall (1986) report molar SO_2/COS of 2,000 to 4,750 for gas samples collected at Mount St Helens from May to September 1981 from radial fumaroles around the lava dome. The mean molar ratios obtained August 31, 2005, using OP–FTIR are much lower than they were in the earlier samples, 350 (table 2, set 3) and 120 (set 2). Mori and Notsu (1997) reported SO_2 / COS of 400 for gases emitted from a fumarole at Aso, Japan, at a temperature of ~740°C.

Conclusions

Several conclusions can be drawn from the results and interpretation presented here:

- The fluxes of magmatic volatiles from Mount St. Helens on August 31, 2005, were 7,200 t/d H_2O, 140 t/d CO_2, 14 t/d HCl, 22 t/d SO_2, 2.0 t/d HF, 54 kg/d CO, and 59 kg/d COS.
- The H_2O/Cl ratio in the gases emitted from stagnant parts of the Mount St Helens lava dome, and the amount of Cl and the H_2O/Cl in the erupted glasses in the melt, are all consistent with a model of closed-system degassing up to ~ 1-km depth (with a fluid-melt partition coefficient, *D*, for Cl of ~10), followed by open-system degassing to the surface (with a *D* of ~2–3). This is similar to models proposed for lava dome-building eruptions elsewhere, where much of the gas loss occurs in the upper 1 km of the conduit, causing cooling, crystallization, and an increase in magma viscosity.
- The gases emitted from the active part of the Mount St Helens lava dome have an H_2O/Cl that is about one order of magnitude higher than that predicted for closed- or open-system degassing or the two-stage model above. This is explained by as much as 90 mol percent of the measured H_2O vapor being nonmagmatic (ground- or glacier-derived) and by some of the Cl being present as alkali chlorides in the gas phase (NaCl and KCl).
- Molar Cl/S in the gases measured in August 2005 is similar to that measured during 1980–86 at Mount St. Helens and at silicic subduction-zone volcanoes elsewhere during similar styles of eruption. This similarity may be caused by a maximum in S solubility when vapor Cl/S ~1, which is valid for the typical range in initial S and Cl (100–300 and 1,000–3,000 ppm, respectively) at silicic subduction-zone volcanoes.
- The gas analyses presented here confirm that remote spectroscopic techniques are capable of measuring the composition of high-temperature gases remotely and safely during lava dome building at silicic volcanoes, provided the measurements can be made using a pathlength ≤1 km with sufficient gas molecules in the path to enable detection. There is scope for automated measurements with more compact instruments that consume less power, enabling the development of time series and further analysis of the degassing regime throughout an eruption.

Acknowledgments

This work was done with the support of the USGS Mendenhall Postdoctoral Fellowship Program and the Center for the Study of Active Volcanoes (CSAV) at the University of Hawai`i, Hilo. Michelle Coombs and Jacob Lowenstern provided detailed and thorough reviews, which improved the manuscript enormously.

References Cited

Blower, J.D., 2001, Factors controlling permeability-porosity relationships in magma: Bulletin of Volcanology, v. 63, no. 7, p. 497–504.

Botcharnikov, R.E., Behrens, H., Holtz, F., Koepke, J., and Sato, H., 2004, Sulfur and chlorine solubility in Mt. Unzen rhyodacitic melt at 850°C and 200 MPa: Chemical Geology, v. 213, no. 1–3, p. 207–225.

Burton, M.R., Allard, P., Mure, F., and Oppenheimer, C., 2003, FTIR remote sensing of fractional magma degassing at Mount Etna, Sicily: Geological Society Special Publication, v. 213, p. 281–293.

Carroll, M.R., and Webster, J.D., 1994, Solubilities of sulfur, noble gases, nitrogen, chlorine and fluorine in magmas: Reviews in Mineralogy, v. 30, p. 231–280.

Dixon, J.E., Stolper, E.M., and Holloway, J.R., 1995, An experimental study of water and carbon dioxide solubilities in mid-ocean ridge basaltic liquids; Part I, Calibration and solubility models: Journal of Petrology, v. 36, no. 6, p. 1607–1631.

Doukas, M.P., 2002, A new method for GPS-based wind speed determinations during airborne volcanic plume measurements: U.S. Geological Survey Open-File Report 02–395, 13 p.

Edmonds, M., Pyle, D.M., and Oppenheimer, C., 2002, *HCl* emissions at Soufrière Hills Volcano, Montserrat, West Indies, during a second phase of dome building, November 1999 to September 2000: Bulletin of Volcanology, v. 64, p. 21–30.

Edmonds, M., Gerlach, T.M., Herd, R.A., Sutton, A.J., and Elias, T., 2005, The composition of volcanic gas issuing from Pu‘u ‘Ō‘ō, Kīlauea Volcano, Hawai‘i, 2004–5 [abs.]: Eos (American Geophysical Union Transactions), v. 86, no. 52, San Francisco, December 5–9, 2005. Fall Meet. Suppl. Abstract, V13G–08.

Francis, P.W., Maciejewski, A., and Oppenheimer, C., 1995, SO_2/HCl ratios in the plumes from Mt. Etna and Vulcano determined by Fourier transform spectroscopy: Geophysical Research Letters, v. 22, p. 1717–1720.

Gerlach, T.M., and Casadevall, T.J., 1986, Evaluation of gas data from high-temperature fumaroles at Mount St. Helens, 1980–1982: Journal of Volcanology and Geothermal Research, v. 28, nos. 1–2, p. 107–140, doi:10.1016/0377-0273(86)90008-9.

Gerlach, T.M., McGee, K.A., and Doukas, M.P., 2008, Emission rates of CO_2, SO_2, and H_2S, scrubbing, and preeruption excess volatiles at Mount St. Helens, 2004–2005, chap. 26 *of* Sherrod, D.R., Scott, W.E., and Stauffer, P.H., eds., A volcano rekindled; the renewed eruption of Mount St. Helens, 2004–2006: U.S. Geological Survey Professional Paper 1750 (this volume).

Horton, K.A., William-Jones, G., Garbeil, H., Elias, T., Sutton, A.J., Mouginis-Mark, P., Porter, J.N., and Clegg, S., 2006, Real-time measurement of volcanic SO_2 emissions—validation of a new UV correlation spectrometer (FLYSPEC): Bulletin of Volcanology, v. 68, no. 4, p. 323–327, doi:10.1007/s00445-005-0014-9.

Keith, T.E.C., Casadevall, T.J., and Johnston, D.A., 1981, Fumarole encrustations—occurrence, mineralogy and chemistry, *in* Lipman, P.W., and Mullineaux, D.R., eds., The 1980 eruptions of Mount St. Helens, Washington: U.S. Geological Survey Professional Paper 1250, p. 239–250.

Kilinc, I.A., and Burnham, C.W., 1972, Partitioning of chloride between a silicate melt and coexisting aqueous phase from 2 to 8 kilobars: Economic Geology, v. 67, p. 231–235.

Le Friant, A., Boudon, G., Komorowski, J.-C., and Deplus, C., 2002. The island of Dominica, site for the generation of the most voluminous debris avalanches in the Lesser Antilles: Comptes Rendus Geoscience, v. 334, no. 4, p. 235–243, doi:10.1016/S1631-0713(02)01742-X.

Le Guern, F., and Shinohara, H., 1985, Etna 1983 composition of the magmatic gases [abs.]: International Association of Volcanology and Chemistry of the Earth's Interior, General Assembly 1985, Giardini-Naxos, Italy, abstract vol. no. QE272 I58 A2 1985.

Le Guern, F., Giggenbach, W., and Tazieff, H., 1975, Equilibres chemiques des gaz eruptifs du volcan Erta`Ale (Ethiopie): Comptes Rendus Hebdominaires des Seances de l'Aacademie des Sciences, Serie D: Sciences naturelles, v. 280, p. 2093–2095.

Lowenstern, J.B., Mahood, G.A., Rivers, M.L., and Sutton, S.R., 1991, Evidence for extreme partitioning of copper into a magmatic vapor phase: Science, v. 252, p. 1405–1409.

Manning, C., 2004. The chemistry of subduction-zone fluids: Earth and Planetary Science Letters, v. 223, p. 1–16.

Metrich, N., and Rutherford, M.J., 1992, Experimental study of chlorine behavior in hydrous silicic melts: Geochimica et Cosmochimica Acta, v. 56, p. 607–616.

Mori, T., and Notsu, K., 1997, Remote CO, COS, CO_2, SO_2, HCl detection and temperature estimation of volcanic gas: Geophysical Research Letters, v. 24, no. 16, p. 2047–2050.

Mori, T., Notsu, K., Tohjima, Y., and Wakita, H., 1993, Remote detection of HCl and SO_2 in volcanic gas from Unzen Volcano, Japan: Geophysical Research Letters, v. 20, no. 13, p. 1355–1358.

Newman, S., and Lowenstern, J.B., 2002, VolatileCalc—a silicate melt-H_2O-CO_2 solution model written in Visual Basic for excel®: Computers and Geosciences, v. 28, no. 5, p. 597–604, doi:10.1016/S0098-3004(01)00081-4.

Pallister, J.S., Thornber, C.R., Cashman, K.V., Clynne, M.A., Lowers, H.A., Mandeville, C.W., Brownfield, I.K., and Meeker, G.P., 2008, Petrology of the 2004–2006 Mount St. Helens lava dome—implications for magmatic plumbing and eruption triggering, chap. 30 *of* Sherrod, D.R., Scott, W.E., and Stauffer, P.H., eds., A volcano rekindled; the renewed eruption of Mount St. Helens, 2004–2006: U.S. Geological Survey Professional Paper 1750 (this volume).

Rasmussen, R.A., Khalil, M.A.K., Dalluge, R.W., Penkett, S.A., and Jones, B., 1982, Carbonyl sulfide and carbon disulfide from the eruptions of Mount St. Helens: Science, v. 215, p. 665–667.

Rutherford, M.J., Sigurdsson, H., Carey, S., and Davis, A., 1985, The May 18, 1980 eruption of Mount St. Helens—1. Melt composition and experimental phase equilibria: Journal of Geophysical Research, v. 90, no. B4, p. 2929–2947.

Shevenell, L., and Goff, F., 1999, Addition of magmatic volatiles into the hot spring waters of Loowit Canyon, Mount St. Helens, Washington, USA: Bulletin of Volcanology, v. 55, no. 7, p. 489–503, doi:10.1007/BF00304592.

Shinohara, H., Iiyama, J.T., and Matsuo, S., 1989, Partition of chlorine compounds between silicate melt and hydrothermal solutions—1. Partition of NaCl-KCl: Geochimica et Cosmochimica Acta, v. 53, p. 2617–2630.

Signorelli, S., and Carroll, M.R., 2002, Experimental constraints on the origin of chlorine emissions at the Soufriere Hills Volcano, Montserrat: Bulletin of Volcanology, v. 62, p. 431–440.

Sparks, R.S.J., Murphy, M.D., Lejeune, A.M., Watts, R.B., Barclay, J., and Young, S.R., 2000, Control on the emplacement of the andesite lava dome of the Soufrière Hills Volcano, Montserrat, by degassing-induced crystallization: Terra Nova, v. 12, no. 1, p. 14–20.

Stoiber, R.E., and Rose, W.I., 1974, Cl, F, and SO_2 in Central American volcanic gases: Bulletin Volcanologique, v. 37, no. 3, p. 454–460.

Symonds, R.B., Rose, W.I., Gerlach, T.M., Briggs, P.H., and Harmon, R.S., 1990, Evaluation of gases, condensates, and

SO_2 emissions from Augustine Volcano, Alaska—the degassing of a Cl-rich volcanic system: Bulletin of Volcanology: v. 52, p. 355–374.

Symonds, R.B., Rose, W.I., Bluth, G.J.S., and Gerlach, T.M., 1994, Volcanic-gas studies—methods, results and applications: Reviews in Mineralogy, v. 30, p. 1–66.

Tabazedeh, A., and Turco, R.P., 1993, Stratospheric chlorine injection by volcanic eruptions; HCl scavenging and implications for ozone: Science, v. 260, no. 5111, p. 1082–1086.

Villemant, B., and Boudon, G., 1999, H_2O and halogen (F, Cl, Br) behaviour during shallow magma degassing processes: Earth and Planetary Sciences, v. 168, p. 271–286.

Wallace, P.J., 2005, Volatiles in subduction-zone magmas—concentrations and fluxes based on melt inclusion and volcanic gas data: Journal of Volcanology and Geothermal Research, v. 140, nos. 1–4, p. 217–240, doi:10.1016/j.jvolgeores.2004.07.023.

Webster, J.D., 1990, Partitioning of F between H_2O and CO_2 fluids and topaz rhyolite melt—implications for mineralizing magmatic-hydrothermal fluids in F-rich granitic system: Contributions to Mineralogy and Petrology, v. 104, p. 424–438.

Webster, J.D., 1992, Water solubility and Cl partitioning in Cl-rich granitic system; effects of melt composition at 2 kbar and 800°C: Geochimica et Cosmochimica Acta, v. 56, p. 679–687.

Webster, J.D., and Holloway, J.R., 1988, Experimental constraints on the partitioning of Cl between topaz rhyolite melt and H_2O and H_2O+CO_2 fluids—new implications for granitic differentiation and ore deposition: Geochimica et Cosmochimica Acta, v. 52, p. 2091–2105.